Structure and Geochronology of the Acquadolce Phyllites and Metasiltstones (Elba Island, Italy)

Master of Science Thesis in Geoscience

Tonje Øvregaard Lunde

Department of Earth Science
University of Bergen
Nov 2020

Abstract

The Oligocene Acquadolce Phyllites and Metasiltstones (APM) of eastern Elba, Italy are high-pressure (HP) rocks related to the Apennine subduction zone. The unit gained newfound attention after the findings of HP minerals (glaucophane and lawsonite), as it was long thought to be greenschist-facies rocks. Parts of the sediments making up these rocks, including detrital zircons, originate from the volcanic arc related to the central Alps. The sediments were deposited in the Apenninic foredeep, subducted shortly after and then rapidly exhumed. In this study, a suggestion for the complex tectonic history of these rocks is made by interpreting the various structures found throughout the unit, as well as providing the first low-temperature thermochronological data using the (U-Th)/He method on zircons (ZHe) in an attempt to constrain the timing of exhumation. The structures found in this study are similar to the ones reported in previous studies (open-isoclinal folds at the micro-meso scale, sheath folds, shear bands, faults, etc.) and show a correlation to other HP units found on mainland Italy such as in the Apuan Alps. Based on these structures, a series of deformational events are described relating to subduction, early exhumation, late exhumation, and post-exhumation. We suggest that the exhumation, always aided by slab retreat, was first driven by buoyancy through an extruding wedge accommodated by compressional and extensional shearing, followed by extension in the orogenic wedge due to gravitational instabilities. The extension was followed by renewed compression reflected by a previously undescribed km-scale antiform in the southern part of the APM. The timing of the exhumation in the region has been constrained to Early-Late Miocene through analyses of other units. The new ZHe ages for the APM yielded 5.9-6.2 Ma and represent cooling through zircon's closure temperature of ca. 180 ºC. This is coeval to the Late-Miocene magmatism that affected Elba, suggesting that the geochronological systems were reset and that the ages represent cooling from the contact metamorphism rather than cooling by exhumation. Magmatism and post-orogenic collapse were results of a rising asthenosphere caused by the eastward migration of the compressional front due to slab retreat and can be seen in the APM by high-angle normal faults.

Acknowledgement

I would first like to thank my main supervisor Prof. Joachim Jacobs (UiB) who has shown faith in me, been great company during the field trip and even paid for my pizza, and of course for giving critical feedback on my work. He has made me aware of how careful one must be when doing scientific work and the importance of being precise and nitpicky. I would also like to thank my co-supervisor Prof. Sergio Rocchi (University of Pisa). Rocchi's input during Teams sessions have been most valuable, and I appreciate the time he took to help me while dealing with the very pressed situation going on in Italy at the time. I am also very grateful to researcher Maria Laura Balestrieri (IGG National Research Council of Italy) and Prof. Andrea Brogi (University of Bari, Italy) for contributing to the discussion of data.

Thank you to Ida Marie Gabrielsen and Åse Hestnes for introducing me to the various stages of mineral separation and always being available when I had questions. My lungs are also particularly grateful after Ida let me borrow her fancy face mask so I could breathe comfortably while crushing rocks. Leif-Erik Pedersen also has my gratitude after helping me several times with SEM and helping me interpret the data. I really appreciate the help I received from Göttingen, Germany where Åse Hestnes picked the zircons and István Dunkl analyzed them. Thanks to Andreas Lambach Viken for preparing my thin sections. Thank you Rebecca Ertesvåg and Brittany Watson for reading my text and giving feedback. Finally, I would like to thank Mike Roche, my fellow student and friend from the University College Dublin who agreed to be my field assistant on Elba and flew down on his own expense to help me. I am sorry the weather was not as promised but know that you made the entire experience a great deal better.

I've not thanked half of you half as well as I should like, and I'll thank less than half of you half as well as you deserve (modified after Bilbo, 3001).

Tonje Øvregaard Lunde
Klepp, November 2020

Table of Contents

1 Introduction

Elba Island is the largest island of the Tuscan Archipelago, situated between mainland Italy and Corsica, bordering the Ligurian and Tyrrhenian Seas (Fig. 1.1). It represents the westernmost outcrop of the Northern Apennines, a mountain chain trending parallel to the Italian Peninsula. Elba has an area of 224 km^2, stretching 29 km in the east-west direction, and 18 km in the north-south direction, with a population just over 32,000. It is famous for its vast variety and abundance of minerals and ores, particularly iron ores. The island was mined extensively and is now conserved by the Island of Elba Mineral Park and Calamita Mineral Park, who protect it from further mining. The minerals in this region were of such good quality that the island gained the name "the Island of Iron and Fire". Its mining history is now open for the public to see through museums and guided tours. The geology of Elba is not only interesting due to its mineral deposits, it also has a number of structures and geological units, such as detachment faults and stacked ophiolite complexes. These structures give insight to the past tectonic and environmental conditions in the Mediterranean region and accompanying subduction systems.

1.1 Study Area

One of the formations on Elba is the Acquadolce Phyllites and Metasiltstones (APM), which will be the focus of this study. This rock unit is mainly exposed in eastern Elba between the Capo d'Arco area in the south and Rio Marina in the north, where it spans between ~200-900 m from east to west. A small section can also be found in central Elba on the southern coast along Felciaio Beach. The main areas where mapping and sampling were carried out were Capo d'Arco, Ortano, Rio Marina, and Felciaio Beach. The quality of exposure varies with location, where some outcrops are highly weathered and vegetated, and others are fresh coastal outcrops. The unit does contain areas where rocks have undergone skarnification, and these were mostly avoided.

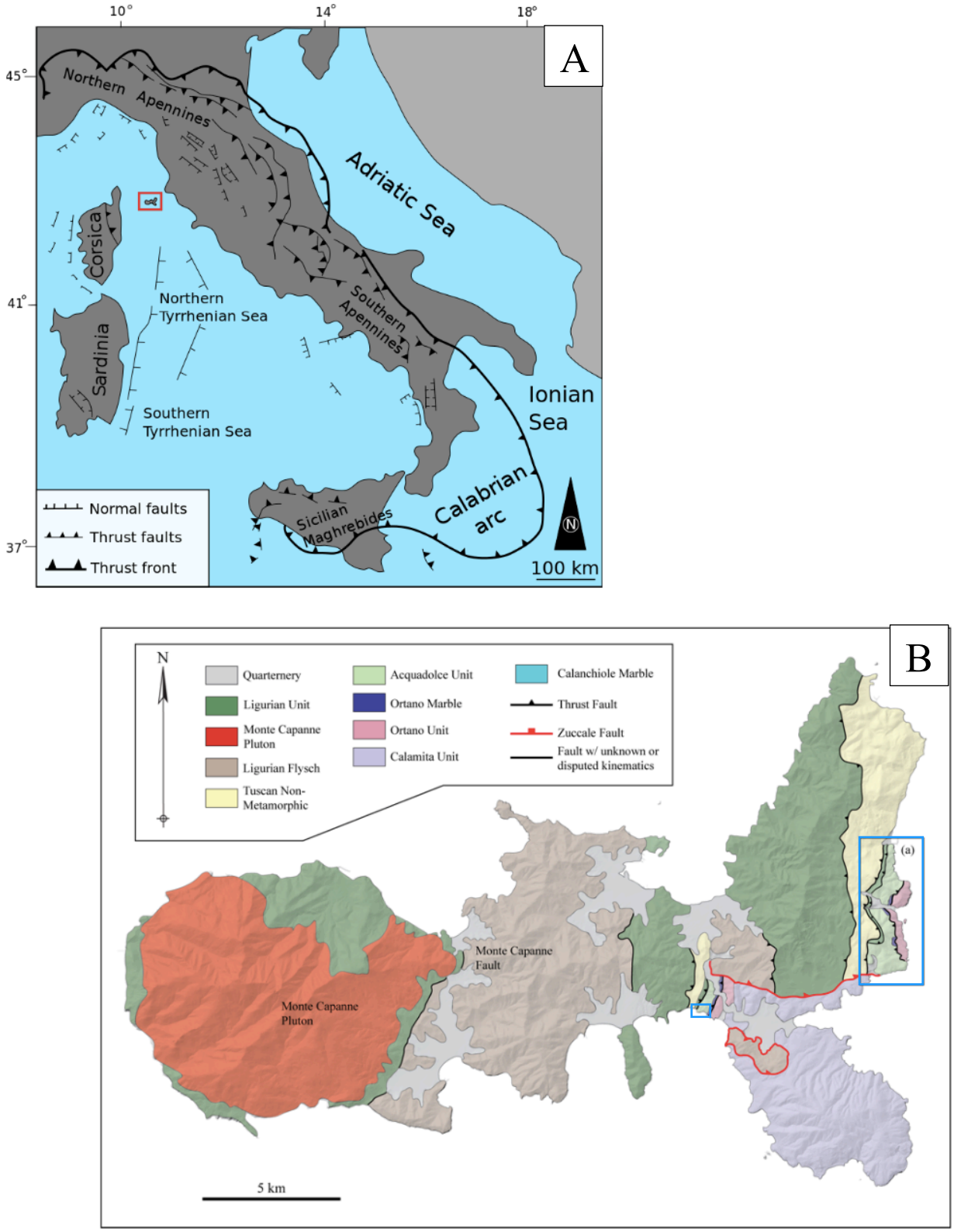

Figure 1.1 – A. An overview map of Italy and its bordering seas, the Tyrrhenian- and Adriatic Sea, showing the main tectonic features and Elba's location (red square). Modified after Rosenbaum and Lister (2004) in Sirevaag (2013).

B. Geological map of Elba Island showing some of the main tectonic features and the two study areas (blue squares). Modified after Mazzarini et al. (2011), Musumeci and Vaselli (2012) and Principi (2015) in Ryan (2017).

1.2 Previous Research

The first major study on Elba Island was conducted by Trevisan (1950), who mapped and described the entire island and lay the foundation for all future studies. One of the main attributes of that study was the division of geological units into complexes. He recognized five separate tectonic complexes (Complex I-V) including metamorphic and sedimentary successions as well as ophiolites, all contained within a nappe stack named the Eastern Elba Nappe Stack (EENS). This sparked newfound interest and was the beginning of several geological studies on Elba. After decades of research ranging from structural to petrological to geochronological, Bortolotti et al. (2001) revisited Trevisan's nappe stack model and further subdivided the five complexes into nine units, which will be described in Chapter 2.3. The focus of this study is the APM, whose origin and affinity, as well as structural evolution, have been debated over the years (Keller and Pialli, 1990; Duranti et al., 1992; Deino et al., 1992; Corti et al., 1996; Bortolotti et al., 2001; Pandeli et al., 2001; Elter and Pandeli, 2001, Benvenuti et al., 2001). The APM was long attributed to the Ligurian Domain, and thought to be Cretaceous in age due to the presence of microfossils (Duranti et al., 1992), but recent studies including Sirevaag (2013) and Bianco et al. (2015) unraveled that they are most likely Oligocene in age and from the Sub-Ligurian or Tuscan Domain. Many have attempted to explain the structurally complex history of the APM. The most obvious tectonic feature is the nappe stack, whose formation was dated by Deino et al. (1992), using the Ar^{40}/Ar^{39} method on muscovite, to 19.68 ±0.15 Ma. Keller and Pialli (1990) described the deformation of Complex II (containing the APM) to be of low grade greenschist facies, but later studies have suggested that the APM are HP-LT rocks, similar to the Schistes Lustrés (Corti et al., 1996, Bortolotti et al., 2001). Bianco et al. (2015, 2019) confirmed this after finding and dating the HP mineral glaucophane to around 19.8 ± 1.4 Ma. A recent study by Jacobs et al. (2018) concluded that due to the Oligocene detrital zircons in the APM, the unit subducted shortly after 32 Ma, and exhumed by 20 Ma during the stacking, with a deformation period of 12 Myr. Papeschi et al. (2020) on the other hand argued that exhumation of the APM *started* around 20 Ma and was exhumed by 6-7 Ma. The most recent deformation including open folding is thought to be caused by the uplift of two magmatic bodies that have been dated to ~6-7 Ma (Elter and Pandeli, 2001; Maineri et al., 2003; Musumeci et al., 2015). The relevant geochronological research from Elba Island and the Northern Apennines used for this study is summarized in Table 1.

Table 1 - Geochronological ages from a variety of rocks found on Elba Island and the Northern Apennines. The ages represent cooling and are sometimes associated with geological events that affected the Northern Apennines. References: 1. Maineri et al. (2013), 2. Bianco et al. (2019), 3. Conticelli, 2001, 4. Musemeci et al., 2011, 5. Musemeci et al., 2015, 6. Tvedt, 2011, 7. Deino et al., 1992, 8. Ryan (2017), 9. Viola et al., 2018, 10. Kligfield et al., 1986, 11. Balestrieri et al., 2003

Sample	*Locality*	*Rock Type*	*Mineral*	*Method*	*Dates*	*Age (Ma)*	*Study*
AZ	Buraccio	Monzogranite, Porto Azzurro (footwall block)	Biotite	40Ar-39Ar	Crystallization	5.9 ± 0.2	1
RMT7A	Rio Marina Harbor	Metabasite	Glaucophane	40Ar-39Ar	Main deformational event	19.8 ± 1.4	2
ST135/10	Monte Castello	Mafic dike	Groundmass of cpx, k-spar, plag, mg, apatit	40Ar-39Ar	Crystallization	5.83 ± 0.14	3
CS14	Calamita Peninsula	Andalusite-cordierite hornfels, Calamita Schist (footwall block)	Muscovite	40Ar-39Ar	Contact metamorphism	6.23 ± 0.06	4
CS16	Calamita Peninsula	Leucogranite sill, Porto Azzurro (hanging wall block)	Muscovite	40Ar-39Ar	Crystallization	6.33 ± 0.07	5
HJ-8	Capo d'Arco Residence	Capo d'Arco Schists	Muscovite	40Ar-39Ar	Cooling below ~425	6.2 ± 1.5	6
AT-12	East of Ex. Vendetta	Porphyroids	Muscovite	40Ar-39Ar	Cooling below ~425	6.32 ± 0.16	6
AT-25	Spiaggia del Lido	Silver-grey phyllites and quartzites	Muscovite	40Ar-39Ar	Cooling below ~425	6.49 ± 0.95	6
TN1	Terra Nera	Diopsite-phlogopite hornfels, Calamita Schist (footwall block)	Phlogopite	40Ar-39Ar	Contact metamorphism	6.76 ± 0.08	5
N/A	Rio Marina	Calcschist	Muscovite	40Ar-39Ar	Main deformational event	19.68 ± 0.5	7
Elb_5	Rio Marina Lighthouse	Calcschist	Muscovite	40Ar-39Ar	Main deformational event	20.99 ± 0.73	8
Elb_7	Ortano	Silver-grey phyllites and quartzites	Muscovite	40Ar-39Ar	Cooling below ~425	6.23 ± 0.02	8
ZUC2	Punta di Zuccale	Fault gouge in Zuccale Fault	Illite	K-Ar	Last fault activity	4.9	9
ZUC4	Punta di Zuccale	Hornfels in Calanchiole Shear Zone	Illite	K-Ar	Calanchione shear zone	6.14 ± 0.64	9
ELB2	Capo Norsi	Fault gouge in serpentinites in Capo Norsi-Monte Arco Thrust	Illite	K-Ar	Last fault activity	4.9 ± 0.27	9
Sample 3	Apuane Alps	Slate	Phengite-Chlorite	K-Ar	D1 foliation	27 ± 1	9
Sample 20	Apuane Alps	Phyllite	Phengite-Chlorite	K-Ar	D2 and D3 foliation	11.5-12	10
CS12	Calamita Peninsula	Andalusite-cordierite hornfels, Calamita Schist (footwall block)	Zircon	U-Pb	Contact metamorphism	6.40 ± 0.15	4
Ap43A	Mt. Falterona	Foredeep deposits	Apatite	U-Th/He	Cooling below ~70	2.72 ± 0.16	11
Ap47A	Mt. Falterona	Foredeep deposits	Apatite	U-Th/He	Cooling below ~70	2.81 ± 0.17	11
Ap48A	Mt. Falterona	Foredeep deposits	Apatite	U-Th/He	Cooling below ~70	3.81 ± 0.23	11
CIP3A	Apuan Alps	"Basement Units"	Zircon	U-Th/He	Cooling below ~180	4.98 ± 0.4	11
AR2A	Apuan Alps	"Basement Units"	Zircon	U-Th/He	Cooling below ~180	7.42 ± 0.59	11

1.3 Research Objectives

With the recent advancements made by Jacobs et al. (2018) regarding the APM's subduction-exhumation cycle, a field-based structural analysis was conducted in an attempt to document the complex structural history of these rocks, also taking into consideration the more recent events such as the Late Miocene magmatism and corresponding fault activity. Despite the several geochronological studies that have been carried out on Elba, thermochronological data for the APM is sparse and non-existent for low-temperature thermochronology specifically. Six samples were collected in order to provide the first thermochronological data for the APM, using (U-Th)/He dating on zircons to determine possible thermal histories and tie that in with the structural history.

2 Geological Background

2.1 Evolution of the Mediterranean and the Apennines

The Mediterranean is a tectonically complex area with several plates and microplates interacting with each other. Collision, back-arc formation, and opening and closing of several oceans are some of the processes responsible for the geology seen today (Lonergan and White, 1997; Doglioni et al., 1997; Jolivet et al., 1998; Gueguen et al., 1998; Stampfli, 2000; Jolivet et al., 2003; von Raumer et al., 2003; Carminati and Doglioni, 2005). Stampfli and Borel (2004) made a series of paleogeographic figures showing the origins of Adria, which the following reconstruction is based on. Adria, the microplate making up parts of Italy and the Adriatic Sea (Fig. 2.1), was part of a long strip of northern Africa called the Cimmerian Superterrane. This superterrane was a continental ribbon that drifted northwards as the Neotethys back-arc basin (Sengör, 1984) started opening in the Late Carboniferous – Early Permian (Fig. 2.2A) (Stampfli et al., 2001). By Middle-Late Triassic times the Cimmerian Superterrane collided with the Eurasian margin, closing the Paleotethys (Fig. 2.2B). In the Jurassic (180 Ma), the opening of the Central Atlantic started to break up Pangea, causing the African pole to change and resulting in northwestward migration and anticlockwise rotation of Africa (Bortolotti et al., 2001). This caused a narrow passage to open between the Atlantic Ocean and the Neotethys, opening yet another Tethys ocean called the Western Tethys, sometimes termed the Alpine Tethys (Fig. 2.2C). In the Cretaceous, Africa eventually closed the Western Tethys as it collided with Europe and Iberia (Fig. 2.2D). This collision involved oblique subduction of Europe underneath Adria, creating a transpressive environment (Marroni and Treves, 1998). It started out as a N-S trending convergence and evolved to a NE-SW convergence (Bortolotti et al., 2001). In the Eocene, the Corsican continental margin and Adria experienced a subduction

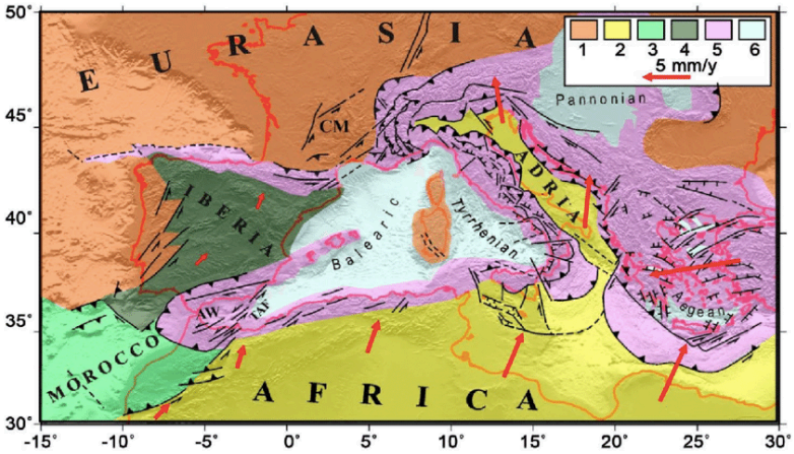

Figure 2.1 - Tectonic map of the Mediterranean, showing Adria surrounded by orogenic belts. Adria is bound by subduction zones, creating the Apennines to the west and Dinarides to the east. 1) Eurasian domain 2) Africa- Adriatic domain 3) Morocco plate 4) Iberian plate 5) Orogenic belts 6) Main extensional basins. Figure from Viti et al. (2016)

flip, as the Adriatic plate developed westward subduction along the back-thrust of the earlier E-dipping subduction zone. This resulted in the detachment of the Corsican slab and the end of eastward subduction (Doglioni et al., 1999; Molli and Malavieille, 2011).

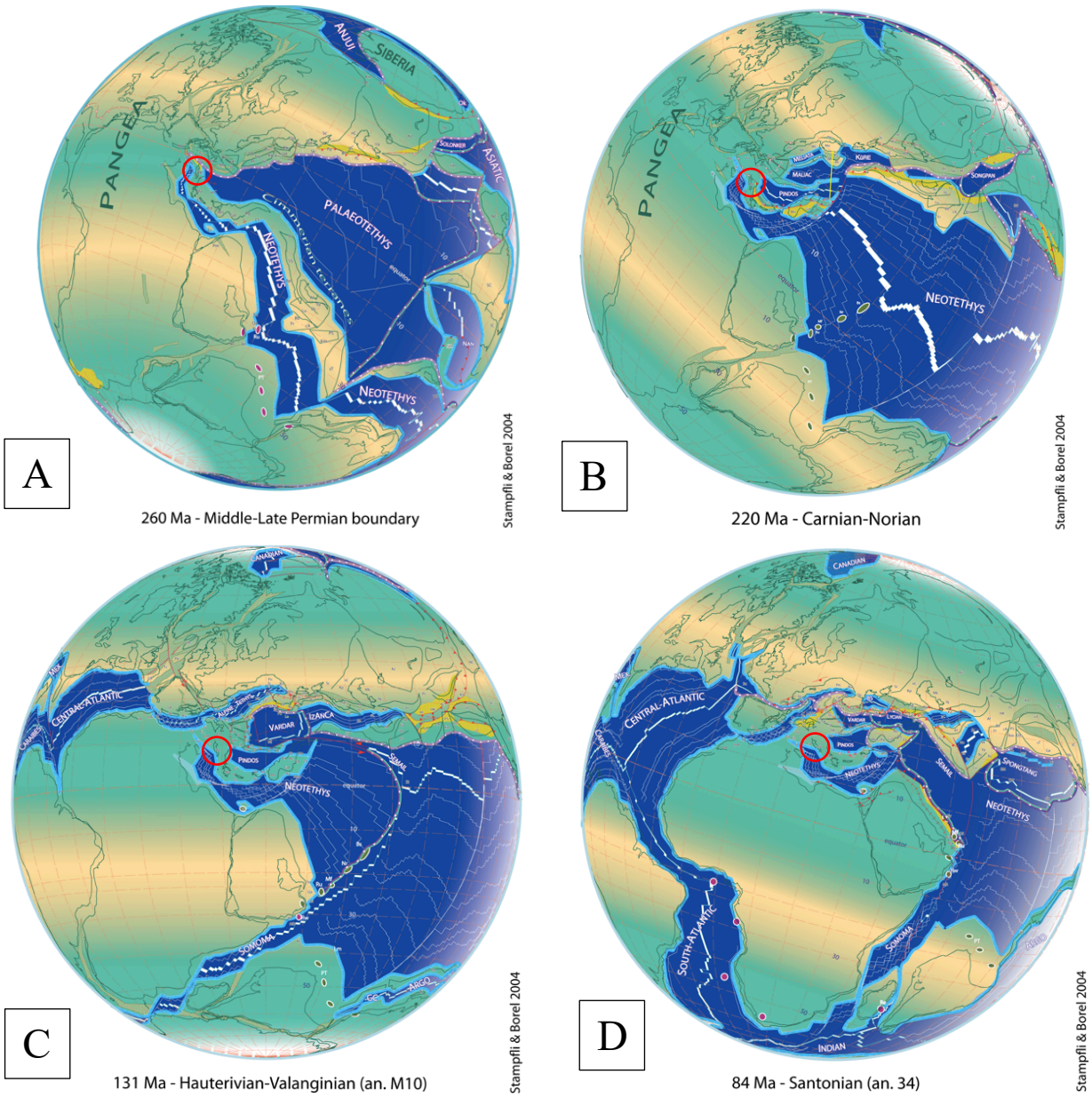

Figure 2.2 - Paleogeography showing Adria's (red circle) migration from Middle Permian to Late Cretaceous. A) Cimmerian Superterrane breaks away from Gondwana as a continental ribbon. B) Cimmerian Superterrane collides with Europe, closing the Paleothethys. C) Central Atlantic opens, causing the formation of the Western Tethys. D) Southern Atlantic opens, Africa + Adria move northwards and later collide with Europe forming the Alps and the Apennines. Figure from Stampfli and Borel (2004).

Sometime in the Neogene, Adria separated from Africa suggested by their different geodetic motion and velocity trends (Battaglia et al., 2004; D'Agostino et al., 2008). In the Late-Oligocene-Early Miocene, slab rollback initiated and affected the region by ripping off the

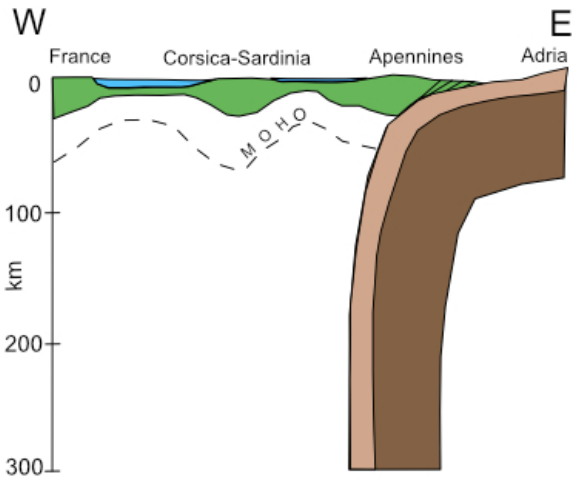

Figure 2.3 – Simplified cross-sectional view of the western Mediterranean today, showing how upwelling asthenosphere (dashed line), caused by slab rollback, thins out the continents creating mega-boudinag. Vertical exaggeration x5. Modified after Gueguen et al. (1998).

Corsica-Sardinia block from France (Robertson and Grasso, 1995; Gueguen et al., 1998), and by 17 Ma opening the back-arc basins that formed the Liguro-Provencal Sea and later on the Tyrrhenian Sea (Séranne, 1999; Malinverno and Ryan, 1986). As the slab sank and the subduction zone retreated, asthenosphere filled the empty space thinning out the crust and forming these basins, making the region appear like mega-boudinage (Fig. 2.3) (Gueguen et al., 1998). The Liguro-Provencal Sea and the Southern Tyrrhenian were thinned to the point where oceanic crust started to form (Hutchison et al., 1985). The entire subduction zone retreated eastward, with most movement happening in Calabria, which resulted in the area rotating anticlockwise 60º to the east (Fig. 2.4). Around 33 Ma, the tectonic regime shifted from solely compressional to compressional *and* extensional, as the accretionary prism started to collapse. The change was due to the increasing rate of slab rollback, caused by lengthening of the slab (Brunet et al., 2000; Faccenna et al., 1996). This is the current situation of the Apennines.

The Apennine's tectonic history most likely initiated in the Late Cretaceous with the development of the west-dipping subduction zone in the Western Tethys, close to Corsica-Sardinia's continental margin (Bortolotti et al., 2001). The subduction zone has been dated to the Late Cretaceous by Maluski (1977) using Ar^{40}/Ar^{39} on glaucophane. This is the only piece of evidence for subduction taking place at this time, as other HP-LT rocks of this region were dated to Middle-Late Eocene. The lack of arc-type magmatic rocks from this period is also puzzling, but can be explained by the oblique collision, slow convergence and hence a very short slab (100 km) (Bortolotti et al., 2001). The Apennines comprise of rocks belonging to both the Ligurian (oceanic) and Tuscan (continental) domains. The Ligurian units were stacked before continental collision during subduction and the formation of an accretionary wedge. Coevally, the deeper parts of the prism started to uplift undergoing ductile deformation (Bortolotti et al., 2001). As continental collision initiated between Adria and Corsica-Sardinia, the Ligurian and Tuscan units were superimposed forming the EENS which has been dated to ca. 19 Ma using Ar^{40}/Ar^{39} on muscovite from the Acquadolce Unit's main schistosity (Deino et

al., 1992). The onset of extension started in the Middle-Late Miocene and the exhumation mechanisms are still being debated but include gravitational collapse in the overthickened accretionary wedge and slab rollback making available space for rising asthenosphere. This extension resulted in normal faulting, including detachment faults, most likely responsible for opening the Corsica Channel (Bortolotti et al., 2001). It is also worth mentioning that extension is sometimes triggered by slab detachment. However, only in the Central-Southern Apennines and the Calabrian region has it been concluded that slab detachment has been completed. There is still some uncertainty pertaining to the Northern Apennines (Wortel and Spakman, 2000).

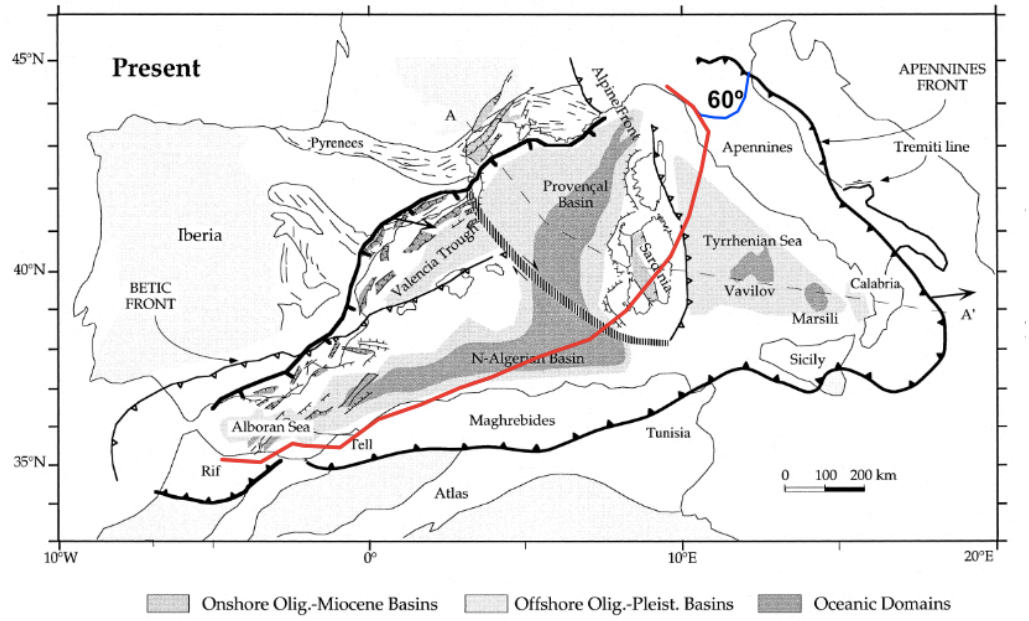

Figure 2.4 – Present-day geography of the western Mediterranean showing the Apennine subduction zone and normal faulting by France and Spain. The red line represents the position of the subduction zone at 23 Ma, which then rotated anticlockwise, 60º to the east, with most of the movement being in the Calabria region. The convergence started out trending NW-SE and has ended up trending NE-SE as observed in the Apennines which stretches along the Italian Peninsula. Modified after Gueguen et al. (1998)

2.2 Subduction Systems

In order to understand the complex tectonic history of Elba and the Northern Apennines, it is useful to have a somewhat understanding of the environment it formed in, which was in a subduction zone. Generally, two subduction styles are recognized, the Chilean- and the Mariana-type, which are commonly referred to as advancing and retreating (Cawood et al., 2009) (Fig. 2.5). In an advancing system, the stress in the back-arc is governed by compression rather than extension as seen in the retreating system (Uyeda and Kanamori, 1979). Royden

and Burchfiel (1989) described these styles in detail, defining advancing systems as when the rate of convergence exceeds the rate of subduction and retreating systems as when the rate of subduction exceeds the rate of convergence. They also listed the different characteristics of the orogenic belts forming over them. Advancing orogens are often the topographically highest, experiencing large amounts of erosion resulting in molasse deposits ending up in the front of the mountain chain. Examples of advancing orogens include the Alps, the Himalayas and the Andes. Retreating orogens are characterized by lower topography, extension in the back-arc region, and flysch deposits. Examples of retreating orogens include the Apennines and the western Pacific. The reason why they have been termed advancing and retreating is because they are not stationary, rather they migrate – advancing subduction zones migrate towards the trench, while retreating subduction zones move away from it. They often start off as retreating due to cold, dense oceanic crust being pulled down by gravity, and end up advancing as buoyant continental crust is subducted, preventing rapid sinking of the slab.

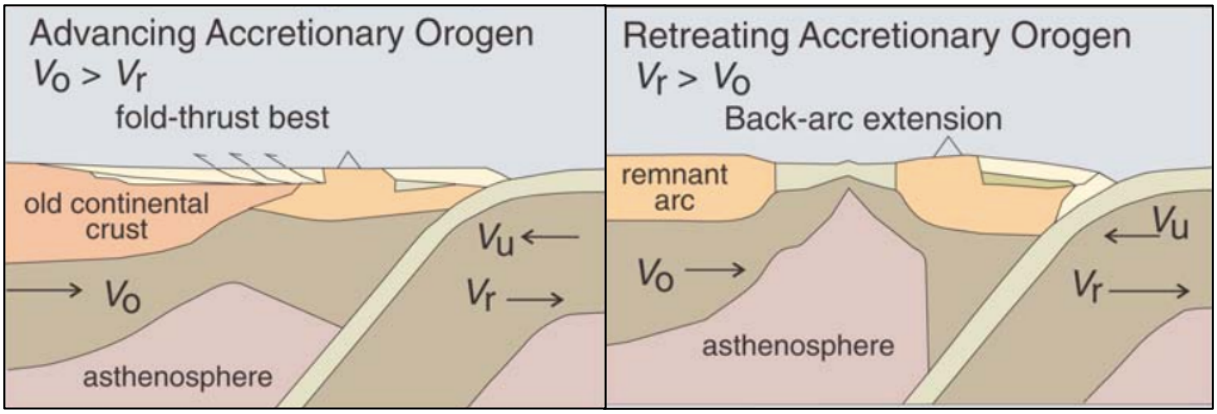

Figure 2.5 - The two endmembers of subduction zones - advancing and retreating. In the retreating subduction, the sinking slab will eventually start to roll back due to increasing density in the oceanic crust, opening a back-arc. $\mathbf{V_O}$: velocity of overriding plate; $\mathbf{V_u}$: velocity of under-riding plate; $\mathbf{V_r}$: velocity of retreat (Cawood, 2009).

As the slab sinks in a retreating system, slab rollback may start to affect the overriding plate's back-arc region (Malinverno and Ryan, 1986). This was the case for the Tyrrhenian Sea, which opened as a result of back-arc extension due to slab rollback (Lonergan and white, 1997). For back-arc extension to occur, the subduction angle needs to be >50º (Lallemand et al., 2005) - in many cases the slab is near vertical (ex. Mariana). This rollback comes to a halt if the slab detaches (Wortel and Spakman, 2000). Decoupling of the plates is another process common for retreating subduction zones and results in distributed stresses, being compressive in the front and extensional in the back, which is the case for the Northern Apennines (Faccenda et al., 2009). Plates that are strongly coupled experience a stronger push against each other, forming large accretionary wedges as sediments are scraped off the ocean floor. Plates with weak coupling have a tendency to drag sediments down in the subduction channel instead of accreting

them on to the other plate, as there is more space between the two plates when the subducting slab is retreating.

In either case, accretionary wedges are formed that deform under the critical taper theory by either thickening or thinning to maintain stability (Fossen, 2016). Davis et al. (1983) defines the critical taper as "the shape for which the wedge is on the verge of failure under horizontal compression everywhere, including the basal décollement" In practice this means that the wedge will build up and deform internally until a certain angle (critical taper) is reached and deformation ceases in the wedge and moves to the basal décollement resulting in sliding. Erosion can affect the wedge by destabilizing it, initiating more build-up until it once again reaches the critical taper. An accretionary wedge is dominated by fold-and-thrust belts resulting in nappe stacking and the formation of several structures often showing opposing vergence (Fig. 2.6) (Costa and Vendeville, 2002). The main processes affecting the wedge geometry is the transfer of sediments from the downgoing slab to the overriding plate which can happen through frontal accretion or underplating in the deeper parts of the subduction channel (Marroni et al., 2004). HP rocks can form in the subduction channel and later be exhumed through the wedge by a variety of processes such as extensional collapse (Dewey, 1993) and buoyancy differences, aided by erosion and tectonics (Chemenda et al., 1995). Whether rocks will exhume rapidly or not depends on the type of subduction, and the only type that allows the rapid exhumation of HP rocks is the continental-type due to its wide accretionary wedge (Guillot et al., 2009).

P-T-conditions of subducted rocks can be recorded by index minerals belonging to different metamorphic facies. The blueschist facies is characterized by high pressure ($P \sim 0.3$-10 GPa) and low temperature ($T < 500°C$) (Ernst, 1972) and is documented by preserved HP-LT minerals that have not undergone retrogressive metamorphism. The minerals vary depending on the protolith's composition, but generally glaucophane, lawsonite, phengite, and epidote are indicative of such conditions (Bucher and Frey, 2002).

Figure 2.6 - Sandbox experiment for a previous course representing plate convergence. The model shows the internal structures of an accretionary wedge. Folds and thrusts verge in opposite directions meaning that relying simply on vergence is not enough to determine the tectonic processes.

2.3 The Geology of Elba

Elba Island is part of the 1200 km long, NW-SE trending Apennine mountain chain and represents the westernmost outcrop of the Northern Apennines. As previously mentioned, the Apennine subduction started retreating in the Late Oligocene-Early Miocene, and the Apennine front has since moved in an anticlockwise direction to its present-day location due to slab rollback (Robertson and Grasso, 1995; Gueguen et al., 1998). This puts the Apennines, and therefore also Elba Island, in both an extensional and compressional tectonic regime. These two regimes have left their imprints in different parts of the island. The east is dominated by thrust tectonics and can be seen as a series of stacked nappes (EENS), while the west is dominated by Mt. Capanne – a granitoid pluton. Another pluton called La Serra-Porto Azzurro (Porto Azzurro for short) later intruded in the east affecting the EENS with its thermal aureole. Together, the two plutons, in conjunction with an extensional upper wedge and later orogenic collapse, put Elba in an extensional setting while being in an overall convergent environment (Bortolotti et. al., 2001). This extensional phase created numerous normal faults, some of them being low-angle detachment faults like the Zuccale Fault. Musemeci et al. (2015) questioned the nature of the Zuccale Fault suggesting that it is actually the flat section in an out-of-sequence thrust with ramp-flat-ramp geometry. These later faults have caused secondary stacking and translated the nappes about six kilometers east (Musumeci, et al., 2015) (Fig. 2.7).

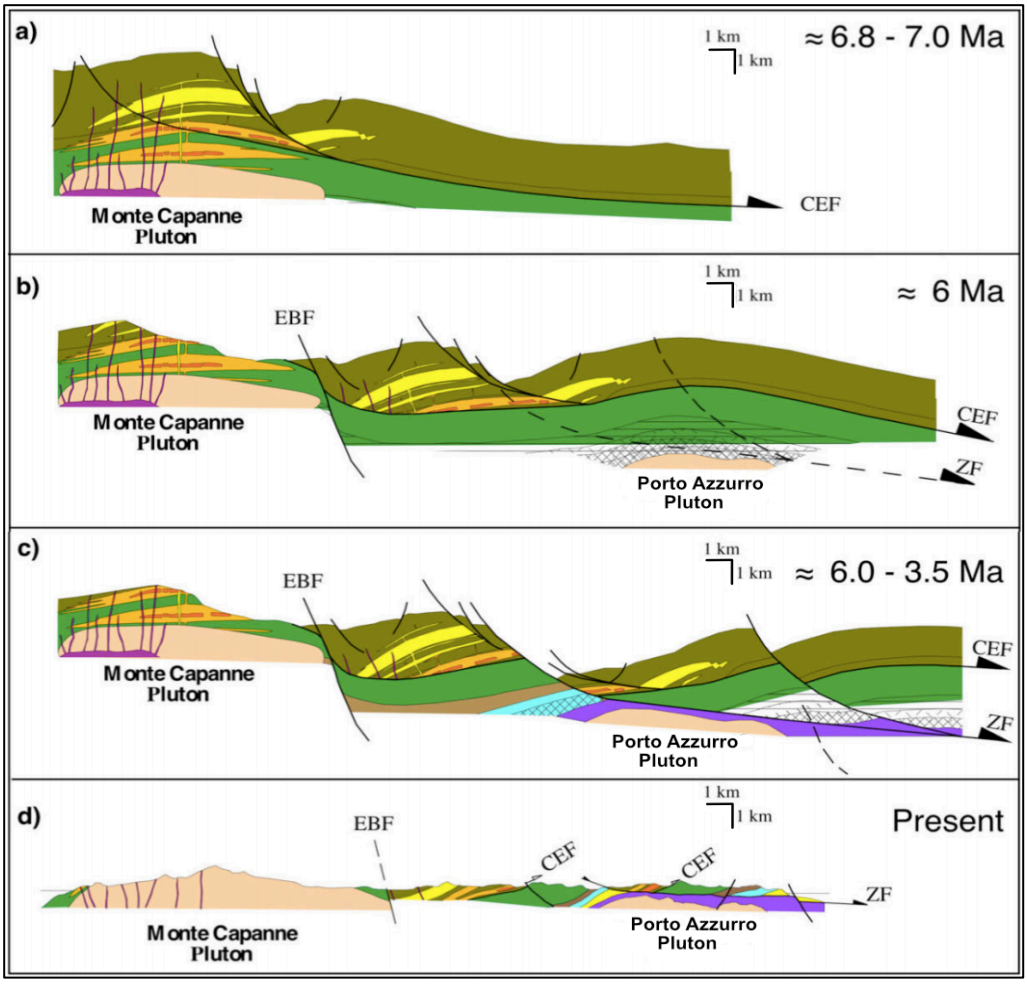

Figure 2.7 – Schematic cross-sections of Elba Island, showing how the uplift of the Mt. Capanne pluton resulted in detachment faults like the Zuccale Fault (**ZF**), which dissected and translated the nappe stack 6 km to the east. a) Mt. Capanne intrudes, creating a laccolith complex in western Elba. b) The Central Elba Fault (**CEF**) translates the laccoliths towards the east. c) The intrusion of the Porto Azzurro Pluton activates the Zuccale Fault which translated the nappe stack 6 km to the east. d) Present-day situation. The APM is in the area shaded blue. Modified after Westerman et al. (2004).

The different lithologies present at Elba Island are found in two units – the continentally derived, mostly autochthonous Tuscan Basement unit, which is overlain by the allochthonous, oceanic sediments in the Ligurian unit. The Tuscan unit includes lithologies from the Adriatic continental margin, while the Ligurian unit's sediments were deposited in the Western Tethys Ocean (Bortolotti et. al., 2001).

Stratigraphy

Elba Island's stratigraphy consists of metamorphic and sedimentary rocks as well as ophiolites and mélanges. The first model that described the stratigraphy and lithologies was the Trevisan model (1950), which grouped them into five complexes. The new model laid forth by Bortolotti et al. (2001), further subdivided the complexes into nine units (Fig. 2.8) whose characteristics are summarized in Table 2.

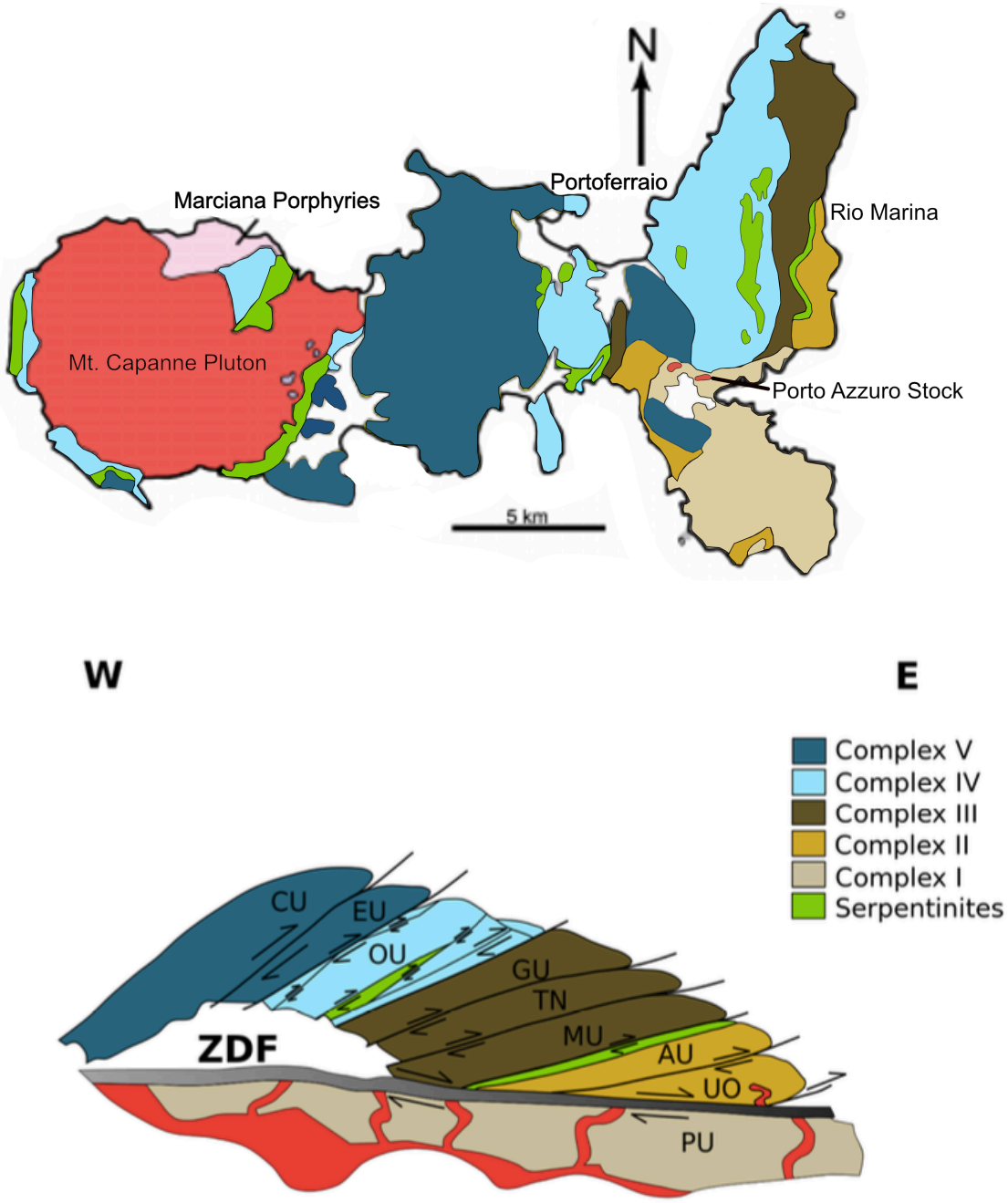

Figure 2.8 - Geological map of Elba showing the distribution of the different complexes, and cross-sectional view of the EENS showing the geometry, layering, and tectonic boundaries. Different units are **PU**: Porto Azzurro; **UO**: Ortano; **AU**: Acquadolce; **MU**: Monticiano-Roccastrada; **TN**: Tuscan Nappe; **GU**: Gràssera; OU: Ophiolites; **EU**: Paleogene Flysch; **CU**: Cretaceous Flysch; **ZDF**: Zuccale Detachment Fault. Modified after Bortolotti et al. (2001) in Sirevaag (2013).

Table 2 - Description of the nine lithological units on Elba Island, showing the associated complexes.

Complex	Unit	Description
I	Porto-Azzurro	Mica schists of Paleozoic age, containing smaller areas of phyllites, quartzites, dolostones, and limestones. They have a thermometamorphic imprint and are cut by dikes from the La Serra-Porto Azzurro pluton. From the Tuscan Domain.
II	Ortano	Ordovician, contact metamorphosed metavolcanics and low-medium grade metamorphic rocks, including phyllites, quartzites and porphyritic schists. Also cut by dikes from the La Serra-Porto Azzurro pluton. Separated from the Porto Azzurro unit by the Zuccale detachment fault. From the Tuscan Domain.
	Acquadolce	Sub-Ligurian/Tuscan, Oligocene massive marbles grading up to calc-schists, phyllites and metasiltstones, topped by serpentinites.
III	Monticiano-Roccastrada	Late Carboniferous to Early Permian graphitic, fossil-rich phyllites and metasedimentary rocks, as well as Triassic quartzites, limestones and calc-schists.
IV	Tuscan Nappe	Consists of eight formations that are mainly Late Triassic dolomitic breccias, calcareous sedimentary rocks, and a variety of limestones and marlstones
	Gràssera	Possibly Cretaceous calc-schists and slates with cm-scale siltstone and limestone beds
	Ophiolites	Several thrust sheets of Late Jurassic-Early Cretaceous, serpentinized ophiolites from the Western Tethys Ocean with a volcanic and sedimentary cover
V	Paleogene Flysch	Middle Eocene, shaly-marly successions with turbiditic limestones, sandstones, and ophiolite breccias. Cut by Mt. Capanne dikes and laccoliths.
	Cretaceous Flysch	Cretaceous ophiolitic shear complex and breccias, and various shales, sandstones, and turbidites consisting of sandstones, marlstones, and shales.

Tectonic Evolution

Benvenuti et al. (2001) explained that Elba's tectonic history can be categorized into three stages; the accretionary, the pre-intrusion extensional, and the syn-and post intrusion. The accretionary stage started in the Eocene and is responsible for stacking parts of the nappes. It refers to the collision between the Western Tethys and Europe, and later Adria and Corsica as oceanic sediments and continental crust were accreted and thrusted on top of each other forming a double-vergence orogenic wedge (Bartole et al., 1990). The early-middle Miocene was the start of the pre-intrusion extensional stage, caused by the asthenosphere rising as a result of slab rollback, and an overthickened wedge compensating by normal faulting. This was also the start of the opening of the Corsica Channel (Bartole et al., 1990). The Miocene-Pliocene syn- and post intrusion stage is responsible for more extension and orogenic collapse as the two granitic magmatic bodies, the Mt. Capanne Pluton and the later Porto Azzurro Pluton intruded (Fig. 2.9). They are part of the Tuscan Magmatic Province, formed by the heat from the upwelling asthenosphere. The two plutons are some of the youngest granites in Europe, emplaced at 6.8-5.4 Ma (Maineri et al., 2003; Musumeci et al., 2015; Bortolotti et. al., 2001). They are responsible for mechanically exhuming the rocks on Elba and triggering several faults. By this time, Elba was most likely exhumed above sea level suggested by the absence of marine sediments (Bortolotti et al., 2001). As a result of these plutons, Elba underwent contact metamorphism at temperatures ranging from 300-650 ºC (hornfels facies) (Duranti et al., 1992).

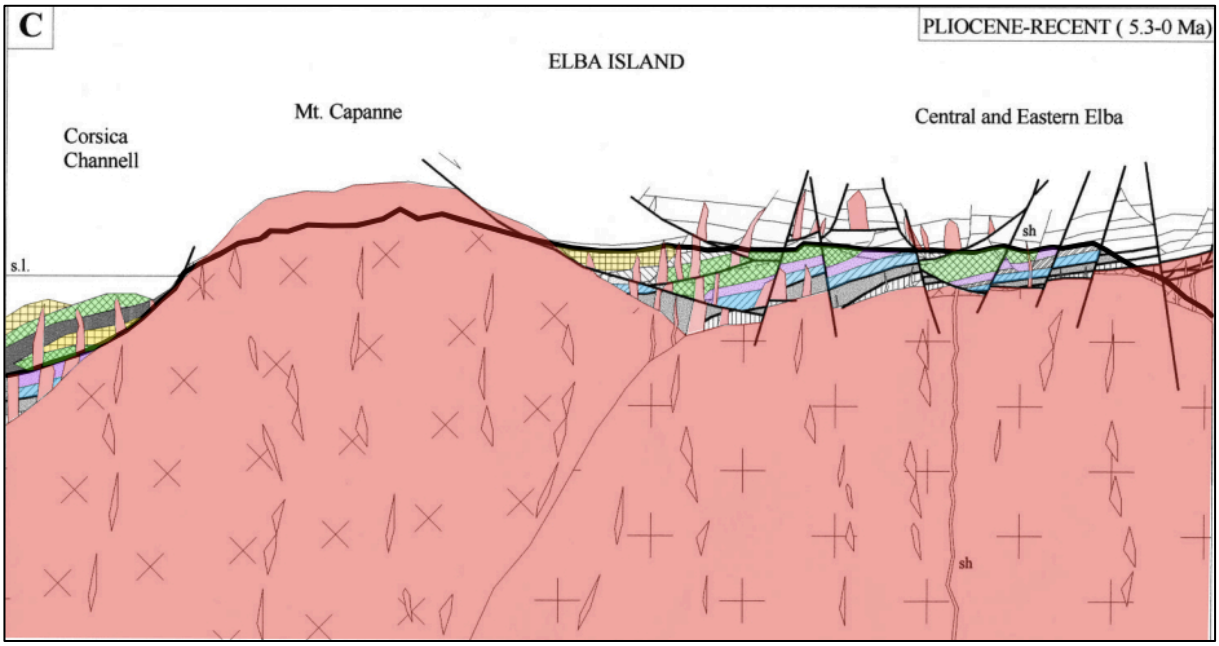

Figure 2.9 - Syn- and post intrusion stage on Elba Island, showing the two magmatic bodies Mt. Capanne and Porto Azzurro and related extensional structures. The bold line shows the present-day W-E topography from Mt. Capanne to Mt. Arco. Modified after Bortolotti et al. (2001).

Geothermal Activity and Mineralization

With a relatively thin crust and high heat flow due to the upwelling asthenosphere (Peccerillo and Donati, 2003), Italy sits on top of a geothermal region called the Tuscan Magmatic Province. The geothermal gradient is on average 25-30 ºC/km, but in places like Larderello, Tuscany it ranges between 75-100 ºC/km (Dini et. al., 2005). This has provided Italy with renewable, geothermal energy since 1911, which is when they were first able to light up four light bulbs. Elba Island is famous for its many minerals, including skarn minerals and especially iron ores. Dünkel (2003) looked at iron ore formation and how they relate to tectonics and found that the iron ores are restricted to a narrow N-S trending belt along the eastern coast. The most typical iron ores include pyrite, hematite in the north, and magnetite, which is more abundant further south. Copper is the dominant ore mineral in central Elba. The ores were deposited by hydrothermal and metasomatic processes during the granite intrusions in the Late Miocene, and are mostly related to three sets of faults; a set of N-S striking thrust faults dipping W, and two sets of normal, high-angle faults, one striking N-S and the other NE-SW.

2.4 Acquadolce Phyllites and Metasiltstones

The Phyllites and Metasiltstones is an approximately 300 m thick unit and makes up the largest chunk of the Acquadolce Unit in Complex II (Bortolotti et al., 2001) and is the main focus of this study. This succession consists of massive marbles, grading up to calc-schists, phyllites and metasiltstones containing lenses of calc-schist and metabasite, and is topped by serpentinites (Bortolotti et al., 2001). Duranti et al. (1992) dated the rocks to the Lower Cretaceous from the presence of relict microfossils. This was long accepted to be the age, until Sirevaag (2013) brought it up for discussion after dating detrital zircons restricting the maximum deposition age to 32 ± 1 Ma.

Pandeli et al. (2001)'s analysis of the composition of K-white mica suggested that the APM are similar to the Schistes Lustrés which are the HP-LT rocks of Corsica and the western Alps that reached pressures of at least 0.8 GPa. This P-T estimate was confirmed by Bianco et al. (2015, 2019) who concluded that the APM are HP-LT rocks with a retrogressive overprint, having reached depths of 40-60 km and metamorphic conditions of >1.6 GPa (blueschist facies). This was concluded after analyzing metabasites embedded in the calc-schist lenses in the APM. The metabasites contain epidote and chlorite as well as relict glaucophane and lawsonite, the latter two being index minerals for HP-LT metamorphism. The recent study by Papeschi et al. (2020) further constrained the P-T conditions to 1.5-1.8 GPa, equating to about

42-50 km depth. This suggests that Elba and the Apennines reached HP conditions in the lawsonite-blueschist facies, retrogressed into the greenschist facies, and disproved previous theories of Elba being in a low-pressure environment (<0.4 GPa and 350 º C) **(**Keller and Pialli, 1990; Keller and Coward, 1996; Musumeci and Vaselli, 2012). These findings made Elba fit in with the rest of the HP tectonic history of the Northern Apennines.

Bortolotti et al. (2001) states that the Acquadolce Unit subducted during the Ligurian events (Eocene-Oligocene). It involved subduction of the Ligurian sedimentary units which produced the HP-LT deformation in the APM, commonly found as tight-isoclinal, meso-scaled folds that are usually overturned or recumbent. With the new advancements from Sirevaag (2013), Jacobs et al. (2018) and Bianco et al. (2015), the maximum age of deposition of the APM is constrained to the Oligocene, and the subducted material was Sub-Ligurian/Tuscan sediments, rather than Ligurian. Therefore, these rocks were long attributed to the Ligurian domain (Bortolotti et al., 2001 and references therein), but Bianco et al. (2015) showed that they belong to the Sub-Ligurian/Tuscan Domain (Fig. 2.10). The Ligurian Domain is the sedimentary cover of Jurassic oceanic crust whose related MORB has a different chemical signature than the metabasites analyzed in the APM. The sediments making up the APM are now associated with the foredeep deposits of the Macigno Formation and Pseudomacigno Unit of the Apuan Alps (Jacobs et al., 2018). The Ligurian events were followed by the Main Apenninic event, which took place in late Oligocene/early Miocene as the Adriatic Plate collided with Corsica. This event deformed the Tuscan Adriatic margin while accreting the APM to the overriding plate by the process of underplating (Bortolotti et al., 2001; Platt, 1986). The 19 Ma age on the main schistosity of the APM is reflective of this event suggesting that nappe stacking took place at this time (Deino et al., 1992). This date has recently been re-interpreted as the age of peak metamorphism (Massa et al., 2017; Papeschi et al., 2020). The stacking eventually caused overthickening in the accretionary wedge, and together with slab rollback (which allowed hot asthenosphere to cause uplift and make the orogen more ductile) resulted in exhumation of the APM and eventually orogenic collapse as the compressional front migrated eastward (Bortolotti et al., 2001). Detachment faults along with the recent Miocene-Pliocene magmatic intrusions weakly folded the entire stack, creating gentle-open folds/kinks in the APM (Elter and Pandeli, 2001). The APM underwent contact metamorphism by the Porto Azzurro Pluton, which has an estimated contact aureole of 6-7 km in diameter and thickness of

700 m (Musemeci et al., 2015). This thermal event formed minerals like andalusite, skarn-related minerals, and cordierite in APM.

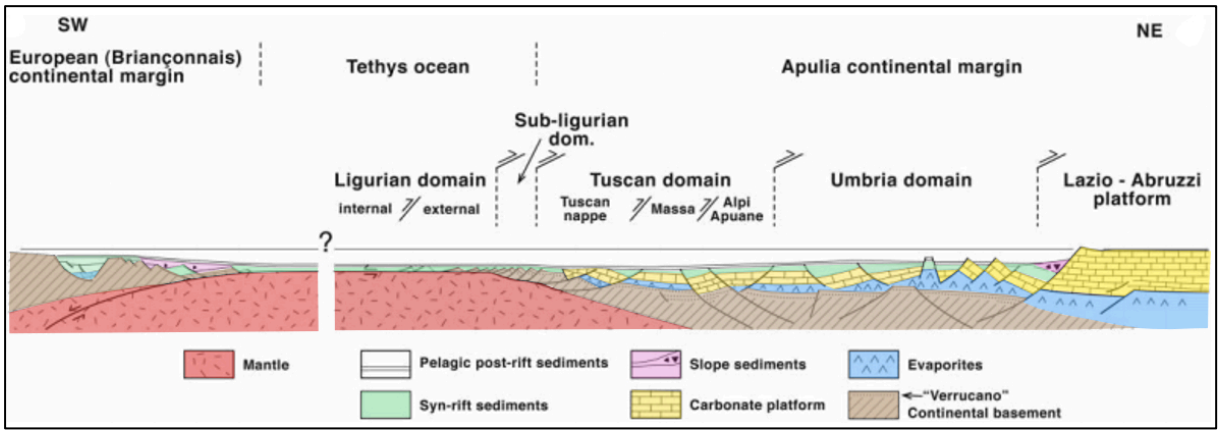

Figure 2.10 - Cross-sectional overview of the Western Tethys and its different domains. The APM were deposited in the Sub-Ligurian/Tuscan domain. The question mark highlights the uncertainty of whether oceanic crust was formed or not. Apulia refers to Adria. Modified after Carmignani et al. (2004).

The tectonic history of the APM took place over 12 Myr as concluded by Jacobs et al. (2018) who argued that the Oligocene zircons originated in a volcanic arc from the Alps created by the convergence of Africa and Europe. The zircons then eroded and travelled 400 km southward to finally be deposited and subducted in the Western Tethys. In their cycle, they considered 32 Ma as the protolith generation and 20 Ma as the age of exhumation. Papeschi et al. (2020) on the other hand, suggested a maximum 15 Myr time frame from peak metamorphism (21-19 Ma) to complete surface exhumation (latest 6-7 Ma).

3 Principles of (U-Th)/He Zircon Dating

3.1 (U-Th)/He System in Zircons

Zircon as a geochronometer has always been popular due to zircon's physical and chemical properties such as resistance to weathering, high U and Th concentrations, and its presence in magmatic, metamorphic, and sedimentary rocks (detrital) (Corfu et al., 2003). Igneous zircons are often euhedral and precipitate from Zr-saturated melts (Watson, 1979), while metamorphic zircons are more rounded and usually preserved from the protolith in low-grade metamorphic rocks or grow during high-grade metamorphism due to the breakdown of garnet and/or hornblende (Fraser et al., 1997). Zircon ($ZrSiO_4$) is an orthosilicate mineral belonging to the tetragonal crystal system and has a crystal structure that is relatively spaced and contains voids. These voids are potential interstitial sites that allow zircon to include a variety of trace elements and REE (Hoskin and Schaltegger, 2003), which is reflected in its empirical formula $Zr_{0.9}Hf_{0.05}REE_{0.05}SiO_4$. This structure is responsible for giving zircon a hardness of 7.5 and a density of $\rho = 4.66$ g/cm^3 (Harley and Kelly 2007), which is relatively high compared to other common minerals like quartz ($\rho = 2.65$ g/cm^3), apatite ($\rho = 3.1$-3.2 g/cm^3), and garnet ($\rho = 3.5$-4.3 g/cm^3).

Zr^{4+} in zircon can be substituted with tetravalent cations of U, Th, and to a lesser extent Sm due to similar ionic radii. This substitution, assuring high concentrations of U (avg. 1330 ppm) and Th (avg. 630 ppm) (Ahrens, 1965), paired with the assumption of lack of initial He in zircon make up the foundation of (U-Th)/He dating. The decay series of radioactive ^{238}U, ^{235}U, and ^{232}Th to ^{206}Pb, ^{207}Pb, and ^{208}Pb result in 6-8 alpha particles/He nuclei being ejected (Fig. 3.1) (Peyton and Carrapa, 2013). At high temperatures, He diffuses out of U- and Th-bearing crystals, but at certain temperatures, called the closure temperature, He is trapped

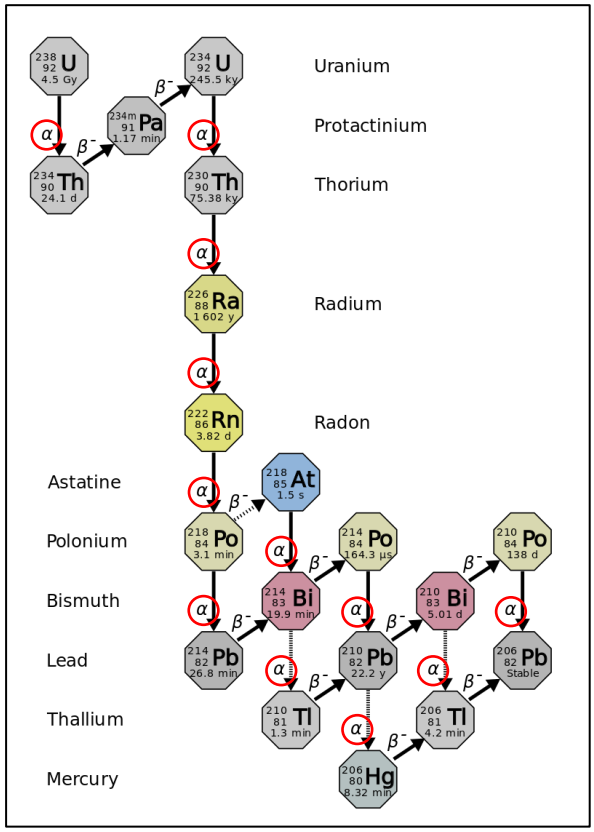

Figure 3.1 - The decay series of ^{238}U to ^{206}Pb, showing the release of alpha and beta particles.

within the crystal. For zircon, this temperature is 170-190 ºC (Reiners et al., 2004), but can vary depending on cooling rate and radiation damage where higher values result in higher closing temperatures (Schuster et al., 2006). The area between the temperatures of full He-loss and full He-retention is the partial retention zone (PRZ) where only part of the He is retained, and this temperature range is 130-200 ºC (Wolfe and Stockli, 2010). Since zircons do not initially contain any He, measuring the amount of trapped He relative to the amount of U, Th, and Sm in zircons can determine when the rock cooled below 130-200 ºC. The accumulation of He is used together with U, Th and Sm concentrations to calculate an age using the decay equation below, with decay constants of λ_{238} = 1.55125 x 10^{-10}/year, λ_{235} = 9.8485 x10^{-10}/year, λ_{232} = 4.948 x 10^{-11}/year, and λ_{147} = 6.539 x 10^{-12}/year, and t = time in years since the system closed (Zeitler, 2014).

$$^{4}\mathrm{He} = 8 \cdot {}^{238}\mathrm{U} \cdot \left(e^{\lambda_{238} t} - 1\right) + 7 \cdot {}^{235}\mathrm{U} \cdot \left(e^{\lambda_{235} t} - 1\right) + 6 \cdot {}^{232}\mathrm{Th} \cdot \left(e^{\lambda_{232} t} - 1\right) + 1 \cdot {}^{147}\mathrm{Sm} \cdot \left(e^{\lambda_{147} t} - 1\right)$$

3.2 (U-Th)/He Analysis

The (U-Th)/He technique of dating was not widely used until Zeitler et al. (1987)'s paper on apatite-He dating (AHe) sparked newfound interest. Farley et al. (1996) and Wolf et al. (1996) further developed the methodology and how to interpret results, using apatite. Apatite is often used as it has the lowest closure temperature (~ 70 ºC). He-dating on zircon was first conducted by Reiners et al. (2002) and proved to be successful as a thermochronometer. As this method records cooling temperatures, it is very useful for calculations of cooling and exhumation, and therefore to determine thermal histories. (Farley et al., 1996). There is no other method that covers this upper crustal temperature regime. The analysis involves degassing the zircon grain for He by heating it with a laser. The He content is then measured before the grain is dissolved in acid. The solution is then measured for U-Th-Sm content using Inductively Coupled Plasma Mass Spectrometry (ICP-MS) which atomizes the solution and allows for U, Th, and Sm to be detected. Sm is not as abundant in zircon as it is in apatite, contributing with very small amounts of He and is therefore sometimes not included.

One of the major challenges using this technique, was highlighted by Farley et al. (1996) who found that as He is ejected it migrates between 10-30 µm, which is referred to as the stopping distance. A more recent study by Ketchman et al. (2011) found that the stopping distance of He for ^{238}U, ^{235}U, and ^{232}Th in zircon are 15.55 µm, 18.05 µm and 18.43 µm

respectively. Depending on grain size and shape, He particles can be ejected out of the crystal or gained through implantation from adjacent grains called “bad neighbors” (Fig. 3.2). This results in a depletion or accumulation of He, which in turn yields ages too young or too old. Removing 20 μm of the crystal rim before analyzing can prevent this over- or underestimation as this is the area that can potentially experience He- gain or loss.

Other possible sources of error are inclusions rich in U and Th, and zonation. Hourigan et al. (2005) found that zonation with U- and Th-enriched cores yielded ages too old, while enriched rims yielded ages too young. With high contents of U and Th, radiation damage/metamictization can take place, which affects the diffusion of He by trapping it and increases the closure temperature, thereby affecting the ages (Schuster et al., 2006).

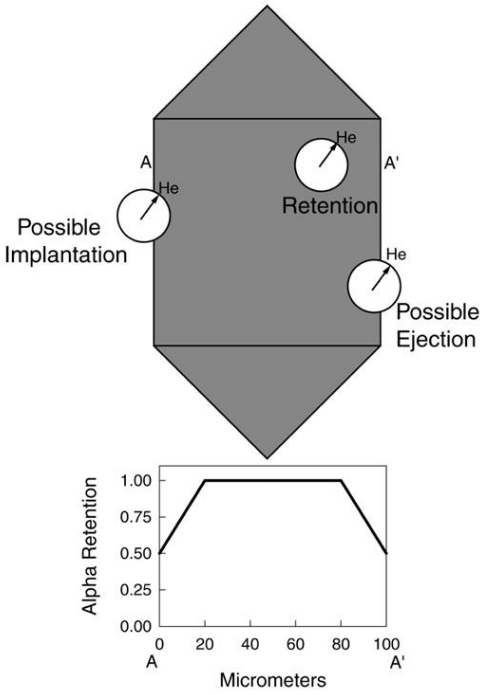

Figure 3.2 - Migration of He in a zircon crystal. He can implant the crystal by having U- and Th-rich "bad neighbors", or it can be ejected out if it is too close to the rim. He has a stopping distance of about 15-18 μm (radius of circle). Cutting away 20 μm of the rim ensures that there is no additional He or lack thereof. The lower graph shows how much He is retained within the crystal. The outer 20 μm only contains 50% He. Figure from Farley (2002).

4 Methods

4.1 Mapping and Sampling

The field areas are shown in Fig. 4.1 and include both eastern and central Elba. During the two-week GEOV252 field course run by the University of Bergen, standard outcrop mapping was completed for parts of eastern Elba. As my fellow students returned to Norway, I stayed behind for one more week to finish the remaining field work. All exposed sections of the APM were walked and studied in detail. Structural measurements were taken for both planar and linear fabrics and later plotted in Stereonet 10 (R. W. Allmendinger).

While mapping, we tried to cover all the outcrops as representative as possible which lead to five thin section samples being collected from both eastern and central Elba (Fig. 4.1). This was done to enable a more detailed petrographic description of the various textures and minerals. The thin sections were later prepared at the University of Bergen.

Six samples were collected for ZHe thermochronology from localities spread throughout the unit (Table 3 and Fig. 4.1) Sampling was based on lithology, where sandier and siltier rocks were preferred as previously collected samples, rich in sand and silt, have shown to contain an abundance of zircon grains (Jacobs et al., 2018). Five of the samples come from eastern Elba and one sample is from Felciaio Beach. The samples were crushed into cobbles at the outcrop and placed in sample bags that were properly sealed with tape to prevent contamination. The samples were then stored at the University of Bergen to await further preparation.

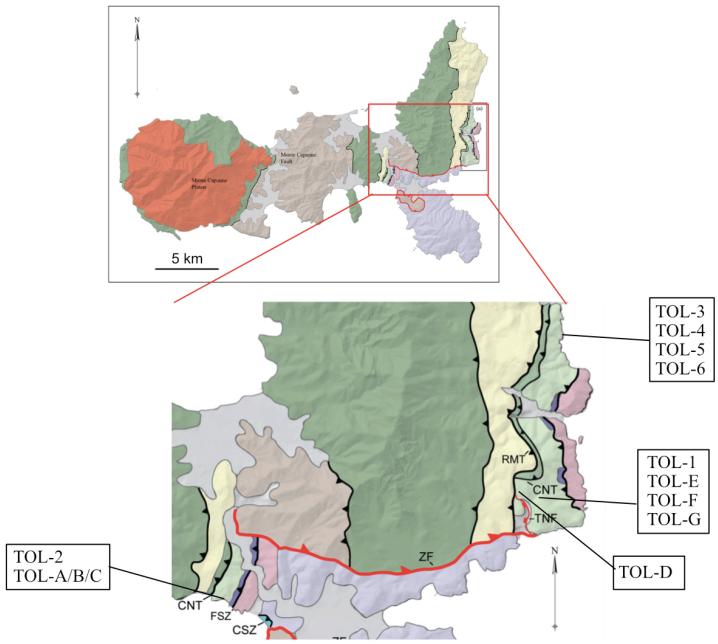

Figure 4.1 - The enlarged map shows sampling locations for thermochronology (labeled TOL followed by numbers) and thin section (TOL followed by letters). TOL-A/B/C are three thin sections from the same sample. Legend is the same as Fig. 1.1B. **CNT** – Capo Norsi Thrust, **FSZ** – Felciaio Shear Zone, **CSZ** – Calanchiole Shear zone, **ZF** – Zuccale Fault, TNF – Terra Nera Fault. Modified after Mazzarini et al. (2011), Musumeci and Vaselli (2012), and Principi (2015) in Ryan (2017)

Table 3 - Sample name, lithology, location, and GPS-coordinates for all the samples analyzed by (U-Th)/He dating on zircon.

Sample	Lithology	Location	GPS-coordinates
TOL-1	Sandy metasiltstone	Capo d'Arco Road	42°78'07'' 10°42'10''
TOL-2	Sandy metasiltstone	Felciaio Beach	42°76'30'' 10°34'80''
TOL-3	Sandy metasiltstone	Rio Marina Coast	42°80'34'' 10°43'12''
TOL-4	Calc-schist	Rio Marina Coast	42°80'65'10°42'83''
TOL-5	Phyllite	Rio Marina Coast	42°80'47'' 10°42'81''
TOL-6	Phyllite	Rio Marina Coast	42°80'44'' 10°42'79''

4.2 (U-Th)/He Thermochronology

4.2.1 Sample Preparation

Crushing and Mineral Separation

Crushing and mineral separation were carried out at the University of Bergen. The six samples were one by one crushed to pebbles, using a sledgehammer on the plastic bags they were contained in. During crushing only one sample was in the lab at a time. The plastic bags were regularly changed as they ripped. Manual crushing was done rather than using the jaw crusher, to further minimize the risk of cross-contamination. The crushed pebbles (1-3 cm) were further crushed in the Fritsch Pulverisette 13 disc mill (Fig. 4.2A) until they were roughly 315 μm. A 315 μm vibrating sieve removed the larger grains, which were put through the disc mill one to two more times and then sieved again. Further sorting was done to the <315 μm grains on the Holman-Wilfey shaking table (Fig. 4.2B), separating light minerals and other fine particles like clay from the heavier minerals like zircon. The first three fractions (out of five) were dried and packed, but only the heaviest fraction was put through magnetic separation.

A hand-held magnet was first used on the first fraction of all the six samples to remove the most magnetic minerals. Once they were out, the Franz Magnetic Separator (Fig. 4.2C) was used with currents of 0.5 mA, 0.1 mA, and 1.2 mA while having a forward and sideways tilt of 15°. This removes weakly ferromagnetic minerals like hematite, which is abundant on Elba. The non-magnetic grains from the 1.2 mA fraction were dropped in the heavy-liquid LST (Low toxicity Sodium heteropolytungstates dissolved in water; $\rho = 2.8$ g/cm^3) to remove quartz and feldspars (Fig. 4.2D). The sink of this fraction was rinsed with deionized water to prevent the LST from binding the grains together due to its rapid crystallization. When fully rinsed, they were packed to dry overnight. Once dry, the final step was to put them through the second heavy-liquid, DIM (Di- Iodomethanedensity; $\rho = 3.1$ g/cm^3) to remove apatite from zircon (Fig. 4.2E). The final batch of grains extracted from the DIM were rinsed thoroughly with acetone,

then packed and put away to dry overnight. Before sending them to the University of Göttingen, Germany for (U-Th)/He analysis, they were checked for zircons in a light microscope. Only TOL-5 and TOL-6 yielded enough zircons to be sent to Göttingen for zircon picking and (U-Th)/He analysis. This can be due to errors during mineral separation, or simply that there were no zircons in the samples.

Zircon Picking and Imaging

At the University of Göttingen, a standard petrographic microscope was used for picking zircons with a good shape, color, and size. A perfect zircon is large (75-150 µm tetragonal prism width), euhedral, whole, clear, and inclusion-free (Reiners, 2005). The particular zircons of interest were the Oligocene zircons used for U-Pb dating in Jacobs et al. (2018), so the selection was based on a guess of resemblance. A total of seven zircons were picked from the two samples. These were then checked in PPL and XPL to look for cracks or inclusions which can be a source of radiation damage. All seven grains were then photographed to determine their actual dimensions before being packed in the Pt capsule to prepare for the (U-Th)/He analysis described in the following section.

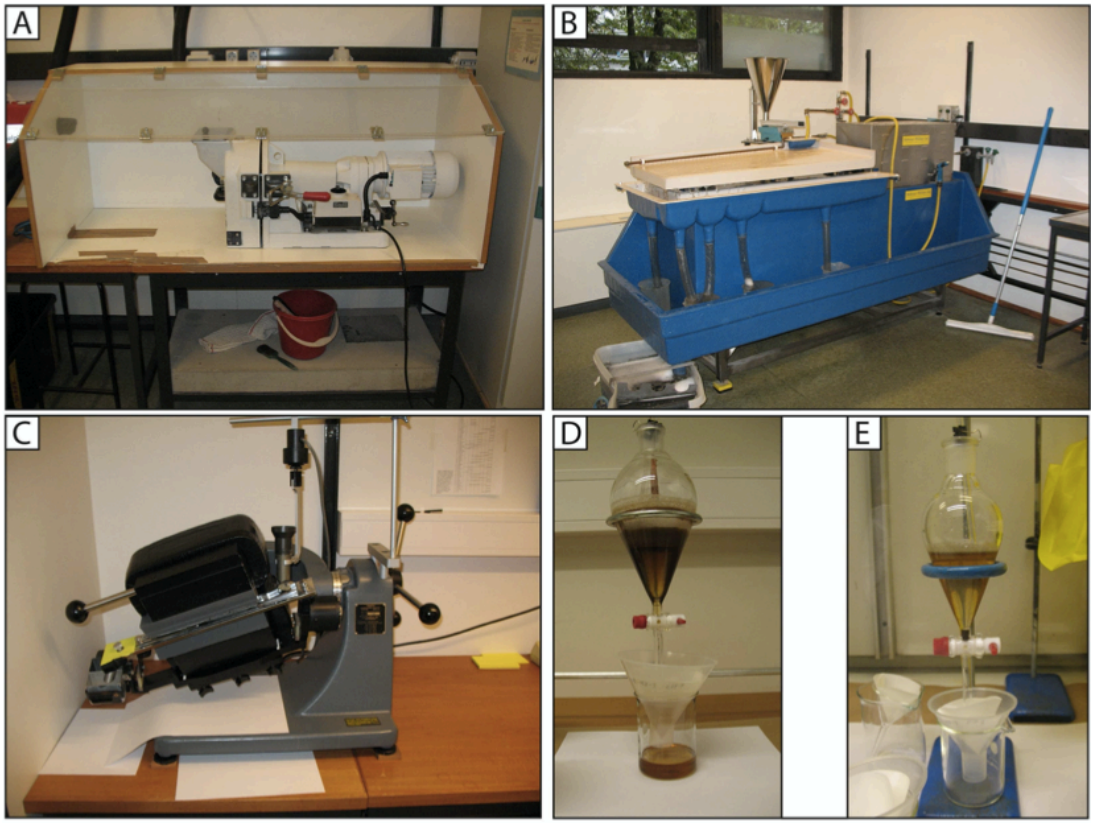

Figure 4.2 - The various instruments and tools used, in order from A-E, for mineral separation at the University of Bergen. A. Fritsch Pulverisette 13 discmill. B: Holman-Wilfey shaking table, showing the five fractions. C: Frantz Magnetic Separator. D: LST heavy-liquid. E: DIM heavy-liquid. Images provided by Johannes Wiest.

4.2.2 (U-Th)/He Analysis

The analytical methods follow the standard procedures outlined by the low-temperature geochronology lab at the University of Göttingen, based on the work of Zeitler et al. (1987) and Farley et al. (1996), and will be summarized briefly. The zircon grains were each carefully placed in a 1 mm^2 Pt capsule. This method of packing the grain in foil (usually Pt or Nd) prior to heating was developed by House et al. (2000) to prevent volatilization and loss of U while ensuring uniform heating. The He extraction was done by heating the capsule with a laser to 1300 ºC for one hour, which results in >99% of the He being extracted (Tagami et al., 2003). A re-extraction might be carried out if the crystal did not react to the usual degassing procedure as expected due to for example inclusions or very large grain size. The degassed crystal was carefully removed from the Pt capsule and dropped in a HF - HNO_3 acid mix in a sealed Teflon vial. This vial was placed in a larger Teflon bomb that contained the same acid mix and kept at 220 ºC for six days. Finally, the dissolved zircon solution was analyzed by a Perkin Elmer Elan DRC II ICP-MS.

4.2.3 Data Processing

Due to the possible errors described in 3.2, there are uncertainties, usually from the properties of the dated zircon, that need to be corrected. If an uncertainty is too large, they are usually left out of the dataset. Any imperfections in crystal morphology are noted as these often have an impact on He diffusion. Ejection correction (Ft) is defined as the total amount of He retained in the crystal (1 - Ft = He), referring to the ejection of He close to the rims. This Ft factor is used to correct ages by dividing the measured age by the Ft factor (Farley et al., 1996). The Ft factor is usually less for smaller grains reflecting the smaller area for He retainment. The uncertainty for Ft is calculated by the following equation: errFt = 15 x (1 - Ft). The first He re-extracts are also considered but are less diagnostic of error as zircons often need several re-extracts. Effective uranium concentration (eU) is also calculated ([U] + 0.235[Th]) to account for any radiation damage that might increase the closure temperature of He (Schuster et al., 2006). The final ages are given in Ma with an error of 2σ, which includes the analytical- and Ft uncertainty.

4.3 Thin Sections and SEM

Several 30 µm thick petrographic thin sections were cut from different parts of the samples and polished at the University of Bergen. Optical images were obtained using an iPhone 11 and a Nikon LV100 POL polarizing microscope equipped with a DS-Fi1 color camera (5.24-megapixel resolution) coupled to NIS-Elements BR 2.30 software. In addition to capturing photos of mineral assemblages and microstructures, the Nikon camera was used make mosaics to better prepare for SEM. The SEM is of the type ZEISS Supra 55VP (Fig. 4.3) with the backscatter detector used for imaging, and the EDS (Energy-dispersive X-ray spectroscopy) detectors used for measurements. Both EDS element maps and EDS spectrums were generated.

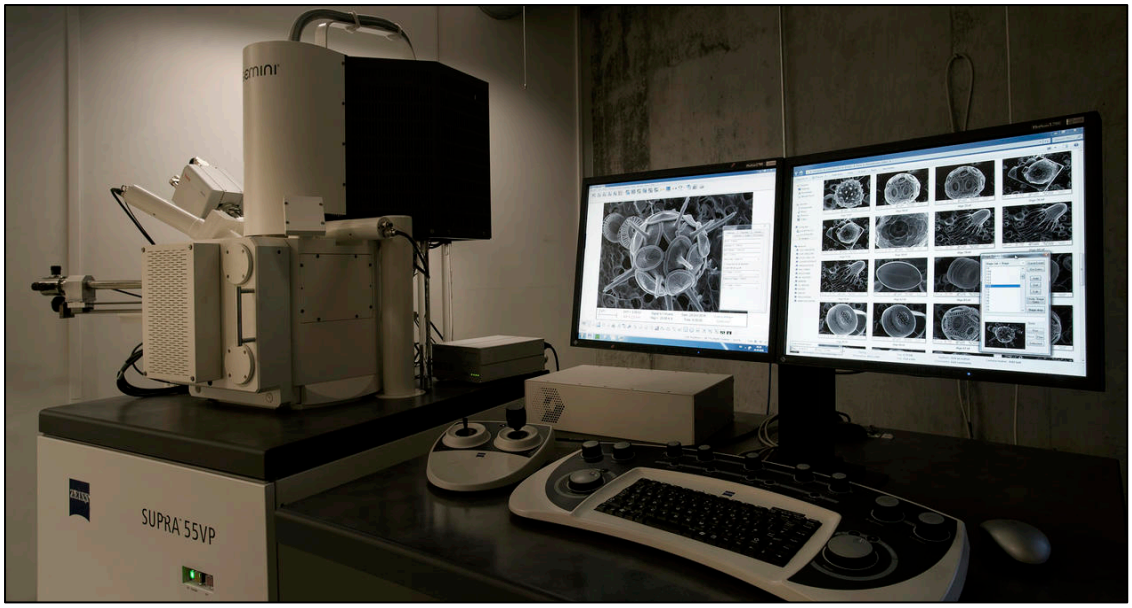

Figure 4.3 - The SEM ZEISS Supra 55VP located at the University of Bergen. Image provided by Irene Heggstad.

5 Results

5.1 Mapping

The results from the mapping are presented in a geological map of eastern Elba and includes outcrops, boundaries/faults, and structural data (Fig. 5.1). 14 outcrops were described during mapping and is summarized in Appendix I. The study is based on 40-50 outcrops, but only 14 were presented in more detail, as many of the outcrops did not provide anything other than structural measurements. The locations for the described outcrops are shown in more detailed maps found in Appendix II. The maps in Appendix II are of eastern and central Elba and were generated by combining the four maps made by the four individual mapping groups in the GEOV252 field course. An accompanying cross-section showing the main features is also provided in Appendix II but excludes the internal structures of the APM as this will be discussed in the next chapter.

The APM stretches from the southern end of Rio Marina straight down to the southern coast through a landscape of rolling hills. A smaller section with great exposure can also be found around Felciaio Beach. Eastern Elba has received majority of the attention in previous studies when describing the unit, but the Felciaio section contains much of interest. The APM is heterogeneous throughout Elba, having a variety of mineral contents, calc-schist lenses, lineations, and folds but generally share a dip-direction to the west, apart from local variations in the Capo d'Arco area, where the foliation dips to the W, NE, and SW.

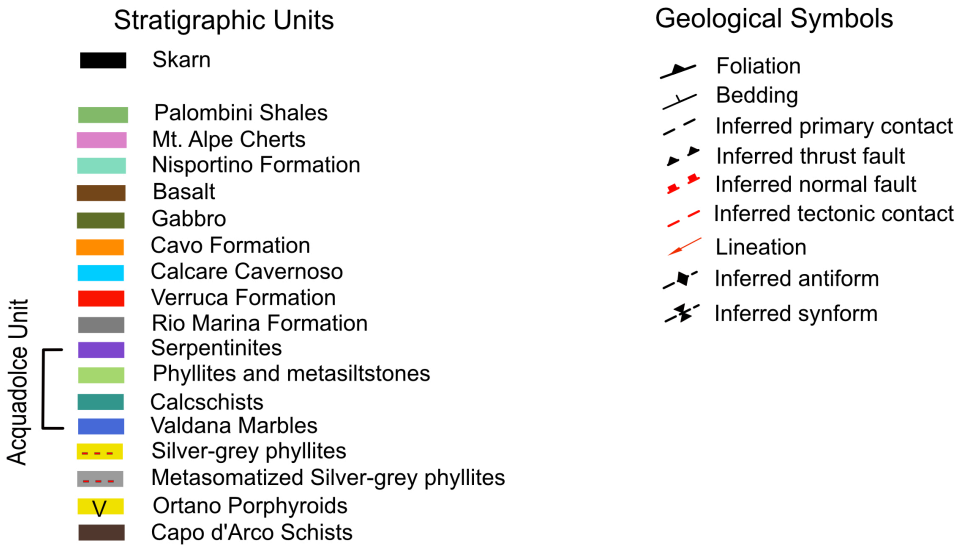

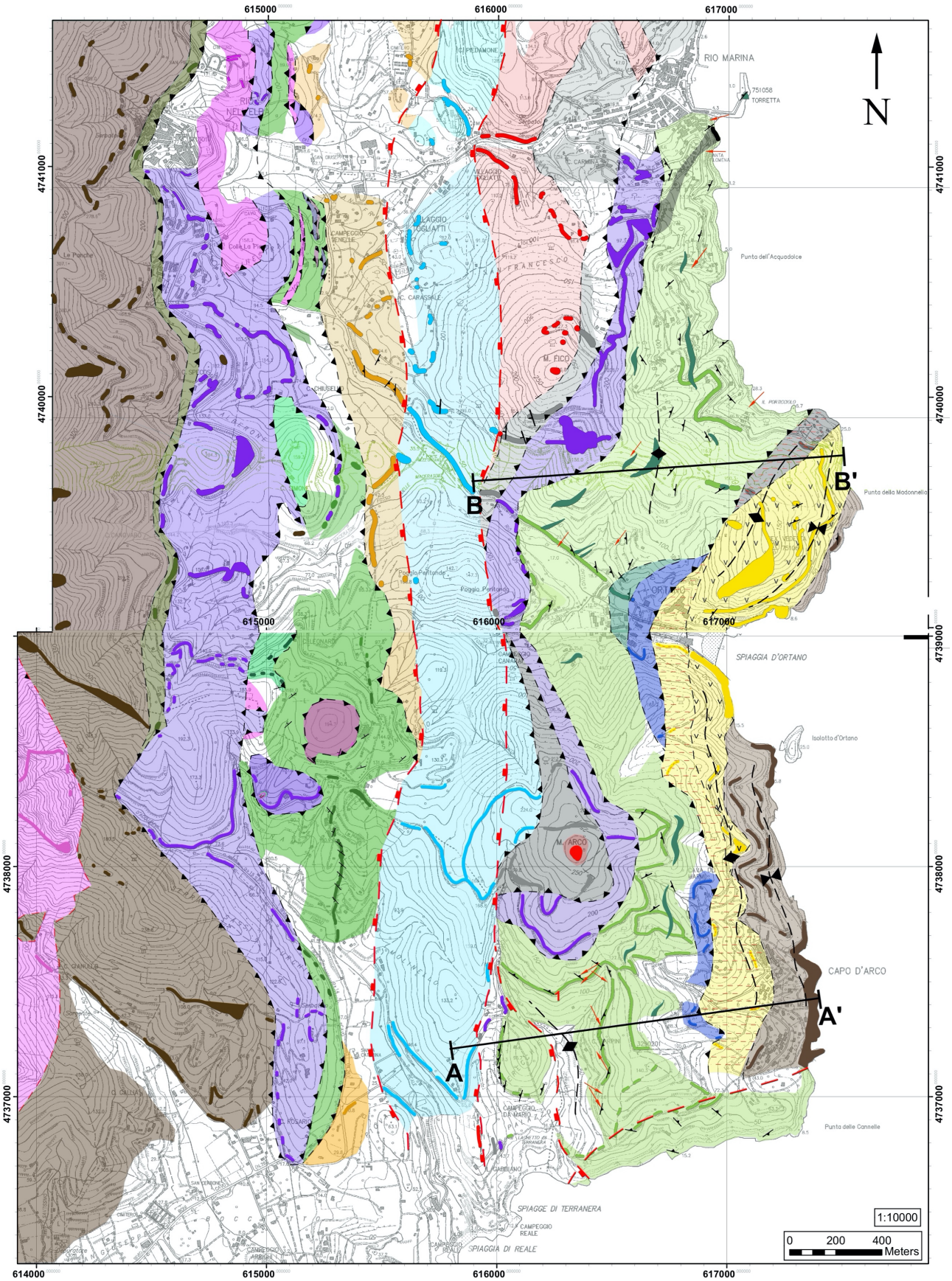

Figure 5.1 – A geological map of eastern Elba, showing the main lithological units and structural measurements. The Acquadolce Phyllites and Metasiltstones are shown in light green with dark green lenses representing calc-schist. The two cross-sections A-A' and B-B' are part of the discussion in Chapter 6. A larger version of the map, including outcrop- and sampling localities, is shown in Appendix II.

5.2 Petrography

Phyllites and metasiltstones are primarily composed of fine-grained quartz and white mica, to which there is no exception here. The unit is quite different in appearance in the two working areas (eastern Elba and Felciaio Beach). The rocks in eastern Elba have a grey and flaky appearance (Fig. 5.2A), sometimes found with elongated white streaks (Fig. 5.2B) that fade in and out laterally. Quartz clasts and veins are usually found in the same sections that contain these white streaks. Sheared clasts and isoclinal folds are especially abundant along Capo d'Arco Road. Local regions of the APM show signs of contact metamorphism, hosting andalusite and hedenbergite (skarn). The andalusite appears to be clustered within thin layers of the phyllites (Fig. 5.2A). In the northern part of the unit, along the Rio Marina coastline, the rocks are more graphitic and contain more, often larger calc-schist lenses (Fig. 5.2C) compared to the Capo d'Arco and Ortano area.

The Phyllites and Metasiltstones at Felciaio Beach (Fig. 5.2D) are part of the rocks left behind in central Elba, as opposed to having been translated east by the Zuccale Fault. This section stands out from the rest of the unit in eastern Elba, with more obvious layering that are folded very differently. In addition to the common minerals, pyrite is often observed in hand-specimens.

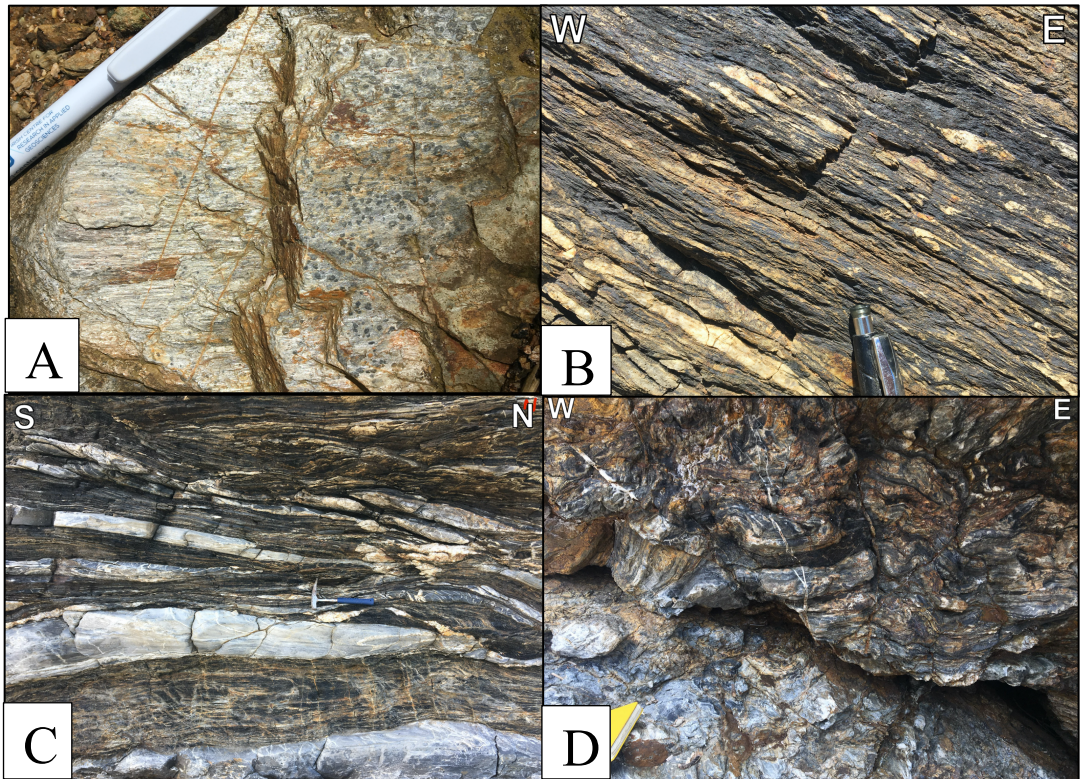

Figure 5.2 - The many looks of the Acquadolce Phyllites and Metasiltstones. A. Typical flaky, shiny phyllite with contact metamorphic minerals disappearing and reappearing within thin layers, found in Ortano. B: Foliated PM in Capo d'Arco, showing elongated streaks and isoclinal folds C. Graphitic PM with calc-lenses in Rio Marina. D. Folded layers at Felciaio Beach.

Rock- and mineral compositions indicate what environment the rock formed in and what P-T conditions it endured during subduction and deformation. To get a more detailed picture of the composition and microstructures, seven thin sections were made from the five samples (Fig. 5.3). However, only A, E, and G will be mentioned as the others did not provide sufficient information.

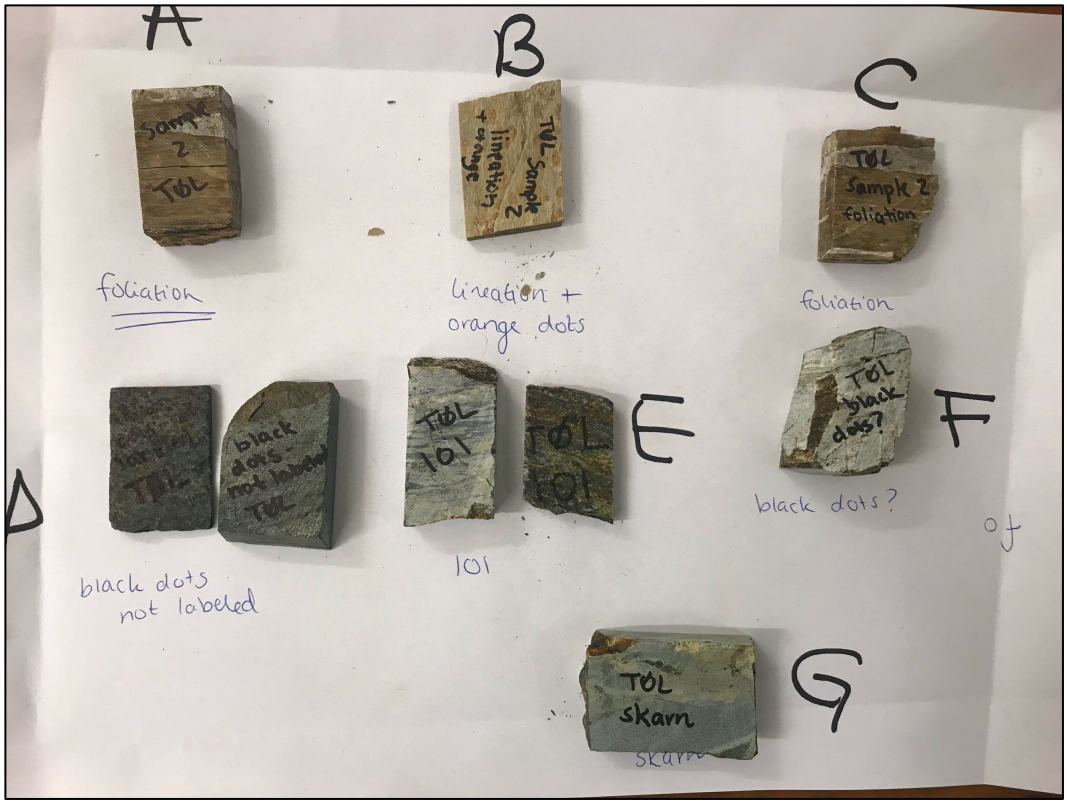

Figure 5.3 - The seven thin section samples before being grinded and polished. A-C are from the same sample, and A proved to be sufficient enough to exclude separate descriptions for B and C. D did not show any structures or obvious minerals and therefore not useful to this study.

The overall composition of the thin sections is dominated by banded quartz and mica, sometimes intertwined with graphite, clinopyroxene, and calcite. The various accessory minerals include biotite, epidote, cordierite, garnet, chlorite (Fig. 5.4). The dark graphitic bands suggest the presence of organic material in the protolith and work well as markers for the microstructures (Fig. 5.4A). Biotite is often intermingled in the muscovite and graphitic bands, while the calcite is found in the quartz bands.

Small round garnets (Fig. 5.4C) are abundant in the sample collected from Felciaio Beach and have a dirty or clear appearance and is usually cracked. They are concentrated in the mica layers, and rarely observed within the quartz layers (Fig. 5.5A). The SEM analyses (Fig. 5.5B and C) show that they are rich in Mn, classifying them as spessartine garnets. However, they also contained smaller amounts of Ca, indicating partial solid solution with

grossular garnet. They have overgrown the foliation, suggesting a post-kinematic origin. Garnets are rarely mentioned in the literature for the APM, and simply described as contact metamorphic garnets (Pandeli et al., 2001).

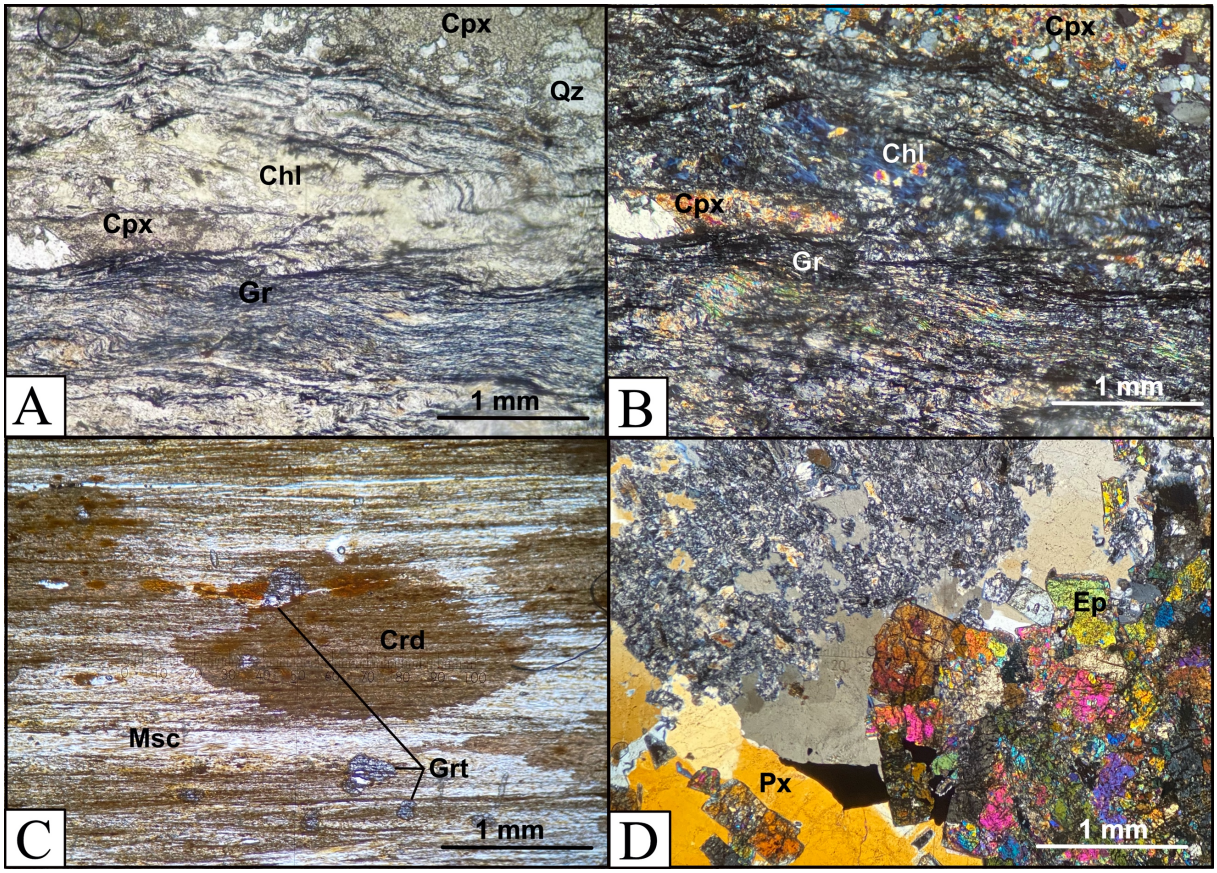

Figure 5.4 - Thin sections from the Acquadolce Phyllites and Metasiltstones. A and B: TOL-E - phyllites from the Capo d'Arco region, in PPL and XPL, showing bands of quartz and graphite, with lenses of clinopyroxene and chlorite. C: TOL-A - Spotted phyllite from Felciaio Beach, showing garnets and altered cordierite. The reddish color is probably a result of iron oxide staining. D: TOL-G - Skarn from the Capo d'Arco region, showing anhedral pyroxene and epidote. Minerals are abbreviated after Whitney and Evans (2009)

Fig. 5.4C shows a muscovite band with darker orange-brown spots. In the field, these were interpreted to be contact metamorphic minerals, and under closer inspection in the petrographic microscope, they do appear to be altered cordierite, a contact metamorphic mineral commonly found together with andalusite. The SEM analysis on these stains showed no different chemical signature to the surrounding muscovite, which is the case as cordierite gets altered to pinite (mica). Cordierite in these rocks has been mentioned in Papeschi et al. (2020) and Musemeci and Vaselli (2012) who also state that the rocks where these samples were collected (Felciaio Beach) are spotted schists rather than spotted phyllites. That would explain why this section lacks the flakiness and sheen that is characteristic of phyllites.

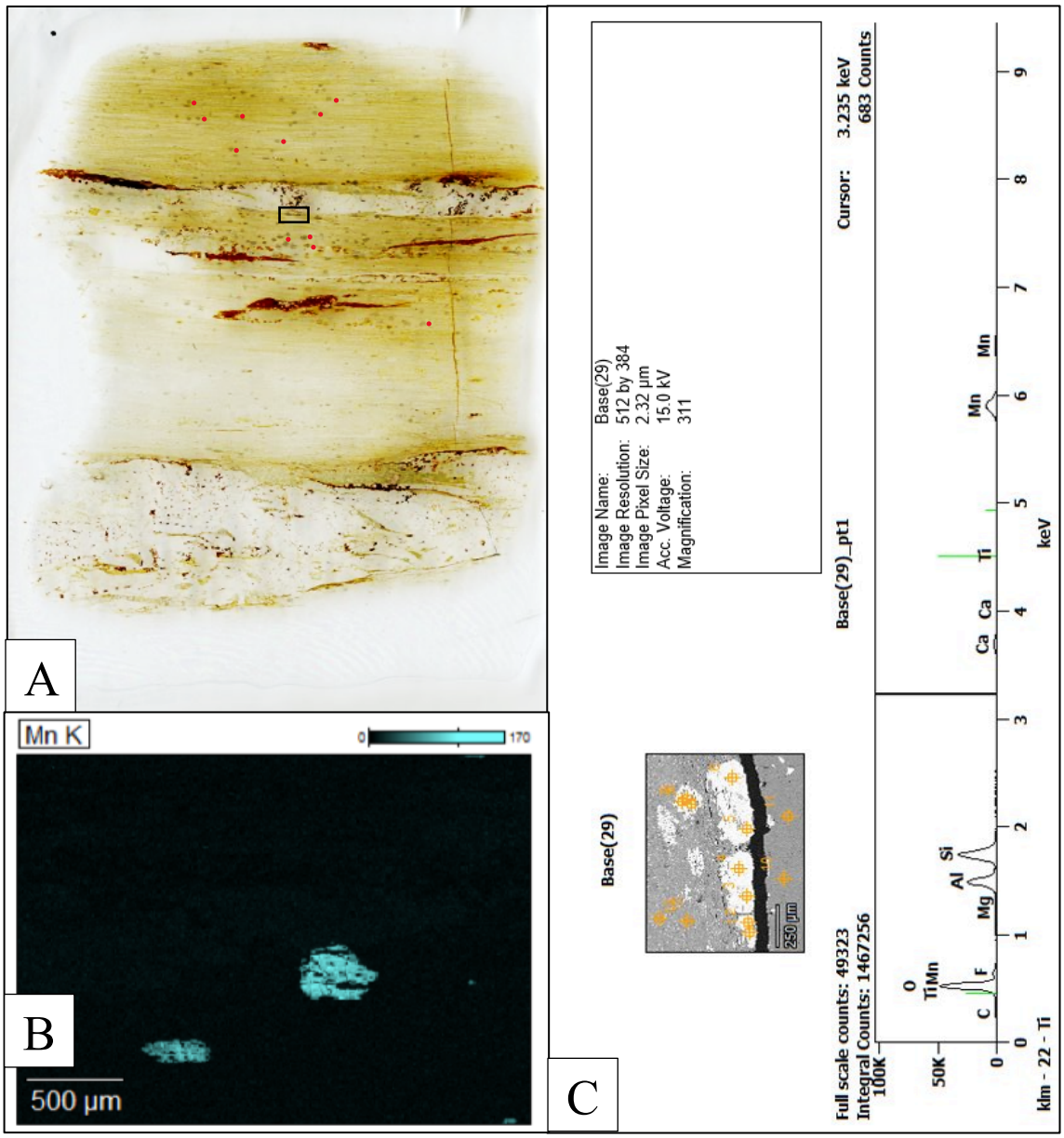

Figure 5.5 - A. TOL-A showing garnet as the small, grey spots highlighted by the adjacent red dots. The black rectangle frames the area used for one of the SEM analyses and is shown as a black and white image in C. B: Mn EDS element map of another area in TOL-A containing garnet. C: EDS spectrum showing Mn and Ca peaks. The white minerals in the black and white image are the garnets.

Clinopyroxene (cpx) is found in several of the samples from eastern Elba but is not a typical mineral for phyllite apart from in metasomatized phyllite (skarn). The cpx, most likely augite, can be found as anhedral crystals in the skarn (Fig. 5.4D), or as elongated lenses within the quartz bands (Fig. 5.4B), possibly suggesting two generations of cpx ; the anhedral cpx related to the skarn formation, and the other related to some metamorphic event seeing as it is aligned with the foliation.

Epidote shows up as apple green in PPL and funky, bright colors in XPL (Fig. 5.4D). Like cpx, epidote is most abundant in the skarn, but is also found as lenses in the more phyllitic rocks that have not been metasomatized. Glaucophane or lawsonite were not found.

5.3 Structure

Folding

Folding in the APM is present at all scales in the study area and vary greatly in style depending on location. The stereonet in Fig. 5.6 shows that the poles to the foliation plot along a great circle, suggesting the presence of a large-scale, NE-verging antiformal fold whose fold axis plunges shallowly to the NNW. The majority of the dip-directions are to the WSW, which could be explained by measuring mostly on the shallower limb, or that the fold is overturned in some areas. This is also supported by the fact that the dip is slightly steeper in the east. The fold axes measured in the field seem scattered, but two patterns emerge – (i) the fold axes in Rio Marina align somewhat on a great circle and (ii) the remaining fold axes trend moderately-shallowly to the ESE. Fold axes aligning on a great circle implies non-cylindrical folding, which fits nicely for Rio Marina being the only area where the highly non-cylindrical sheath folds (trending E-W) have been observed. The lineations trend primarily to the SW, plotting on the western limb of this possible megafold. The SE/NW lineations and the ESE fold axes are sub-parallel to the main fold axis of the larger fold, suggesting the fold axis might be non-cylindrical and undulating.

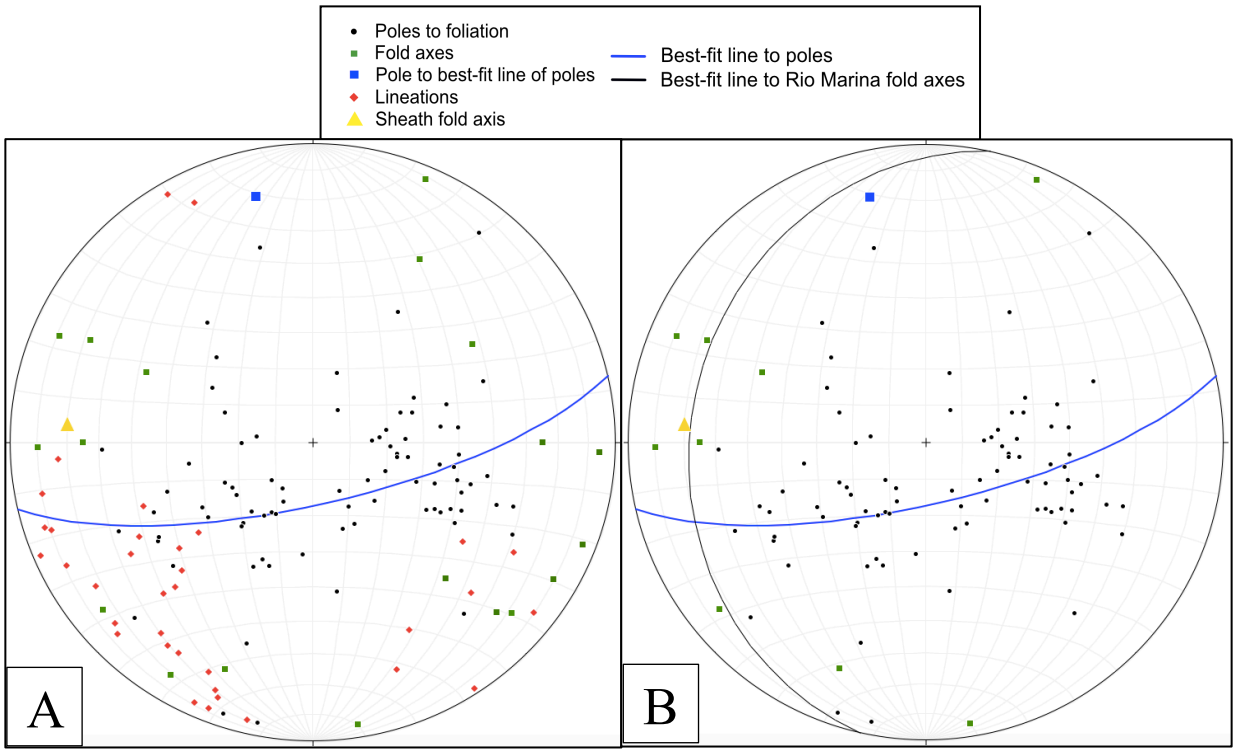

Figure 5.6 – A: Stereonet summarizing data collected from the entire working area in Elba. The poles align somewhat on a great circle indicating a fold with a fold axis trending NNW. The fold axes trend in all directions. The lineations trend SW and SE/NW. B: Stereonet showing the Rio Marina fold axes plotted on a great circle, suggesting high non-cylindrical folding in the area.

The observed folding will be described by location due to the large variations, in the following order: Capo d'Arco, Rio Marina, and Felciaio Beach. The main style of folding in the Capo d'Arco area is found as rootless, cm-scaled, tight-isoclinal, similar folds (Fig. 5.7A, B, D). In sections that are more phyllitic, the foliation undulates creating m-scaled, asymmetrical, open and upright folds or kinks. (Fig. 5.7C). The less deformed, smaller folds show mostly E-NE vergence, but some verge to the W. The W-verging folds often continue into transposed folds and might therefore not show the original vergence. The measured fold axes plunge shallowly to the ESE with a few trending to the NE.

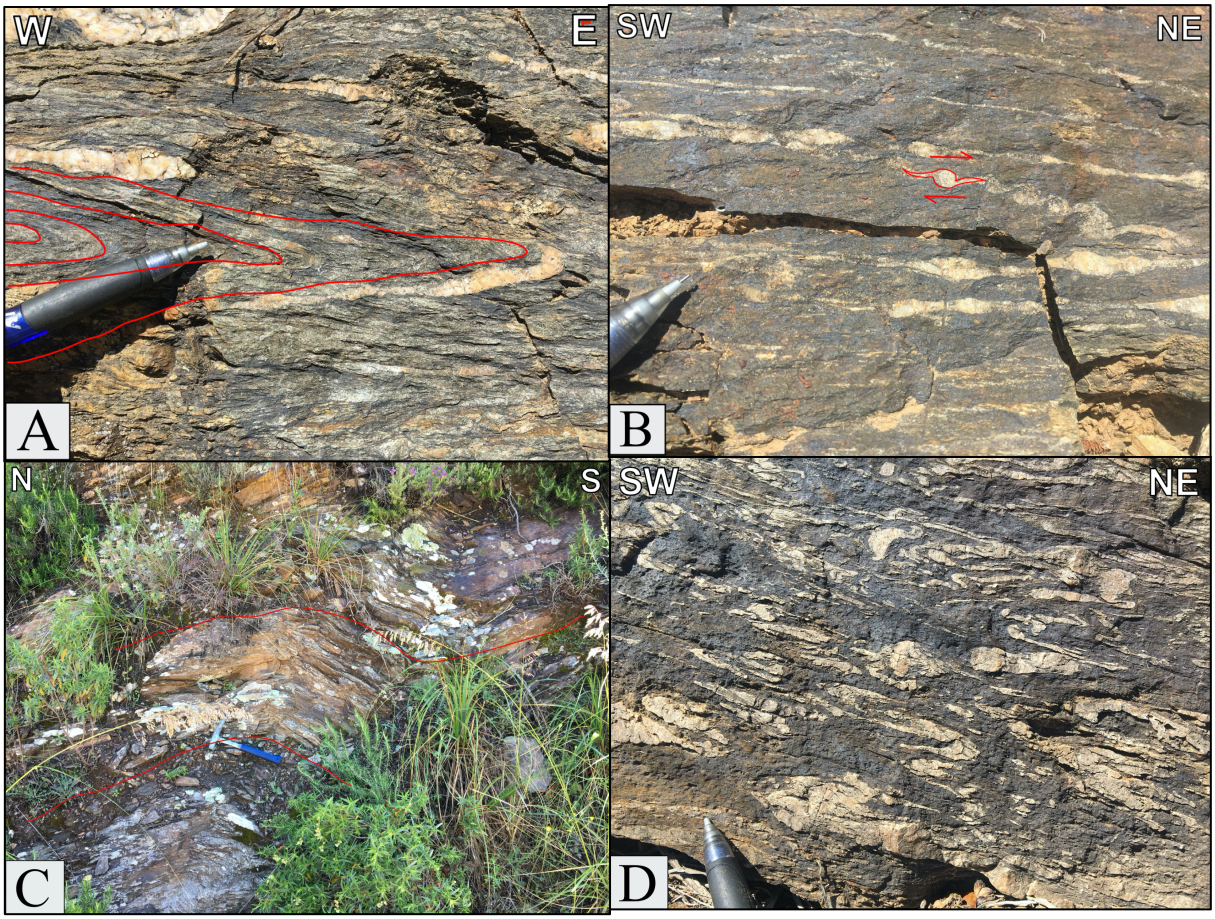

Figure 5.7 – Different styles of folding in Capo d'Arco. A: Recumbent, tight-isoclinal fold. B: In the field, the structures outlined in red were thought to be folds with varying thickness, but they are probably sheared delta clasts. C: Undulating foliation making open folds and kinks. D: Rootless, isoclinal, broken-up and pulled-apart quartz veins.

In Rio Marina, most of the folding observed is found in the large calc-schist lens by the lighthouse in Rio Marina harbor. The colorful layers form tight to isoclinal similar folds and sheath folds (Fig. 5.8). The similar folds have fold axes trending in all directions except from east. The sheaths folds are recognized only by the elongated, flattened eye shape that represents the tip of this highly non-cylindrical fold. The sheath fold's fold axis appears to trend sub-horizontally to the WNW, and measures 20º/274, but this is a rough measurement. Rough or

not, the trend corresponds with the general direction of E-W shearing in Elba. Ptygmatic folding in quartz veins were occasionally observed further south along the coast.

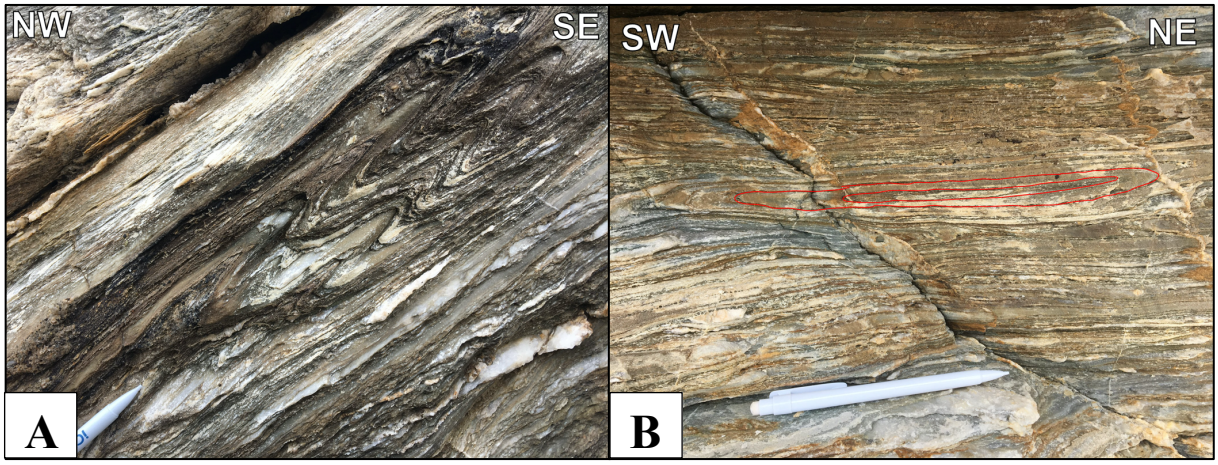

Figure 5.8 - Folding in the calc-schist lense at the lighthouse in Rio Marina. A: Similar folds in the foliation. B: Sheath fold's eye shape outlined in red.

Felciaio Beach has as mentioned a different style of folding as well as very local variations. The rocks cropping out on the sandy beach are mostly planar, getting increasingly more folded to the west. Thin quartz veins folded in a chaotic manner that protrude from the host rock is the first style encountered (Fig. 5.9). Similar to Capo d'Arco, majority of the smaller folds verge in an eastern direction, with a few verging to the W. Some sections have very strong layering which is folded concentrically and sometimes refolded (Fig. 5.10), showing a clear distinction between the competent quartz layers and incompetent finer-grained layers. This is the only place in the study area where refolding is interpreted at the meso-scale and the folds appear to be type 3 refolded folds (Fig. 5.10A and B). Parts of the outcrops are broken off and highly weathered, increasing the uncertainty about whether these are refolded folds or not.

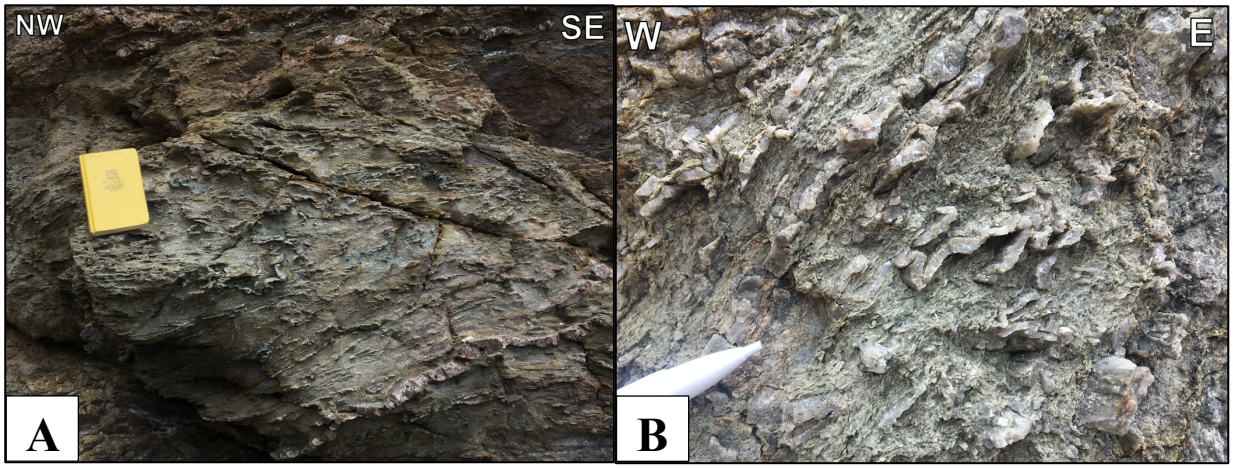

Figure 5.9 - Chaotically folded quartz veins protruding from the host rock at Felciaio Beach. B is a close up of the veins in A.

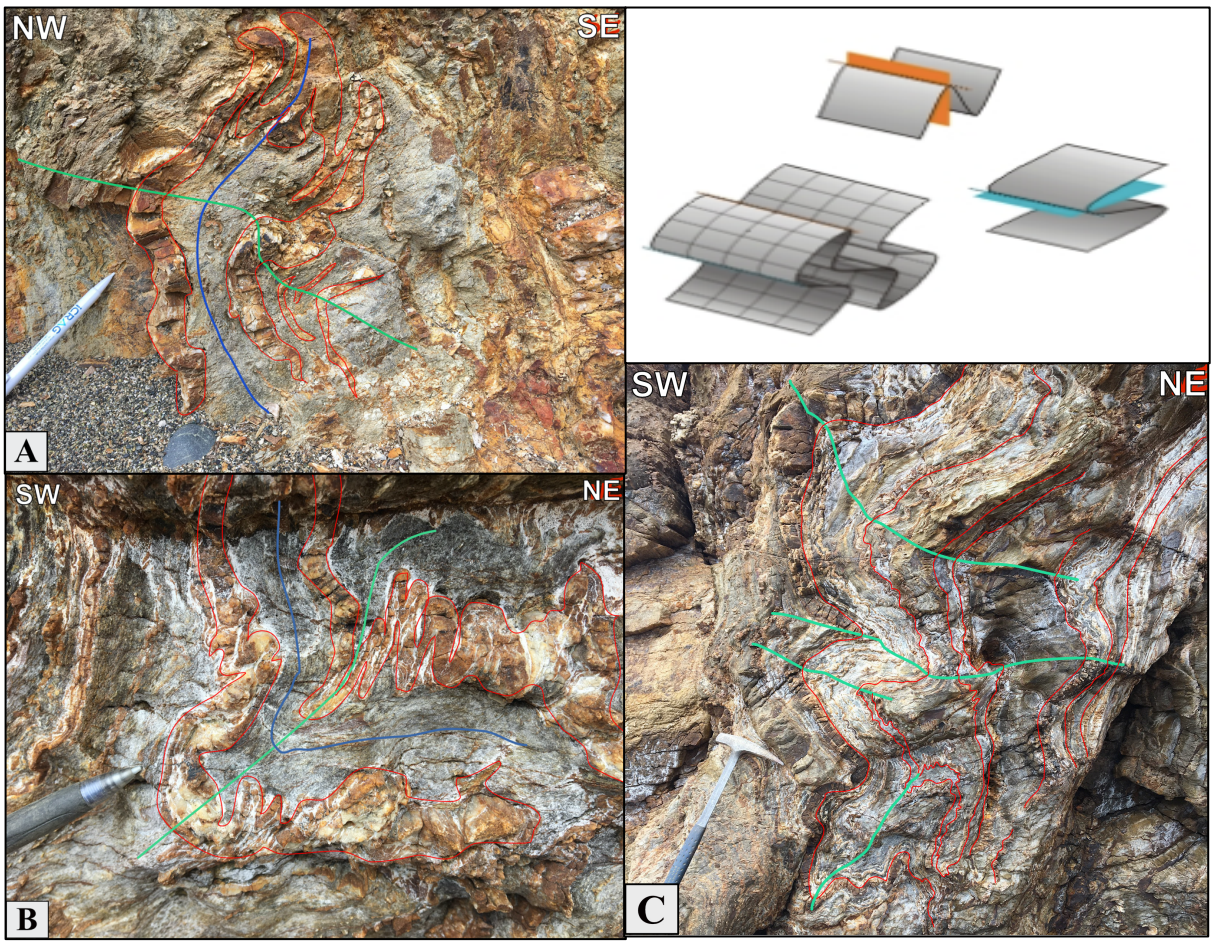

Figure 5.10 - Folds at Felciaio Beach. A and B: Refolded folds. Blue line represents the axial plane from the first generation, and the green line represents the new axial plane. C: Concentric folds outlined in red with green lines showing the fold axes. The upper-right hand sketch shows the process of how a type 3 fold forms, by combining folds that have axial planes perpendicular to one another.

Lineations

Lineations are abundant throughout both working areas and include mineral stretching lineations and possibly crenulation- and intersection lineations (Fig. 5.11). There are two main lineation directions as seen in Fig. 5.6. The majority plunge shallowly-moderately shallow to the SW, and represents the lineations measured at Rio Marina, Ortano, and Felciaio Beach. The SE/NW trending lineations reside in the Capo d'Arco area, which again is the outlier when it comes to structural homogeneity. The stretching lineations are highlighted by cordierite and rodding (Fig. 5.11A, C and D). The cordierite is elongated in the NE-SW direction, and shortened in the SE/NW direction, implying constrictional strain with the formation of an L-tectonite. Cordierite is a contact metamorphic mineral and is probably a result from contact metamorphism by the Porto Azzurro Pluton (5.9 Ma), suggesting that the stretching post-dates the intrusions.

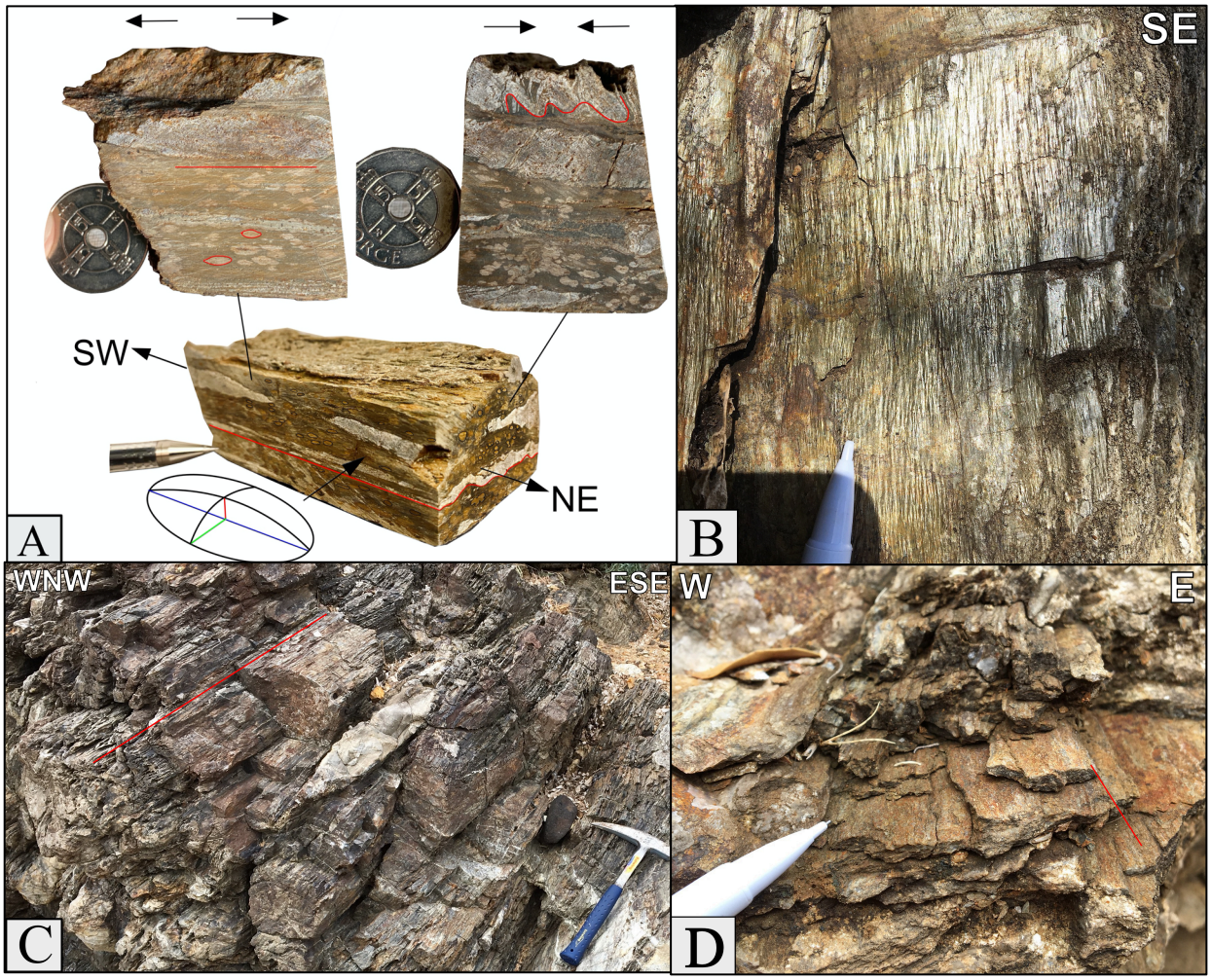

Figure 5.11 - A: Sample from Felciaio Beach, showing a stretching lineation on cordierite, elongated in the NE-SW direction, and folded quartz layers shortened in the SE-NW direction, also represented by a strain ellipsoid. B: Possibly crenulation or intersection lineations by Rio Marina coast trending SW**.** C: Rodding lineations at Felciaio Beach trending SW with an average plunge of average 13º. D. Rodding lineations trending SSE by Ortano Road.

Microstructures

Microstructures are abundant in the thin sections, and the most prominent one is crenulation cleavages. Crenulation cleavages form as an older foliation is folded, creating several microscopic folds, indicating that the rock underwent stress from two different directions (Fossen, 2016). In TOL-E, the crenulations are highlighted by the graphitic bands (Fig. 5.12A, B) and verge both left and right which is common for crenulations as they often kink. S-C' fabrics (Fig. 5.12C, D) can also be seen in the same thin section, showing a sinistral sense of shear. Unfortunately, the thin sections were not oriented so they cannot be used to determine movement direction, but high strain can be inferred as well as an extensional setting. S planes represent the curved, rotated foliation, while C′ planes are miniature shear zones within the shear zone. C' planes differ from C planes in that they are formed at a later stage during

shearing. The rocks might not appear highly deformed at first glance, but at closer inspection, the thin sections record various phases of deformation as transposed folds can be found wrapped around the crenulations (Fig. 5.12B).

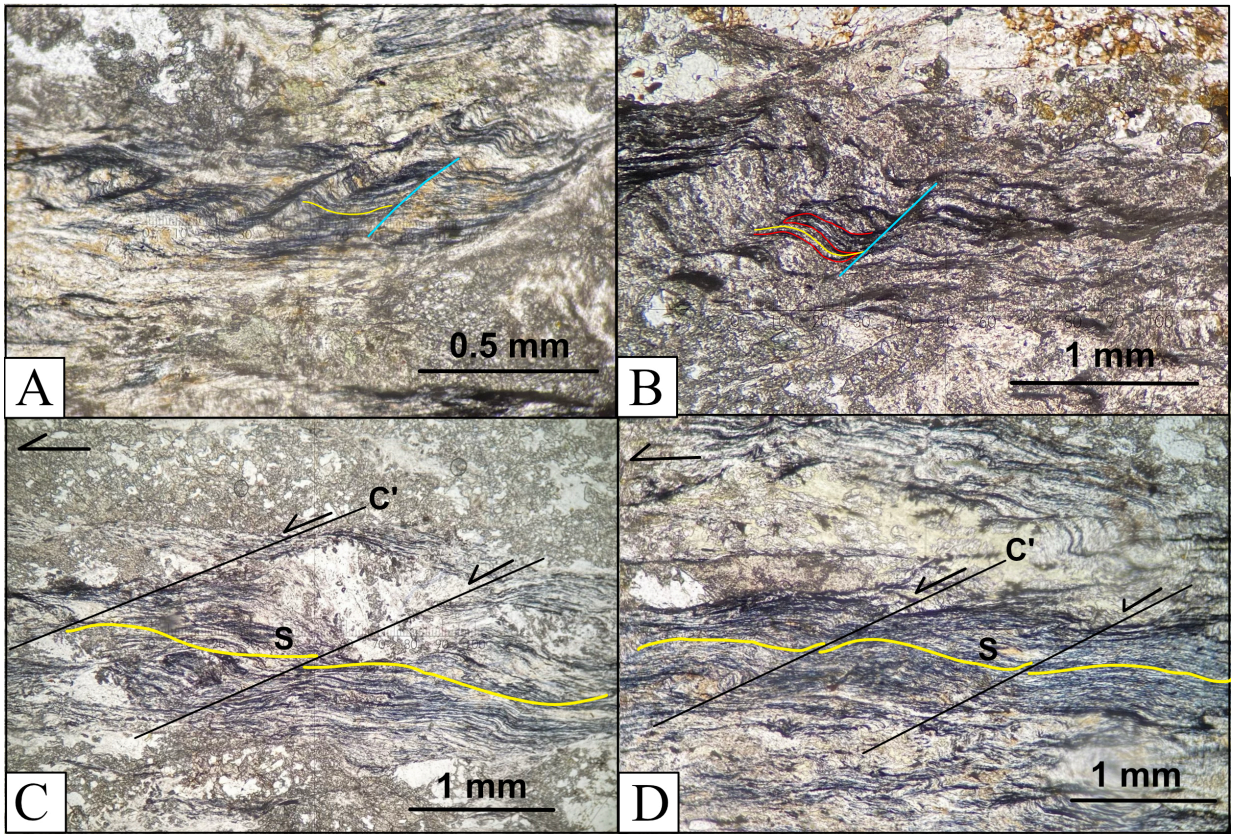

Figure 5.12 - Microstructures in TOL-E from Capo d'Arco Road highlighted by graphitic bands. A: Crenulation cleavage viewed at 10x magnification. The yellow line is the old foliation, and the blue is the newer foliation. B: Crenulation cleavage folding the older foliation together with the transposed folds, viewed at 4x magnification. The yellow line represents both the older foliation and the transposed fold's fold axis. Blue line is once again the new foliation. C and D: S-C' fabric showing a top-to-the-left movement by extensional shear bands. Viewed at 4x magnification.

Brittle deformation

Brittle deformation was observed in the form of normal faulting across the entire unit (Fig. 5.13). The faults show both TTW and TTE movement with displacement varying between tens of cm to m. They most likely relate to the two normal fault systems trending N-S and NE-SW that were mentioned in Chapter 2.3. The fault planes are characterized by either well-defined slip surfaces or fault gouges approximately 5-10 cm wide. The largest fault was observed by the sampling location of TOL-3 and has ca. 10 m exposed with the foliation showing normal drag. Collectively, the fault dips range between 30º to near vertical. Older structures, such as open folding, are crosscut by these normal faults.

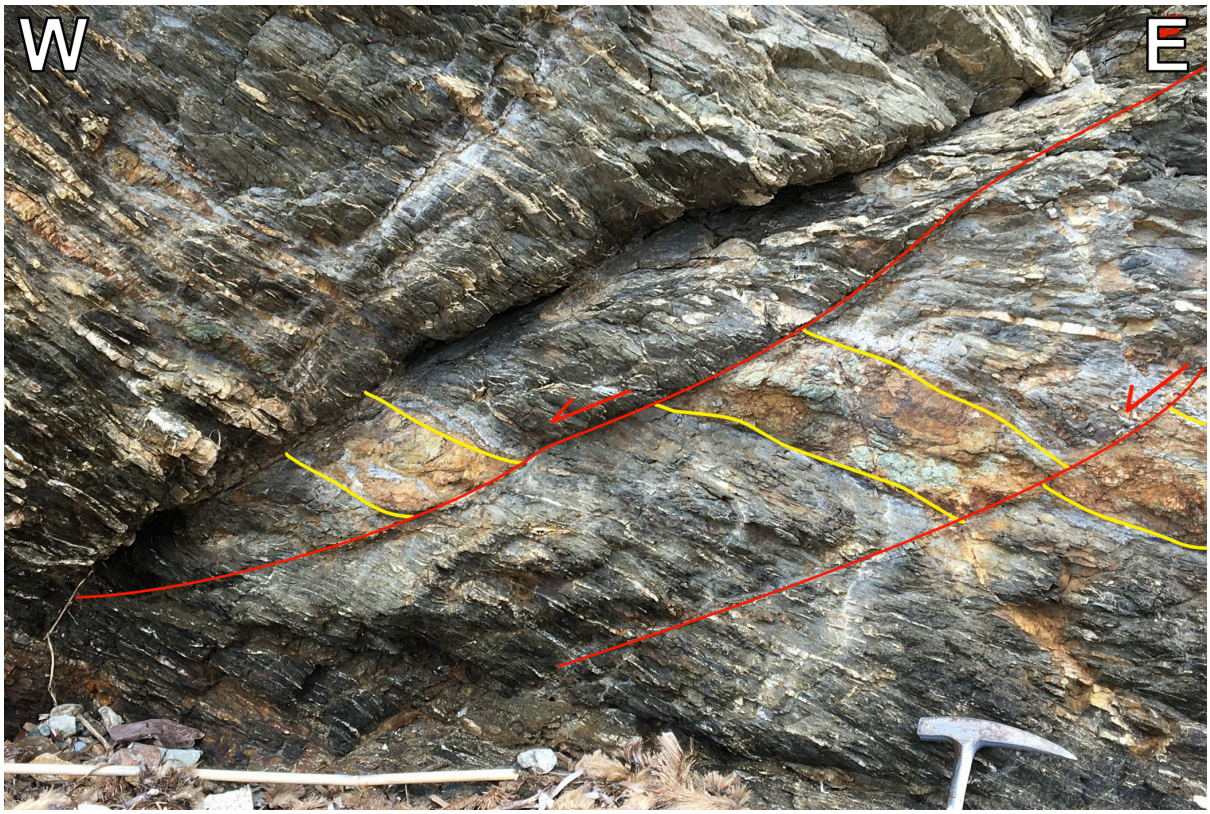

Figure 5.13 – Brittle, W-dipping faults showing normal displacement of about 20-30 cm. They are probably related to the Late Miocene-Pliocene normal faulting that took place on Elba during extension and collapse.

5.4 (U-Th)/He Analysis

Out of the six samples collected, only two yielded zircons, TOL-5 and TOL-6. The two samples were collected only a few tens of meters apart and it was quite surprising that these were the ones to contain the most zircon, as they looked the least sandy and more like proper flaky phyllites (Fig. 5.14). (U-Th)/He thermochronology of zircon from TOL-5 and TOL-6 has resulted in seven single-grain ages. The analyzed zircon grains are euhedral with spherical radii of 37-61 μm. They all have small inclusions, but none are broken (Fig. 5.15). The concentrations for U, Th, and Sm ranged between 276-1161 ppm, 25-181 ppm, and 0-12 ppm respectively. Sm is significantly lower than U and Th, which is normal for zircon and why it is not included when calculating the effective uranium concentration (eU). The eU ranges between 291-1190 ppm, averaging at 605 ppm. The correction ejection (Ft) ranges between 0.684 and 0.799 and has a positive correlation with the grain size. A He re-extraction was also completed, where five of the grains range between 0.1 and 1.2%, while the remaining two had values of 7.2% and 13.6%, the latter being the largest grain of the seven.

Figure 5.14 - The location where TOL-5 was sampled, right behind the hammer. The rocks are on the more phyllitic side rather than sandy side, and quite weathered.

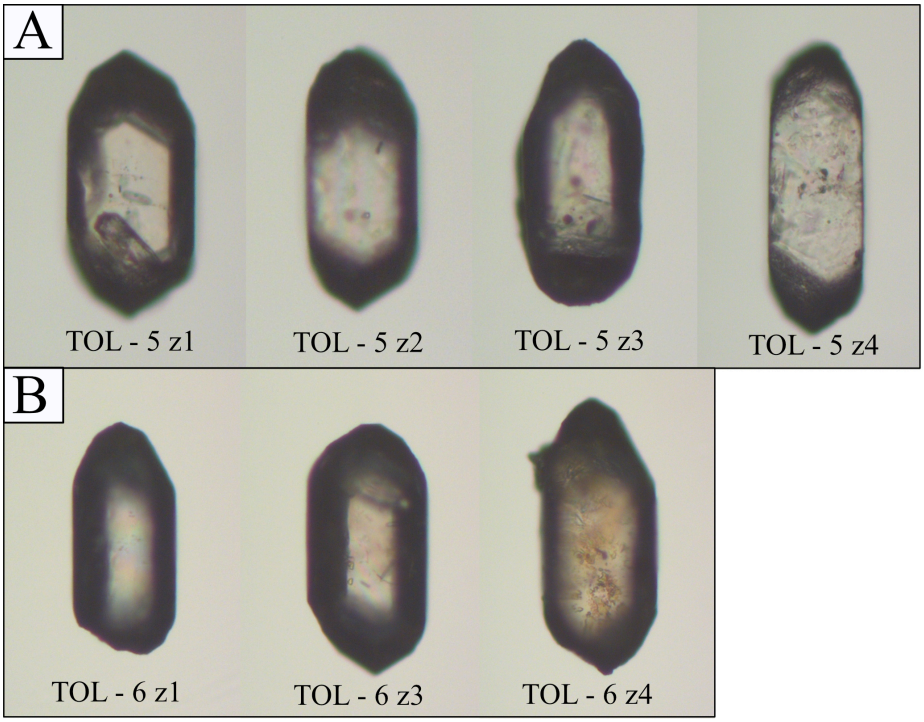

Figure 5.15 – The seven zircons used for (U-Th)/He thermochronology in this study. A: The four zircons picked from TOL – 5 have widths of 85 µm, 60 µm, 81 µm, and 76 µm (z1-z4). B: The three zircons picked from TOL – 6 have widths of 76 µm, 93 µm, and 98 µm (z1, z3, z4). All the grains are euhedral and contain small inclusions. Their mass is listed in Table 3.

The (U-Th)/He analyses of the seven grains resulted in similar ages from 5.06 Ma to 6.37 Ma, with the mean age being 5.7 Ma for TOL-5, and 5.9 Ma for TOL-6, both with an error margin of 0.3 Ma. Whether the youngest and/or oldest ages are outliers can be established to some degree by interpretation of He re-extraction, the Ft, crystal properties, and the eU. The youngest ages, 5.06 Ma (TOL–5 z4) and 5,22 Ma (TOL–6 z4), have the highest He re-extracts of 7.2% and 13.6%, while the older ages are all below 1.2%. If the value is >5% it is often excluded from the dataset. TOL-6 z4 has the highest Ft value, and TOL-5 z4 has the second highest Ft value for TOL-5, but this is expected for the largest grains. The estimated uncertainty of Ft is the same or less as the other grains (3.0-4.7%). The grain morphology is similar in all the grains, being euhedral with minor inclusions, but TOL-5 z4, and especially TOL-6 z4 are rather cloudy compared to the other clear grains. The eU shows no correlation with the ages, and a correlation, either negative or positive, is expected if the dispersion of ages is due to radiation damage (Anderson et al., 2017). These results are summarized in Table 3. All in all, this suggests that the younger dates might not be as accurate as the older ones. Excluding the two youngest outliers, the new ages are 5.9 Ma for TOL-5 and 6.2 Ma for TOL-6, and they are both within the margins of error of each other (0.3 Ma). Looking back at Table 1, the ages could be related to the thermal effects of the Porto Azzurro Pluton (5.9 Ma) and/or the Calanchiole Shear Zone (6.1 Ma)

Table 3: (U-Th)/He zircon data from TOL-5 and TOL-6. The unweighted average ages are 5.7 Ma for TOL-5 and 5.9 Ma for TOL-6.

	He		U			Th				Sm			Ejection	*Uncorr.*	Ft-Corr.		Sample unweighted					
	vol.	1σ	mass	1σ	conc.	mass	1σ	conc.	Th/U	mass	1σ	conc.	correct.	*He-age*	He-age	2σ	aver. ± 2 s.e.					
Sample	[ncc]	[%]	[ng]	[%]	[ppm]	[ng]	[%]	[ppm]	ratio	[ng]	[%]	[ppm]	(Ft)	*[Ma]*	[Ma]	[Ma]	[Ma]	[Ma]	TAU [%]	First He re-extract [%]	eU [ppm]	sphere radius [µm]
TOL-5 z1	**0.842**	1.0	**1.356233893**	1.8	310	**0.3393594**	2.4	78	0.25	**0.014**	6.2	3	**0.763**	*4.86*	**6.37**	0.52			1.9	**1.2**	328	51
TOL-5 z2	**0.657**	1.1	**1.336629369**	1.8	878	**0.0927508**	2.4	61	0.07	**0.005**	6.2	3	**0.684**	*4.01*	**5.86**	0.61			2.1	**0.2**	892	37
TOL-5 z3	**0.573**	1.1	**1.090504387**	1.8	276	**0.2527189**	2.4	64	0.23	**0.006**	6.2	2	**0.752**	*4.13*	**5.48**	0.46			2.0	**0.1**	291	49
TOL-5 z4	**2.764**	0.9	**5.848643032**	1.8	1161	**0.6114463**	2.4	121	0.10	**0.058**	6.2	12	**0.756**	*3.82*	**5.06**	0.42	**5.7**	0.3	1.9	**7.2**	1190	50
TOL-6 z1	**0.556**	1.1	**0.982624569**	1.8	343	**0.0709822**	2.5	25	0.07	**0.001**	6.2	0	**0.742**	*4.61*	**6.21**	0.54			2.0	**0.7**	349	47
TOL-6 z3	**2.023**	1.0	**3.253305466**	1.8	620	**0.9707406**	2.4	185	0.30	**0.022**	6.2	4	**0.781**	*4.81*	**6.17**	0.47			1.9	**0.4**	663	56
TOL-6 z4	**2.057**	1.0	**4.035592019**	1.8	519	**0.2372774**	2.4	30	0.06	**0.021**	6.2	3	**0.799**	*4.17*	**5.22**	0.38	**5.9**	0.3	2.0	**13.6**	526	61

Footnote:
Amount of helium is given in nano-cubic-cm in standard temperature and pressure.
Amount of radioactive elements are given in nanograms.
Ejection correct. (Ft): correction factor for alpha-ejection (according to Farley et al., 1996 and Hourigan et al., 2005).
Uncertainties of helium and the radioactive element contents are given as 1 sigma, in relative error %.
Uncertainties of the radioactive element concentrations are ca. 10% (due to the high uncertainty in the crystal mass estimation).
Uncertainty of the single grain age is given as 2 sigma in Ma and it includes both the analytical uncertainty and the estimated uncertainty of the Ft.
Uncertainty of the sample average age is 2 standard error, as (SD)/(n)1/2; where SD=standard deviation of the age replicates and n=number of age determinations.

6 Discussion

The style of folding, refolding, opposing vergences and kinematic indicators in the APM all point towards a multi-deformational tectonic history which can be somewhat unraveled using thermochronology. Previous studies have provided first-order interpretations for the deformation of the APM, but few of them were done solely on this unit. As a result, there is lack of data and debate surrounding the existing explanations of the APM's tectono-thermal evolution. This study gives special focus to the APM and provides additional structural data as well as the first ZHe thermochronological data for the APM, which will be discussed in the following section.

6.1 Structure

6.1.1 Comparison of Structural Data with Selected Previous Studies

The general structural picture of this study is similar to what Elter and Pandeli (2001) found, with foliations dipping mostly to the WSW like the rest of the EENS, and lineations plunging mainly to the SW and NE. Foliations in the eastern section of Capo d'Arco deviate from this trend, dipping towards the ENE, as also noted in most studies dealing with the structural analysis of the APM (Fig. 6.1). Although the majority of the mineral lineations trend to the SW, a number of SE-plunging lineations were also found in this study. SE-plunging lineations are very sparse or absent in the selected previous studies (Fig. 6.1B, D). Kinematic indicators found by Pandeli et al. (2001) and Bortolotti et al. (2001) show transport directions to the NE, SW, top-to-the SW (TTSW), and top-to-the SE (TTSE). Few kinematic indicators were observed in this study, but they show transport directions to the NE (asymmetric folds and clasts) and W (normal faults). Combining the results from this work and previous studies shows the varied distribution of structural data, which can be explained by a series of deformational events.

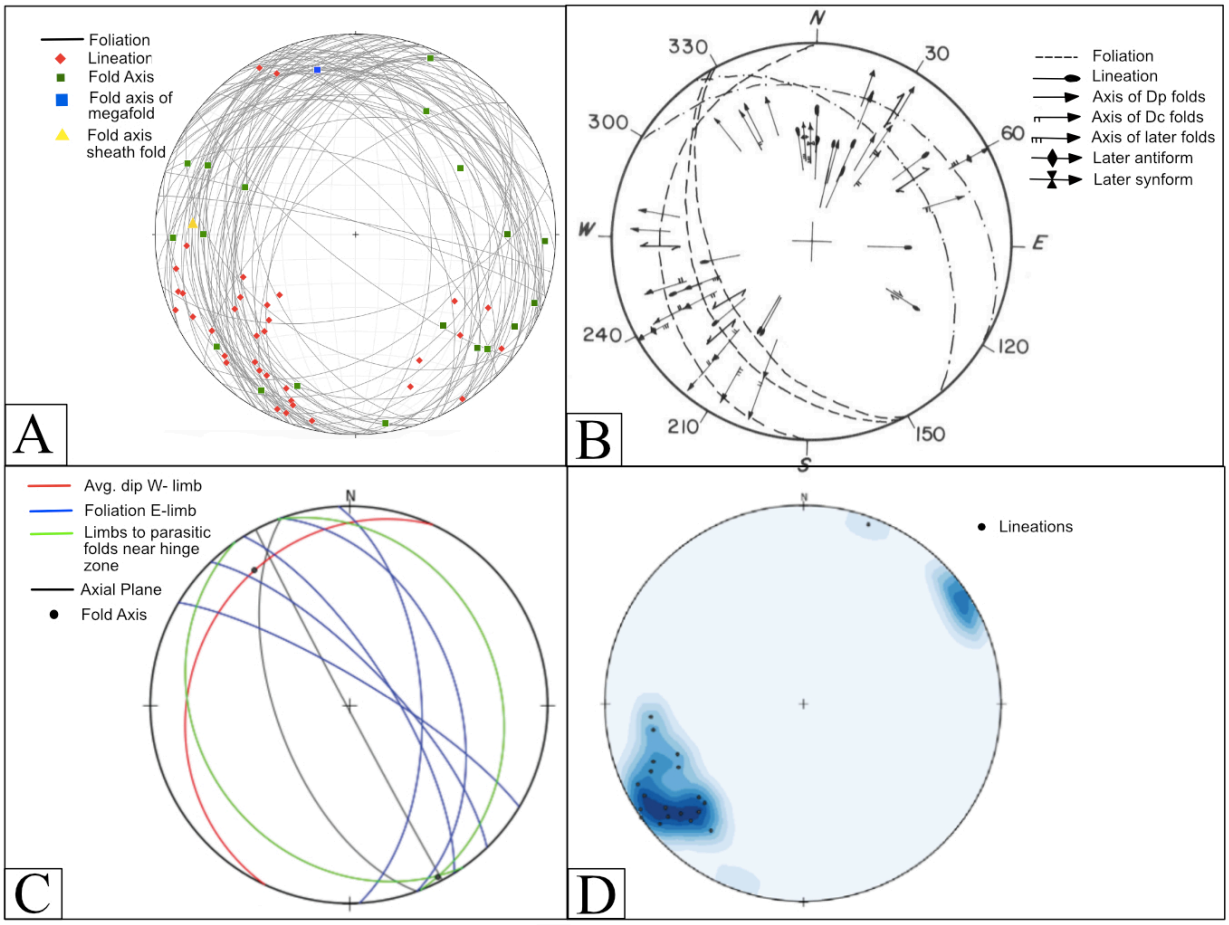

Figure 6.1 – Comparisons of structural data. A: Stereonet of all structural measurements taken in this study. B: Stereonet for APM showing lineations fold axes related to Dp (main deformational event), Dc (later crenulation event), and later folds (Elter and Pandeli (2001) This is a rather unusual representation linear data, clearly showing the trend, but whether the plunge is at the arrowhead or tail is not specified. C: Stereonet of the megafold in the APM (Ryan, 2017). D: Lineations in the APM (Ryan, 2017). The datasets are relatively similar to each other.

6.1.2 Deformational Events

Different events and deformation mechanisms have been suggested based on structures and accompanying ages. Generally, there are two-three main deformation phases recognized – the prograde metamorphic related to subduction, and the retrograde related to exhumation and extension, and finally deformation related to pluton emplacement and post-orogenic collapse.

Pre-subduction

The collision between Africa and Europe initiated in the Late Cretaceous as Europe subducted underneath Adria in the north forming the Alps, and later Adria subducted underneath the Corsica-Sardinia block further south creating the Apennines (e.g. Carmignani and Kligfield, 1990; Gueguen et al., 1998 and references therein). The APM were originally thought to be Early Cretaceous in age after the findings of relict microfossils (Duranti et al., 1992) and from

the Ligurian Domain that had undergone low-P metamorphism (Keller and Coward, 1996; Garfagnoli et al., 2005; Musumeci and Vaselli, 2012). The Ligurian affinity and low-P metamorphism was questioned by Bianco et al. (2015) who instead suggested a Tuscan affinity based on the chemistry of metabasites and HP-metamorphism based on relict HP minerals in the same rocks. The age of these sediments is controversial. Microfossils were not observed in this study and have not been reported in other studies succeeding Duranti et al. (1992). Whether fossils would even be preserved after the intense deformation and metamorphism is questionable (Moorbath, 2005), but fossils have been found in Triassic HP rocks from the Alps (Bernard et al., 2007). Sirevaag (2013) dated detrital zircons in the APM using the U-Pb LA-ICPMS method obtaining a cluster of minimum ages around the 32 Ma peak**,** constraining the maximum deposition age to the Oligocene. Jacobs et al. (2018) confirmed this by dating zircons using the more accurate U-Pb SIMS method (Kosler et al., 2002), obtaining an age of 31.6 Ma, making them coeval to the foredeep deposits of the Macigno and Pseudomagicno units of the Apuan Alps in the Northern Apennines. The depositional age is important as it constrains the age of the first deformation to <31.6 Ma. Finding the source and origin of these sediments was discussed by Sirevaag (2013) who suggested an igneous source based on the euhedral morphology of the zircons, and an Iberian origin based on the igneous activity in Sardinia that lasted from 32-15 Ma, yet peaked at 20 Ma (Lustrino et al., 2009), postdating the zircons. However, Jacobs et al. (2018) analyzed the Hf isotopic composition on the zircons, which showed similarities to the Bergell plutons of the Central Alps. Its volcanic roof is now fully eroded, and its erosional products are found in the Oligocene Aveto-Petrignacola Formation in the Northern Apennines. The zircons could therefore originate directly from the Bergell volcanic roof or from the erosional products in the Aveto-Petrignacola Formation. Instead of eroding from W to E from the Iberian Plate into the subduction zone as proposed by Sirevaag (2013), the zircons must have travelled longitudinally about 400 km south, from the Central Alps to the Apennine foredeep, and was then subducted (Jacobs et al., 2018).

Subduction and HP/LT Metamorphism

There is no doubt that the APM has a subduction history based on the relict HP minerals contained in the metabasites (Bianco et al., 2015, 2019) The APM subducted to depths that experienced lawsonite-blueschist facies peak metamorphism, reaching P-T conditions of 1.5-1.8 GPa and 320-370 °C (Papeschi et al., 2020; Bianco et al., 2015, 2019). This is the first of the many deformational events that the APM endured and its timing is currently being debated

after new data from Jacobs et al. (2018) came forth, suggesting that the peak metamorphism happened at 19 Ma rather than 30 Ma as previously interpreted (Bortolotti et al., 2001; Balestrieri et al., 2011; Deino et al., 1992). This event is reflected best in the Capo d'Arco region indicated by the presence of isoclinal and rootless folds observed at both the mesoscale (Fig. 5.7D) and microscale (Fig. 5.12B). Due to the relationship between the Corsica-Sardinia block and Adria, it is expected that these structures should be dominated by TTE movement. However, determining any asymmetry in these old structures is near impossible as they are poorly preserved after being strongly deformed to the point of transposition onto the later foliation. Shear zones have been present from subduction to pluton emplacement, making it difficult to constrain the timing of the formation of the Rio Marina sheath folds. Sheath folds have for example been found in central Elba, associated with the Late Miocene Felciaio Shear Zone (Musumeci et al., 2012). Nonetheless, this study interprets the Rio Marina sheath folds as a result of the intense shearing during the subduction stage, based on the E-W trend of the fold axes and the associated E-W- and NE-SW-trending, penetrative stretching lineations (Papeschi et al., 2020) reflecting the NE-SW plate motion (Carmignani et al., 1978). This is supported by the similar findings in the Tuscan metamorphic units of the Apuan Alps who also host subduction-related sheath folds with fold axes subparallel to the pervasive N60-80-trending stretching lineations (Vanneschi et al., 2014).

Early Exhumation

Exhumation in the Northern Apennines is one of the more debated topics as it includes the puzzle of exhumation- timing and mechanisms of (U)HP rocks. The processes that have been suggested for the exhumation of the metamorphic units in the Northern Apennines include syn-orogenic extrusion (Storti, 1995; Jolivet et al., 1998; Rossetti et al., 2002; Molli, 2008; Molli et al., 2018), post-orogenic extension (Carmignani & Kligfield, 1990; Carmignani et al., 1994), slab rollback, delamination and buoyancy (Brun and Faccenna, 2008; Ernst et al., 1997), and repeated underplating (Jolivet et al., 1998; Malavieille, 2010). Thomson et al. (2010) pointed out that it is most likely a combination of these, as one single process cannot account for the variety of structures seen across the Northern Apennines.

After being subducted to depths of 42-50 km, the APM underwent rapid, near-isothermal exhumation in the greenschist-facies reaching temperatures of <380–420°C (Papeschi et al., 2020). Open-tight and E- and W-verging folds, shear bands, crenulation cleavages, and boudinage/pinch-and-swell are associated with the high ductile strain during the

various stages of exhumation. The high strain structures are mostly found in the far north and south, suggesting the strain was heterogenous. The early stage of this phase deformed the older isoclinal structures to the point of transposition onto the main foliation. This is also seen in the areas abundant in calc-schist lenses where alternating layers appear to represent stratigraphy but is in reality transposed layers. This event could also account for the incorporation of the lower nappes into the accreted, unmetamorphosed nappes (e.g. Tuscan Nappe, Ligurian units), but the distinction between nappe stacking of the upper and lower units are often not differentiated, leading to some stating that nappe stacking took place during subduction (Carmignani and Kligfield, 1990; Jolivet et al., 1994; Musumeci et al., 2015) and some at the beginning of exhumation (Deino et al., 1992; Massa et al., 2017; Papeschi et al., 2020). Extensional shear bands associated with exhumation are found cutting the main foliation. Due to the unfortunate fact that the thin sections were not oriented one cannot determine whether the bands show TTW- or TTE extensional shearing. TTW extensional shearing has been reported in previous literature for the Acquadolce Unit (Elter and Pandeli, 2001; Ryan, 2017), but the similar HP units of Gorgona Island (the northernmost island in the Tuscan Archipelago) show TTE extensional shearing (Rossetti et al., 1999). Either way, both TTW and TTE extensional structures, like detachment faults, can form in an orogenic wedge during extension (Fossen, 2016).

The APM consists of HP rocks from the subduction channel, an environment characterized by very rapid exhumation of continental material that is mainly driven by buoyancy as opposed to the slower extension found in the overlying wedge (Jolivet et al., 2003). The positive buoyancy of continental rocks will only exhume them to depths of about 30-40 km (Boutelier et al., 2004; Brun and Faccenna, 2008) which is often located at the base of the orogenic wedge (Jolivet et al., 2003). Syn-convergent extrusion can occur via rigid wedge extrusion or ductile channel flow (Chemenda et al., 1996; Boutelier and Chemenda, 2008; Grujic, 2006). At a certain depth, the effective interplate pressure can become lower than the lithostatic pressure due to buoyancy, triggering the detachment of a rigid extruding wedge (Boutelier and Chemenda, 2008) (Fig. 6.2). This wedge is bound by the main basement thrust and an upper extensional fault (Chemenda et al., 1996) possibly causing both the TTW extensional-and TTE compressional structures in the APM. Strain is mostly concentrated along the fault boundaries whereas the core experiences little to no deformation (Grujic, 2006). Channel flow is similar to wedge extrusion, involving the upward ductile movement of rocks in a low-viscosity layer (Cloos, 1982; Shreve and Cloos, 1986) and results in distributed

deformation. This was suggested by Ryan (2017) to account for the TTW, conjugate, and TTE structures. Grujic, (2006) pointed out that if the ductile channel falls below a critical temperature it will convert to an extruding wedge.

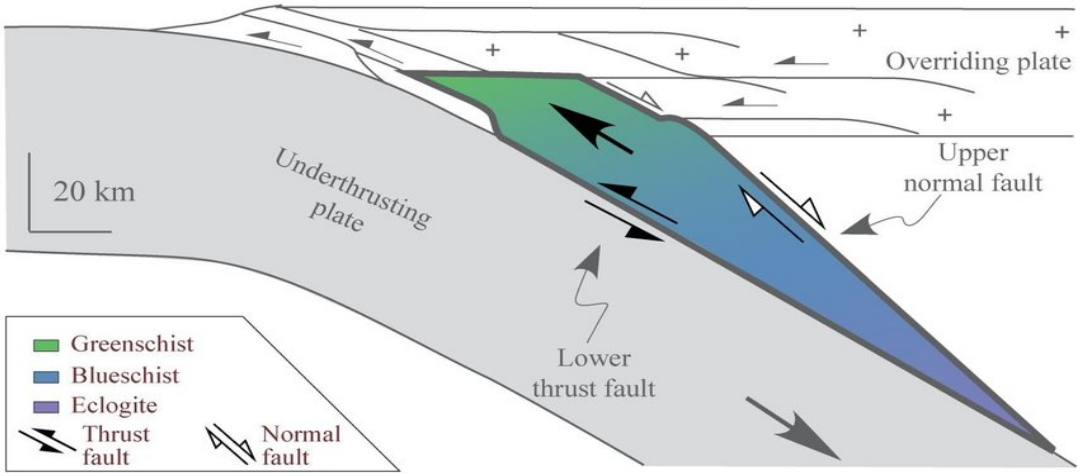

Figure 6.2 - Subduction zone showing the extrusion of a detached, more buoyant wedge bound by a basal thrust fault and an upper normal fault. Modified after Ring & Glodny (2010).

Slab rollback initiated between the Late Oligocene-Early Miocene (Gueguen et al., 1998) resulting in a wide subduction channel and wedge and created more space for return flow and uplift of the buoyant rocks as well as further heating and upwelling by the asthenosphere. Even with the upwelling asthenosphere, the exhumation happened in an overall cool regime due to the continuous underthrusting of cold continental crust (Jolivet et al., 1996, 2003), but did experience a slight increase in temperature during the greenschist retrograde metamorphism (Papeschi et al., 2020).

Brun and Faccenna (2008) suggested that the exhumation of HP rocks in the Calabria-Apennine belt is driven by the subduction of a small continental block, slab rollback, and buoyancy. Their model shows that exhumation initiates when the continental block is completely decoupled from the underlying mantle as the compressional front of the wedge reaches the ocean-continent boundary, which in turn triggers slab-retreat. Slab retreat widens the subduction channel, and the upwelling asthenosphere can cause core complex exhumation. This model is probably more applicable to the Southern Apennine-Calabria region considering the lack of evidence of oceanic subduction after the initial continental collision took place in the Northern Apennines. However, most of the concepts correlate with syn-orogenic extrusion apart from what triggered rollback. If not triggered by the continental block, retreat was most likely caused by an increase in the subduction angle as a result of the downward gravity of the high-density slab (Zhang and Wang, 2020). Ultimately, the concept of positive buoyancy is

probably what exhumed the APM to crustal levels of 30-45 km. Platt (1993) even claimed that buoyancy-driven exhumation is the only way to exhume deeply buried rocks in the early stages.

Late Exhumation

Once at mid-crustal levels, different processes started governing after the equilibration of buoyancy forces. Extrusion could still take place, but it would be due to other mechanisms than buoyancy. The retreating slab along with wedge dynamics caused extension in the wedge. (Platt, 1986; Carmignani and Kligfield, 1990; Jolivet et al., 1998). Repeated underplating/antiformal stacking has been proposed for the exhumation of HP units like the Tuscan metamorphic core complex in the Apuan Alps (Jolivet et al., 1998; Malavieille, 2010) and could have aided with some of the exhumation for the APM. This process is often a response to the everchanging wedge-geometry, which switches between frontal accretion and underplating to maintain gravitational stability, resulting in phases of compression followed by extension (Gutscher et al., 1996, 1998). Repeated underplating and frontal accretion will ultimately result in an overthickened wedge that will start to deform by extensional faulting through normal- and detachment faults verging both to the E and W (Storti, 1995; Clemenzi et al., 2014; Massa et al., 2017). Both upper crustal listric normal faults and shear zones are recorded in the Northern Apennines (Apuan Alps) (Carmignani and Kligfield, 1990).

W-verging tight folds are associated with exhumation in the wedge. Platt (1983) explains W-verging structures can form in the retrowedge due to local compression. Indeed, a phase of renewed compression during the Middle-Late Miocene interrupted the extensional tectonics taking place in the Northern Apennines (Bonini et al., 2014; Musumeci et al., 2015; Massa et al., 2017; Viola et al., 2018). This is also highlighted by the delta clasts (Fig. 5.7B) which are made of boudinaged quartz veins suggesting extension. They were then affected by TTE-shearing indicating a later compressional event. This was possibly caused by wedge instabilities that were accommodated by compression in the internal wedge (Ryan, 2017). The most prominent structures to come out of this event were km-scale folds**,** which have been described for the Apuan Alps (Carosi et al., 2004; Molli and Meccheri, 2012), and recently also on Elba (Massa et al., 2017). Bortolotti et al. (2001, 2016) mentioned large-scale folds in the lower Ortano units, but their isoclinal nature makes them more likely to be related to subduction or early exhumation. The later large-scale folds are characterized by NE-vergence, trending to the NNW, sometimes with a flat-lying axial plane. The inferred large-scale fold in the APM, now referred to as the Acquadolce Antiform, was initially noticed in the Capo d'Arco

area after finding opposite dip-directions indicating an antiform. The geometry of the fold is non-cylindrical, asymmetrical, verging to the NE, with an undulating fold axis overall plunging to the NNW. This fold could explain the NW-SE lineations if interpreted as intersection lineations and rods, as one would expect these to form parallel to the fold axis. Megafolds in the APM has only been reported once before by Ryan (2017) who interpreted the foliation, just north of Ortano Valley in the Rio Marina area, to define an overturned fold (Fig. 6.3A), similar to the Rio Marina Antiform described by (Massa et al., 2017) (Fig. 6.3B). In the Rio Marina area, the Acquadolce Antiform is described as having a short, steep E-dipping limb and a shallow W-dipping limb. Comparing this to the one found in this study shows that the western limbs seem to be similar, but the short eastern limb in the Capo d'Arco area dips more shallowly to the NE which was interpreted to be a result of later deformation caused by normal faulting (Ryan, 2017). The interpretation of late normal faulting explains the wide variety of dip-directions observed in this particular region. The structural measurements from this study that were taken in the Rio Marina area do not show any steep E-dipping foliation. What was observed instead was constant W-dipping foliation, where the higher end of the dip values did not exceed 65º.

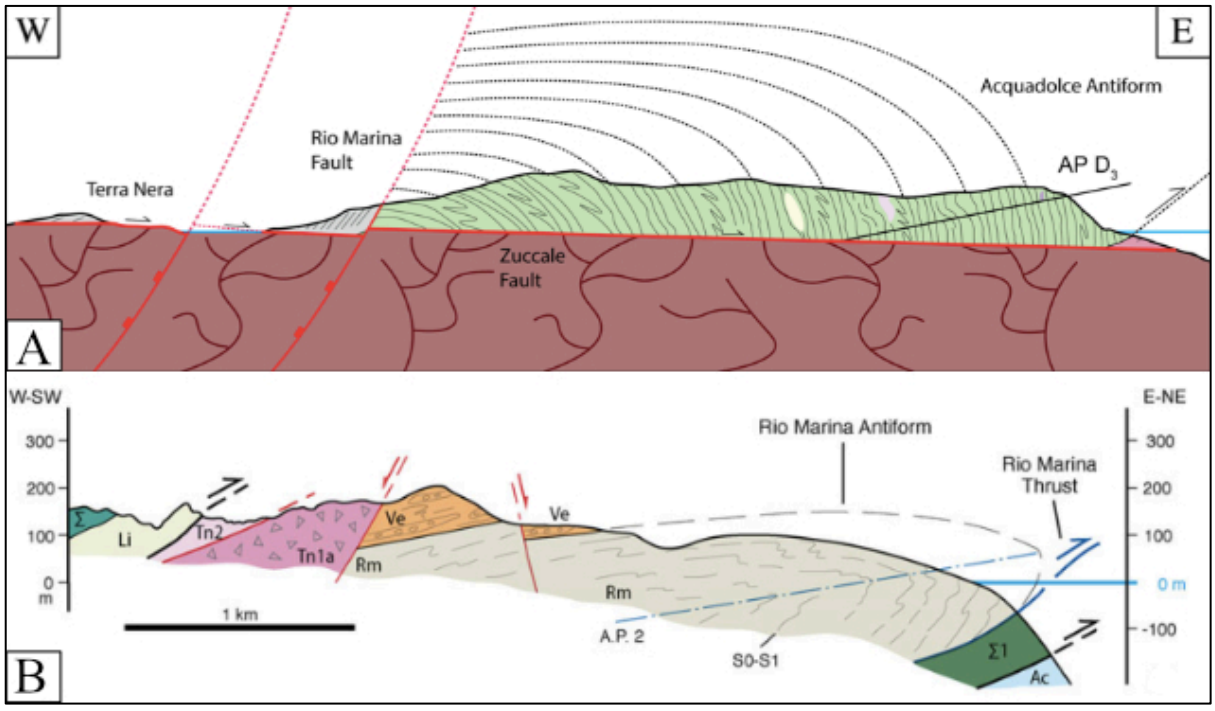

Figure 6.3 - Previously described megafolds in the EENS. A: The Acquadolce Antiform north of the Ortano Valley. The eastern limb is cut off by the Rio Marina Fault. The western limb might invert at depths (Ryan, 2017). B: The overturned Rio Maria Antiform just north of Rio Marina. **Σ** – Serpentinites; **Li** – Mesozoic Sedimentary Cover; **Tn**; Calcare Cavernoso; **Ve** – Verruca Fm; **Rm** – Rio Marina Fm; **Ac** – Acquadole Unit (Massa et al., 2017).

Based on our own measurements and the fold interpretation of Ryan (2017) two cross-sections were drawn, showing the southern antiform in Capo d'Arco (Fig. 6.4A), and the northern antiform near Rio Marina (Fig. 6.4B). Naturally, the northern antiform has a slightly different geometry than the one drawn by Ryan (2017) in Fig. 6.3B due to our partially different measurements. Another explanation for the varying orientation of the eastern limb could be its contact to the Felciaio Shear Zone. This shear zone was active during the Late Miocene pluton emplacement (Musumeci and Vaselli, 2012) and could have caused ductile deformation directed upwards by its reverse motion until the eastern limb finally dipped to the E.

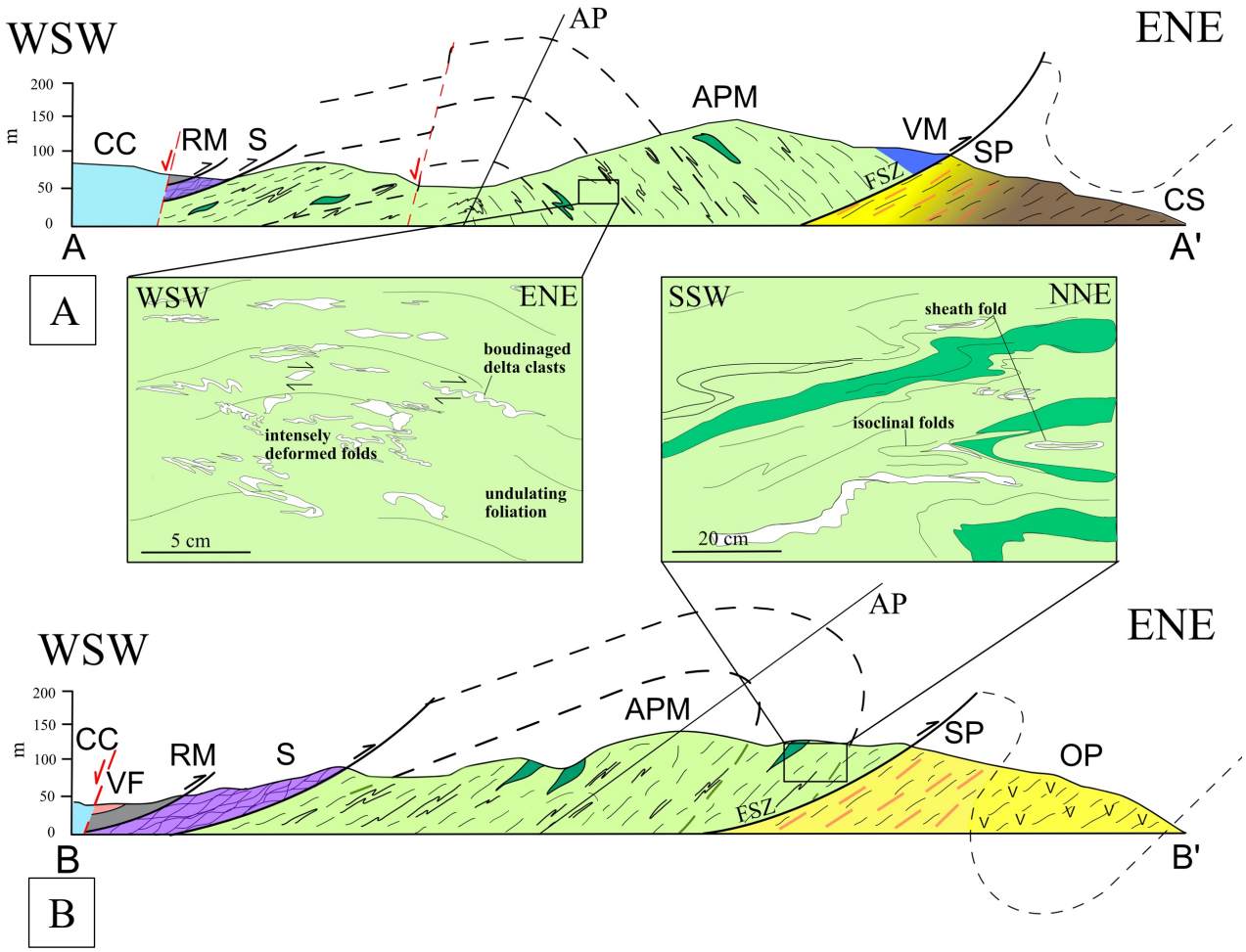

Figure 6.4 - Cross-sections from Eastern Elba, showing the relationship between interpreted folds and structures. A: The top cross-section is from the Capo d'Arco area showing the NE-verging Acquadolce Antiform that formed in a compressional event in the Middle-Late Miocene. Later, the fold suffered deformation by normal faulting, slightly changing the geometry of the fold. The E-dipping shorter limb is possibly a result from this later brittle, normal faulting or from the reverse motion from the ductile Felciaio Shear Zone. Capo d'Arco contains structures mostly related to the subduction event, as shown in the left-hand zoomed-in box, showing the transposed, isoclinal folds, as well as some later clasts showing TTE movement. The Ortano folds are included in the cross-section, but the Ortano Porphyroids are not exposed in the southern area due to the NNW-plunging fold axis.
B: The lower cross-section represents the area around Rio Marina, north of Ortano Valley. The Acquadolce Antiform is overturned as reflected by the same dip-direction across the unit. The Ortano Porphyroids are now exposed due to being located further up in the fold. The northern part of the APM contains more calc-schists and skarn which are intensely sheared in areas like the Rio Marina lighthouse. This is the only area where sheath folds have been observed showing E-W movement. **AP** – axial plane; **FSZ** – Felciaio Shear Zone; **CC** – Calcare Cavernosso; **VF** – Verruca Formation; **RM** – Rio Marina Formation; **S** – Serpentinites; **APM** – Acquadolce Phyllites and Metasiltstones; **SP** – Silvergrey Phyllites and Quartzites; **OP** – Ortano Porphyroids; **CS** – Capo d'Arco Schist.

Post Exhumation

With a continuously rising asthenosphere, the monzogranite Porto Azzurro Pluton was emplaced at depths of approximately 6.2 km, intruding Eastern Elba at 5.9-6.5 Ma (Maineri et al., 2003; Gagnevin et al., 2011). The pluton generated enough heat allowing for ductile deformation to take place rather than brittle which is expected for rocks at very shallow crustal levels. A new phase of Late Miocene-Early Pliocene compression was recognized by reverse motion in thrusts and shear zones (e.g. Felciaio Shear Zone, Capo-Norsi Thrust, possibly Zuccale Fault) (Musumeci et al., 2015; Papeschi et al., 2017; Massa et al., 2017) creating local mylonites and open folds (Fig. 5.7C). Mineral stretching lineations of quartz and the contact metamorphic mineral cordierite form an L-tectonite (Fig. 5.11A) trending SW, (sub)parallel to the local shear zones found at Felciaio Beach. The stretching probably relates to the Felciaio Shear Zone, indicating ductile deformation taking place syn- or post intrusion. The pluton's main effect on the APM was the formation of skarn and contact metamorphic minerals such as the spessartine-grossular garnets. The garnets overgrow both the main foliation and the cordierite, suggesting they are post-kinematic in origin or deformed brittlely due to insufficient heating. As for the question of the composition of the garnets, Mn/Ca-rich garnets are usually regarded as a mineral belonging to the greenschist facies produced in low-grade phyllites, but can also be a product of contact metamorphism seeing as the formation of Mn/Ca-garnets is mostly dependent on the availability of these elements in the protolith rather than P-T conditions (Hsu, 1980). This period, marked by very high heat flow, was similar to today's Larderello geothermal field with its impressive geothermal gradient of 75-100 ºC/km. Papeschi et al. (2020) states that the northernmost parts of the APM largely escaped HT-LP metamorphism, but obliterated most of the HP minerals in the southern portion.

The final phase of deformation that affected the APM is the upper crustal brittle deformation marked by N-S striking high-angle normal faults dipping to the west. The observed faults are likely to be part of the same normal fault systems described in previous literature relating to orogenic collapse and the rifting of the Tyrrhenian Sea (Trincardi and Zitellini, 1987; Bortolotti et al., 2001). The observed faults are relatively small and did not affect the overall geometry of the APM other than offsetting thin layers. The larger faults on the other hand, like the Rio Marina Fault, are responsible for offsetting the nappes, which can be seen in the cross section in Appendix II. A summary of the tectonic evolution is shown in Fig. 6.5.

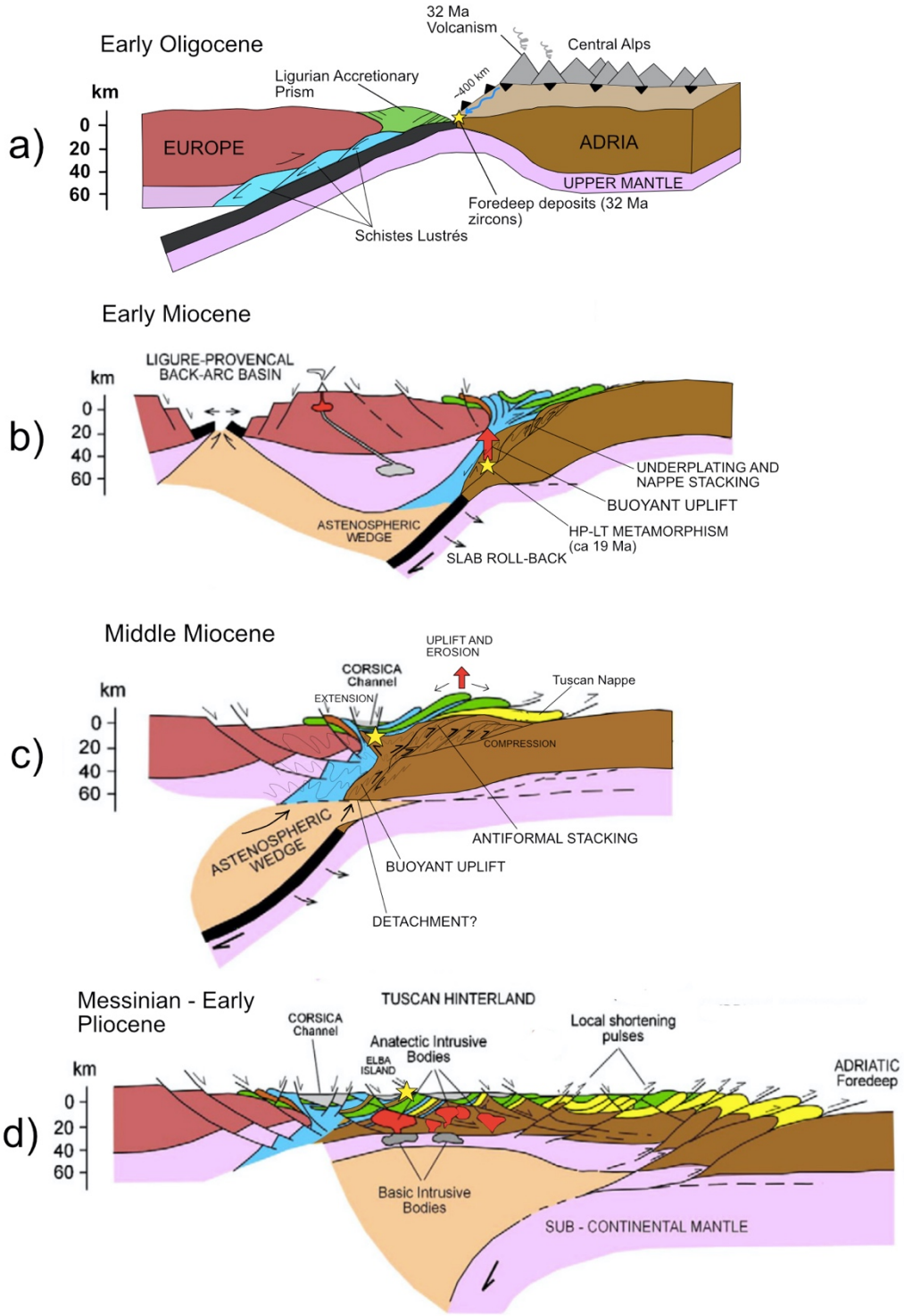

Figure 6.5 - Tectonic evolution of the Northern Apennines showing the journey of the Oligocene zircons from the APM (yellow star). a) Subduction of the Western Tethys, which accreted and subducted oceanic sediments. Volcanism in the Central Alps provided the 32 Ma zircons, which eroded and traveled 400 km south, ending up in the Apennine foredeep before being subducted shortly after. b) Continental collision initiated in the Late Oligocene-Early Miocene, accreting Tuscan rocks either by frontal accretion or underplating. At 19 Ma, the APM were subducted to depths of 42-50 km, experiencing peak metamorphism in the lawsonite-blueschist facies before exhuming isothermally through the episode-blueschist to greenschist facies, which was driven by buoyancy. Slab-rollback started shortly after, triggering extension in the upper wedge and upwelling of the asthenosphere, promoting further uplift. c) The APM probably reached upper crustal levels by the Middle Miocene, undergoing further exhumation by extension in the upper crust. At this time, the APM experienced a compressional event in-between the extension, creating km-scale folds. Detachment of the subducting slab has been suggested for the Southern Apennines/Calabria, but uncertainty remains around the detachment in the Northern Apennines. d) Continuous thinning of the crust by the upwelling asthenosphere caused plutons like the Porto Azzurro and Mt. Capanne Pluton to intrude Elba. The whole region then experienced post-orogenic collapse as the compressional front migrated to the east. Modified after Balestrieri et al. (2020).

6.2 Thermochronology

The (U-Th)/He analysis was conducted in order to obtain information about cooling and exhumation history of the APM. The zircons' euhedral shapes likely make them the Oligocene volcanic zircons we were after. Based on the zircons' morphology, Ft values, He re-extractions, and eU, the ages of 5.9 Ma and 6.2 Ma were interpreted to represent cooling through the closure temperature for retention of He in zircon at ca. 180 °C. The beginning of exhumation was said to initiate shortly after peak metamorphism, which was previously thought to have occurred at 30 Ma (Balestrieri et al., 2011), but more recent studies suggest that the 19 Ma age (Deino et al., 1992; Bianco et al., 2019) more likely represents peak metamorphism (Massa et al., 2017; Papeschi et al., 2020). This study will interpret the results using the younger age.

Constraining Elba's exhumation has been done in various ways. Bortolotti et al. (2001) suggested that Elba was already above sea-level by the Late Miocene pluton emplacement due to the absence of marine sediments. Duranti et al. (1992) calculated that HT-LP metamorphism in the Acquadolce Unit experienced a maximum pressure of 0.2 GPa, equating to depths of 5-6 km (Papeschi et al., 2020), suggesting that it was *not* fully exhumed by pluton emplacement. Due to the fact that Elba was probably already at shallow depths by the Late Miocene, Early-Middle Miocene ages were expected as the 180°C isotherm would be at depths of ca. 7 km using a geothermal gradient of 25/km. Previous thermochronological work has also suggested that exhumation in the Apuan Alps occurred at 12 Ma (Kliegfield et al., 1986). Papeschi et al. (2020) was published during this study and showed that the APM experienced near-isothermal exhumation through a cold geothermal gradient similar to oceanic subduction gradients of 5-10°C/km. This means that the 180°C isotherm was probably located at depths of 36-18 km. If the 5.9-6.2 Ma ages represent cooling by exhumation, then the exhumation rate would be very slow (0.46-2.4 km/Myr). The APM is always described as being rapidly exhumed (Jacobs et al., 2018) and HP rocks exhuming in collision zones can exhume at rates of 30 km/Myr (Brun and Faccenna, 2008) and even 50-100 km/Myr (Boutelier et al., 2004).

Balestrieri et al. (2003) did ZHe dating in the Apuan Alps and reported similar young ages (7.42 – 4.98 Ma). Specifically, the Pseudomacigno Unit (metamorphosed Macigno foredeep deposits and are also found on Elba) has been correlated to the APM, and showed an age of 7.4 Ma (Balestrieri et al., 2003) and 3.61-6.93 Ma (Fellin et al., 2008), which was interpreted to represent cooling by exhumation as there is no evidence of nearby magmatism. Whether parallels can be drawn between this unit and the APM is questionable. The Pseudomacigno only subducted to 20-30 km (Molli and Vaselli, 2006; Malusà et al., 2015) and

could have a different exhumation history. It is therefore unlikely that our obtained ages represent exhumation.

Reset Ages by the Porto Azzurro Pluton

If the ages do not represent exhumation, then the other possibility is that the zircons were reset by the Porto Azzurro Pluton and/or deformation/hydrothermal fluids. Tvedt (2011) dated muscovite from the Capo d'Arco Schists and Ortano Porphyroids in eastern Elba, and the Silver-grey phyllites and quartzites in central Elba at the beach adjacent to Felciaio Beach. These units are all in close proximity of the APM. The ages obtained were around 6.2-6.5 Ma and were interpreted to represent cooling to below muscovite's closure temperature of 350-400°C (e.g. Hames and Bowring, 1994) after getting heated and reset by the Porto Azzurro Pluton. The results are relatively similar to the zircon ages in this study (5.9-6.2 Ma), suggesting that they probably share the same thermal history. To reset zircon ((U-Th)/He system) and muscovite (Ar^{40}/Ar^{39} system), temperatures need to be above at least 180 °C and 350-400 °C respectively over a period of time. In some cases, high temperatures are not enough to fully reset the minerals and requires interactions with hydrothermal fluids and/or deformation (Wölfler et al., 2010; Ault et al., 2016). The simplest explanation for the young ages is that they were reset by the Porto Azzuro Pluton with or without the aid of hydrothermal fluids and/or deformation. The Porto Azzurro Pluton is dated to 5.9-6.5 Ma (Maineri et al., 2013; Musemeci et al., 2015) reaching peak temperatures of ca. 600 °C in the lower units (Duranti et al., 1992) while the Calanchiole Shear Zone is dated to 6.14 Ma (Viola et al., 2018) with the Felciaio Shear Zone probably being coeval. These two features could provide both the temperature and/or circulation of hydrothermal fluids required for resetting. Nearby skarns in Rio Marina that formed by metasomatic processes confirm the presence of hydrothermal fluids close to the sampling location. Further observations strengthening the interpretation of reset is the presence of contact metamorphic minerals in the APM. Both andalusite and cordierite have been observed in the field, which require at least 450 ºC to form (Deer et al., 1992).

The uncertainties with this explanation lie within the general uncertainties pertaining to the extent of the Porto Azzurro Pluton**.** The pluton is not documented as well as the Mt. Capanne Pluton due to the lack of outcrops. The contact aureole has been estimated to have a diameter of 6-7 km (Musemeci et al., 2015) or 9.5 km from north to south (Caggianelli et al., 2018). Whether the aureole actually affected our sampling localities, and to what degree, is still debatable. Papeschi et al. (2020) states that the northern unit largely escaped contact

metamorphism. They also show that the isograd for cordierite and andalusite ends just north of the Ortano Valley, which puts our sampling localities in the biotite zone, indicative of low-grade contact metamorphism. This corresponds to the findings in this study, as cordierite has only been observed in the south at Felciaio Beach, and andalusite has not been observed north of the Ortano Valley. On the other hand, Ryan (2017) computed isotherms for the APM relating to the Porto Azzurro Pluton, showing a 450 °C isotherm going through the location where TOL-5 and TOL-6 were collected. One of the remaining questions is whether these temperatures were upheld for long enough to reset the geochronological systems. Currently, Andrea Brogi and his colleagues are conducting a study on the emplacement and cooling of the Porto Azzurro Pluton, which can provide us with the information about this being a short pulse of heating or a longer-lasting event. They state that the Porto Azzurro emplacement and exhumation did not exceed 2 Ma. (personal communication, October 10, 2020). Our best guess using the previous evidence is that these ages most likely represent cooling related to cooling after contact metamorphism.

7 Summary and Conclusion

This study aimed to document and explain the structural history of the Acquadolce Phyllites and Metasiltstones (APM) on Elba Island, and provide new thermochronological data using (U-Th)/He dating on zircons. The APM show a complex structural history not easily determined, but is represented by folds at all scales, shear zones, lineations, and sheath folds. The Acquadolce Unit was deposited in the Apenninic foredeep in the Oligocene before being subducted to depths of 42-50 km, undergoing HP-LT metamorphism at ca. 19 Ma (Jacobs et al., 2018; Papeschi et al., 2020; Deino et al., 1992). HP-LT minerals are only preserved as relict glaucophane and lawsonite pseudomorphs in the metabasites in the APM (Bianco et al., 2015; Papeschi et al., 2020), while the rest have been obliterated by later retrograde metamorphism. Shortly after the closure of the Western Tethys Ocean, continental collision between Adria and Europe took place in the Early Miocene initiating slab rollback (Robertson and Grasso, 1995; Gueguen et al., 1998), allowing for hot asthenosphere to fill in the mantle wedge. The APM probably underwent buoyancy-driven uplift from the upper mantle to the lower crust. This was followed by further uplift caused by a combination of processes related to the stability of the wedge, such as underplating, causing extension in the very shallow crust compensated by compression in the deeper crust. This resulted in a km-scale fold called the Acquadolce Antiform, similar to the Rio Marina Antiform described by Massa et al. (2013, 2017). In the Late-Miocene/Pliocene, eastern Elba was intruded by the Porto Azzurro Pluton where the APM was affected by HT-LP metamorphism, mostly in the southern portion of the unit. This activated reverse shear zones possibly overprinting the larger folds. During orogenic collapse and the extension and opening of the Tyrrhenian Sea, the APM, along with the other units on Elba, were subject to brittle deformation by normal faulting (Bortolotti et al., 2001).

New thermochronological data were obtained, aimed at constraining the exhumation of the APM and yielded ages of 5.9-6.2 Ma. These ages are surprisingly young and fall within the age range of the Porto Azzurro Pluton (5.9-6.5 Ma), which most likely makes them a product of either contact metamorphism or the circulation of hydrothermal fluids related to the pluton, rather than exhumation ages.

8 Future work

In order to build on this work and take on some of the limitations and questions raised, there are several things that could be done in future studies.

Thermochronology

One of the major limitations to the work was knowing whether the rocks were affected by contact metamorphism/metasomatism or not. Mapping the contact aureole and skarn bodies using a variety of low-temperature thermochronological systems would be beneficial. With muscovite already dated, it would be interesting to try U-Pb dating in apatites or Ar^{40}/Ar^{49} dating on hornblende to explore the 500°C range.

It is unknown why we did not find any zircons in the Capo d'Arco region after plenty of zircons were found in Jacobs et al., (2018) at the same location. Another attempt to constrain the timing of exhumation could be done using ZHe again, but ideally AHe should also be used to see when the rocks reached the upper 7-14 km of the crust. Luckily, apatites were found in our samples. The Pseudomacigno Unit found in northern Elba in Cavo is most likely outside of the contact aureole. Due to its correlation to the APM, this unit could also be dated using ZHe and AHe to track exhumation paths.

Structure

An in-depth structural analysis of the APM would be beneficial while having the previously undescribed Acquadolce Antiform in mind, looking for clues and structures relating to potential hinge zones and overturned limbs that would help confirm these large-scale folds.

Petrology

Although this project did not focus on petrology, some of the findings still sparked interest in this field. One of the more puzzling minerals observed in the phyllites was clinopyroxene (cpx). Some of the cpx is clearly related to skarn, but the cpx aligned with the foliation found in Capo d'Arco is more difficult to determine. Are they related to skarn or are they relict cpx either from the subducting sediments or the mantle? The spessartine garnets are also interesting as neither of us have seen garnets like this, with such a rounded, dirty appearance. Garnets are great for geobarometry and could be analyzed to determine if they are in fact related to skarn or burial. A microprobe analysis would be beneficial, looking at zoning and trace elements.

9 References

Ahrens, L. (1965). Some observations on the uranium and thorium distributions in accessory zircon from granitic rocks. *Geochimica Et Cosmochimica Acta*, *29*(6), 711-716. https://doi.org/10.1016/0016-7037(65)90064-5

Anderson, A., Hodges, K., & van Soest, M. (2017). Empirical constraints on the effects of radiation damage on helium diffusion in zircon. Geochimica Et Cosmochimica Acta, 218, 308-322. https://doi.org/10.1016/j.gca.2017.09.006

Ault, A., Frenzel, M., Reiners, P., Woodcock, N., & Thomson, S. (2016). Record of paleofluid circulation in faults revealed by hematite (U-Th)/He and apatite fission-track dating: An example from Gower Peninsula fault fissures, Wales. *Lithosphere*, *8*(4), 379-385. https://doi.org/10.1130/l522.1

Balestrieri, M., Bernet, M., Brandon, M., Picotti, V., Reiners, P., & Zattin, M. (2003). Pliocene and Pleistocene exhumation and uplift of two key areas of the Northern Apennines. *Quaternary International*, *101-102*, 67-73. https://doi.org/10.1016/s1040-6182(02)00089-7

Balestrieri, M., Pandeli, E., Bigazzi, G., Carosi, R., & Montomoli, C. (2011). Age and temperature constraints on metamorphism and exhumation of the syn-orogenic metamorphic complexes of Northern Apennines, Italy. *Tectonophysics*, *509*(3-4), 254-271. https://doi.org/10.1016/j.tecto.2011.06.015

Bartole, R., Torelli, L., Mattei, G., Peis, D. & Brancolini, G. 1991. Assetto stratigrafico-strutturale del Tirreno Settentrionale. *Studi Geologici Camerti*, volume speciale, 1, 115-140

Battaglia, M., Murray, M., Serpelloni, E., & Bürgmann, R. (2004). The Adriatic region: An independent microplate within the Africa-Eurasia collision zone. *Geophysical Research Letters*, 31(9), n/a-n/a. https://doi.org/10.1029/2004gl019723

Benvenuti, M., Bortolotti, V., Conticelli, S., Pandeli, E., Principi, G., 2001. 2 – Elba Island – A – Introduction. *Ofioliti,* 26, 321-330.

Bernard, S., Benzerara, K., Beyssac, O., Menguy, N., Guyot, F., Brownjr, G., & Goffe, B. (2007). Exceptional preservation of fossil plant spores in high-pressure metamorphic rocks. *Earth And Planetary Science Letters*, 262(1-2), 257-272. https://doi.org/10.1016/j.epsl.2007.07.041

Bianco, C., Brogi, A., Caggianelli, A., Giorgetti, G., Liotta, D., & Meccheri, M. (2015). HP-LT metamorphism in Elba Island: Implications for the geodynamic evolution of the inner Northern Apennines (Italy). *Journal Of Geodynamics*, *91*, 13-25. https://doi.org/10.1016/j.jog.2015.08.001

Bianco, C., Godard, G., Halton, A., Brogi, A., Liotta, D., & Caggianelli, A. (2019). The lawsonite-glaucophane blueschists of Elba Island (Italy). *Lithos*, *348-349*, 105198. https://doi.org/10.1016/j.lithos.2019.105198

Bonini, M., Sani, F., Stucchi, E., Moratti, G., Benvenuti, M., Menanno, G., & Tanini, C. (2014). Late Miocene shortening of the Northern Apennines back-arc. *Journal Of Geodynamics*, *74*, 1-31. https://doi.org/10.1016/j.jog.2013.11.002

Bortolotti, V., Fazzuoli, M., Pandeli E., Principi, G., Babbini, A., and Corti, S., 2001a, Geology of central and eastern Elba Island, Italy: *Ofioliti*, 26(2a), 97-150.

Boutelier, D., & Chemenda, A. (2008). Exhumation of UHP/LT rocks due to the local reduction of the interplate pressure: Thermo-mechanical physical modelling. *Earth and Planetary Science Letters*, 271(1-4), 226-232. https://doi.org/10.1016/j.epsl.2008.04.011

Boutelier, D., Chemenda, A., & Jorand, C. (2004). Continental subduction and exhumation of high-pressure rocks: insights from thermo-mechanical laboratory modelling. *Earth And Planetary Science Letters*, *222*(1), 209-216. https://doi.org/10.1016/j.epsl.2004.02.013

Brunet, C., Monié, P., Jolivet, L., & Cadet, J. (2000). Migration of compression and extension in the Tyrrhenian Sea, insights from 40Ar/39Ar ages on micas along a transect from Corsica to Tuscany. *Tectonophysics*, 321(1), 127-155. https://doi.org/10.1016/s0040-1951(00)00067-6

Bucher, K., & Frey, M. (2002). *Petrogenesis of Metamorphic Rocks* (7th ed., p. 313). Springer.

Caggianelli, A., Zucchi, M., Bianco, C., Brogi, A., & Liotta, D. (2018). Estimating P-T metamorphic conditions on the roof of a hidden granitic pluton: an example from the Mt. Calamita promontory (Elba Island, Italy). *Italian Journal Of Geosciences*, 137(2), 238-253. https://doi.org/10.3301/ijg.2018.11

Carmignani, L., Conti, P., Cornamusini, G., Meccheri, L., 2004. The internal Northern Apennines, the northern Tyrrhenian Sea and the Sardinia-Corsica block. *Intern. Geol. Cong.* IGC 32, 59-77.

Carmignani, L., Giglia, G., & Kligfield, R. (1987). Structural Evolution of the Apuane Alps: An Example of Continental Margin Deformation in the Northern Apennines, Italy. *The Journal of Geology*, 86(4), 487-504.

Carmignani, L., & Kligfield, R. (1990). Crustal extension in the northern Apennines: The transition from compression to extension in the Alpi Apuane Core Complex. *Tectonics*, *9*(6), 1275-1303. https://doi.org/10.1029/tc009i006p01275

Carminati, E., Doglioni, C., 2004. Mediterranean Tectonics. Encyclopedia of Geology, vol. 1. Elsevier, pp. 135–146.

Carosi, R., Montomoli, C., & Pertusati, P. (2004). Late tectonic evolution of the Northern Apennines: the role of contractional tectonics in the exhumation of the tuscan units. *Geodinamica Acta*, 17(4), 253-273. https://doi.org/10.3166/ga.17.253-273

Cawood, P., Kröner, A., Collins, W., Kusky, T., Mooney, W., & Windley, B. (2009). Accretionary orogens through Earth history. *Geological Society, London, Special Publications*, *318*(1), 1-36. https://doi.org/10.1144/sp318.1

Chemenda, A., Mattauer, M., & Bokun, A. (1996). Continental subduction and a mechanism for exhumation of high-pressure metamorphic rocks: new modelling and field data from Oman. *Earth and Planetary Science Letters*, 143(1-4), 173-182. https://doi.org/10.1016/0012-821x(96)00123-9

Chemenda, A., Mattauer, M., Malavieille, J., & Bokun, A. (1995). A mechanism for syn-collisional rock exhumation and associated normal faulting: Results from physical modelling. *Earth and Planetary Science Letters*, 132(1-4), 225-232. https://doi.org/10.1016/0012-821x(95)00042-b

Chen, X., Schertl, H., Cambeses, A., Gu, P., Xu, R., & Zheng, Y. et al. (2019). From magmatic generation to UHP metamorphic overprint and subsequent exhumation: A rapid cycle of plate movement recorded by the supra-subduction zone ophiolite from the North Qaidam orogen. *Lithos*, *350-351*, 105238. https://doi.org/10.1016/j.lithos.2019.105238

Clemenzi, L., Molli, G., Storti, F., Muchez, P., Swennen, R., & Torelli, L. (2014). Extensional deformation structures within a convergent orogen: The Val di Lima low-angle normal fault system (Northern Apennines, Italy). *Journal Of Structural Geology*, 66, 205-222. https://doi.org/10.1016/j.jsg.2014.05.019

Cloos, M. (1982). Flow melanges: Numerical modeling and geologic constraints on their origin in the Franciscan subduction complex, California. Geological Society Of America Bulletin, 93(4), 330. https://doi.org/10.1130/0016-7606(1982)93<330:fmnmag>2.0.co;2

Conticelli, S., Bortolotti, V., Principi, G., Laurenzi, M. A., D'Antonio, M., Vaggelli, G. (2001) Petrology, mineralogy and geochemistry of a mafic dike from monte castello, Elba island, Italy. *Ofioliti*, 26 (2a), 249-262.

Corti S., Dini c., Pandeli E. and Principi G. (1996.) Le unità tettoniche dell 'Isola d 'Elba orientale (Toscana): nuovi dati e ipotesi di correlazione. *In: 78ª Riunione Estiva S.G.I. "Geologia delle Dolomiti", San Cassiano (BZ), Riass.,* 65-66.

Corfu, F., Hanchar, J., Hoskin, P., & Kinny, P. (2003). Atlas of Zircon Textures. *Reviews In Mineralogy And Geochemistry*, *53*(1), 469-500. https://doi.org/10.2113/0530469

Costa, E., & Vendeville, B. (2002). Experimental insights on the geometry and kinematics of fold-and-thrust belts above weak, viscous evaporitic décollement. *Journal Of Structural Geology*, *24*(11), 1729-1739. https://doi.org/10.1016/s0191-8141(01)00169-9

D'Agostino, N., Avallone, A., Cheloni, D., D'Anastasio, E., Mantenuto, S., & Selvaggi, G. (2008). Active tectonics of the Adriatic region from GPS and earthquake slip vectors. *Journal Of Geophysical Research*, 113(B12). https://doi.org/10.1029/2008jb005860

Davis, D., Suppe, J., & Dahlen, F. (1983). Mechanics of Fold-and-Thrust Belts and Accretionary Wedges. *Journal Of Geophysical Research*, 88(B2), 1152-1172.

Deer, W. A. & Zussman, J. (Jack), 1924- & Howie, R. A. (Robert Andrew) & Deer, W. A & Howie, R. A et al. (1992). An introduction to the rock-forming minerals (2nd ed, 696p). Longman Scientific & Technical; New York, NY: Wiley, Harlow, England.

Dewey, J., Ryan, P., & Andersen, T. (1993). Orogenic uplift and collapse, crustal thickness, fabrics and metamorphic phase changes: the role of eclogites. *Geological Society, London, Special Publications,* 76(1), 325-343. https://doi.org/10.1144/gsl.sp.1993.076.01.16

Duranti, S., Palmeri, R., Pertusati, P.C., and Ricci, C.A., 1992, Geological evolution and metamorphic petrology of the basalt sequences of eastern Elba (Complex II): *Acta Vulcanologica*, 2, 213-229.

Deino, A., Keller, J., Minelli, G. And Pialli, G. (1992) Datazioni 40Ar/39Ar del metamorfismo dell'Unitá di Ortano-Rio Marina (Isola d'Elba): risultati preliminiari, *Studi Geologici Camerti*, 2, 187-192.

Dini, A., Gianelli, G., Puxeddu, M., & Ruggieri, G. (2005). Origin and evolution of Pliocene–Pleistocene granites from the Larderello geothermal field (Tuscan Magmatic Province, Italy). *Lithos*, *81*(1-4), 1-31. https://doi.org/10.1016/j.lithos.2004.09.002

Doglioni, C., Gueguen, E., Harabaglia, P., & Mongelli, F. (1999). On the origin of west-directed subduction zones and applications to the western Mediterranean. *Geological Society, London, Special Publications*, 156(1), 541-561. https://doi.org/10.1144/gsl.sp.1999.156.01.24

Doglioni, C., Gueguen, E., Sàbat, F., & Fernandez, M. (1997). The Western Mediterranean extensional basins and the Alpine orogen. *Terra Nova*, *9*(3), 109-112. https://doi.org/10.1046/j.1365-3121.1997.d01-18.x

Dünkel, I., Kuhlemann, J., & Nohlen, U. (2003). Iron ore formation and neotectonic evolution in Elba (Tuscany, Italy) during Messinian plutonism. *Neues Jahrbuch Für Geologie Und Paläontologie - Abhandlungen*, *230*(2-3), 391-407. https://doi.org/10.1127/njgpa/230/2003/391

Elter, F. M. and Pandeli, E. (2001) Structural Evolution of Anchi-/Epimetamorphic Uits of Centrla and Eastern Elba (Ortano, Acquadolce, Monticiano Roccastrada and Grassera Units) *Ofioliti*, 2001, 26 (2a), 219-228

Ernst, W. (1972). Occurrence and mineralogic evolution of blueschist belts with time. *American Journal Of Science*, *272*(7), 657-668. https://doi.org/10.2475/ajs.272.7.657

Ernst, W., Maruyama, S., & Wallis, S. (1997). Buoyancy-driven, rapid exhumation of ultra-high-pressure metamorphosed continental crust. *Proceedings Of The National Academy Of Sciences*, *94*(18), 9532-9537. https://doi.org/10.1073/pnas.94.18.9532

Faccenda, M., Minelli, G., & Gerya, T. (2009). Coupled and decoupled regimes of continental collision: Numerical modeling. *Earth And Planetary Science Letters*, *278*(3-4), 337-349. https://doi.org/10.1016/j.epsl.2008.12.021

Faccenna, C., Davy, P., Brun, J., Funiciello, R., Giardini, D., Mattei, M., & Nalpas, T. (1996). The dynamics of back-arc extension: an experimental approach to the opening of the Tyrrhenian Sea. *Geophysical Journal International*, 126(3), 781-795. https://doi.org/10.1111/j.1365-246x.1996.tb04702.x

Farley, K., Wolf, R., & Silver, L. (1996). The effects of long alpha-stopping distances on (U-Th)/He ages. *Geochimica Et Cosmochimica Acta*, *60*(21), 4223-4229. https://doi.org/10.1016/s0016-7037(96)00193-7

Fossen, H. (2016). Structural geology (2nd ed., p. 1029-1339). Cambridge University Press.

Fraser, G., Ellis, D., & Eggins, S. (1997). Zirconium abundance in granulite-facies minerals, with implications for zircon geochronology in high-grade rocks. *Geology*, *25*(7), 607. https://doi.org/10.1130/0091-7613(1997)025<0607:zaigfm>2.3.co;2

Gagnevin, D., Daly, J., Horstwood, M., & Whitehouse, M. (2011). In-situ zircon U–Pb, oxygen and hafnium isotopic evidence for magma mixing and mantle metasomatism in the Tuscan Magmatic Province, Italy. *Earth And Planetary Science Letters*, 305(1-2), 45-56. https://doi.org/10.1016/j.epsl.2011.02.039

Garfagnoli, F., Menna, F., Pandeli, E., & Principi, G. (2005). The Porto Azzurro Unit (Mt. Calamita promontory, south-eastern Elba Island, Tuscany): stratigraphic, tectonic and metamorphic evolution. *Bollettino Della Società Geologica Italiana*, *3*, 119-138.

Grujic, D. (2006). Channel flow and continental collision tectonics: an overview. *Geological Society, London, Special Publications, 268*(1), 25-37. https://doi.org/10.1144/gsl.sp.2006.268.01.02

Gueguen, E., Doglioni, C., & Fernandez, M. (1998). On the post-25 Ma geodynamic evolution of the western Mediterranean. *Tectonophysics*, *298*(1-3), 259-269. https://doi.org/10.1016/s0040-1951(98)00189-9

Guillot, S., Hattori, K., Schwartz, S., & Vidal, O. (2009). Exhumation processes in oceanic and continental subduction contexts: A review. *Subduction Zone Geodyanmics*, *In: Lallemand S., Funiciello F. (eds) Subduction Zone Geodynamics. Frontiers in Earth Sciences. Springer, Berlin, Heidelberg.*, 172-205. https://doi.org/https://doi.org/10.1007/978-3-540-87974-9_10

Gutscher, M., Kukowski, N., Malavieille, J., & Lallemand, S. (1996). Cyclical behavior of thrust wedges: Insights from high basal friction sandbox experiments. *Geology*, *24*(2), 135. https://doi.org/10.1130/0091-7613(1996)024<0135:cbotwi>2.3.co;2

Gutscher, M., Kukowski, N., Malavieille, J., & Lallemand, S. (1998). Episodic imbricate thrusting and underthrusting: Analog experiments and mechanical analysis applied to the Alaskan Accretionary Wedge. *Journal Of Geophysical Research: Solid Earth*, *103*(B5), 10161-10176. https://doi.org/10.1029/97jb03541

Harley, S., Kelly, N., & Moller, A. (2007). Zircon Behaviour and the Thermal Histories of Mountain Chains. *Elements*, *3*(1), 25-30. https://doi.org/10.2113/gselements.3.1.25

Hoskin, P., & Schaltegger, U. (2003). The Composition of Zircon and Igneous and Metamorphic Petrogenesis. *Reviews In Mineralogy And Geochemistry*, *53*(1), 27-62. https://doi.org/10.2113/0530027

Hourigan, J., Reiners, P., & Brandon, M. (2005). U-Th zonation-dependent alpha-ejection in (U-Th)/He chronometry. *Geochimica Et Cosmochimica Acta*, *69*(13), 3349-3365. https://doi.org/10.1016/j.gca.2005.01.024

House, M., Farley, K., & Stockli, D. (2000). Helium chronometry of apatite and titanite using Nd-YAG laser heating. *Earth And Planetary Science Letters*, *183*(3-4), 365-368. https://doi.org/10.1016/s0012-821x(00)00286-7

Hsu, L. (1980). Hydration and phase relations of grossular-spessartine garnets at P H 2O=2 Kb. Contributions To Mineralogy And Petrology, 71(4), 407-415. https://doi.org/10.1007/bf00374712

Husson, L., Brun, J., Yamato, P., & Faccenna, C. (2009). Episodic slab rollback fosters exhumation of HP-UHP rocks. *Geophysical Journal International*, *179*(3), 1292-1300. https://doi.org/10.1111/j.1365-246x.2009.04372.x

Hutchison, I., Von Herzen, R., Louden, K., Sclater, J., & Jemsek, J. (1985). Heat flow in the Balearic and Tyrrhenian Basins, western Mediterranean. *Journal Of Geophysical Research: Solid Earth*, *90*(B1), 685-701. https://doi.org/10.1029/jb090ib01p00685

Jacobs, J., Paoli, G., Rocchi, S., Ksienzyk, A., Sirevaag, H., & Elburg, M. (2018). Alps to Apennines zircon roller coaster along the Adria microplate margin. *Scientific Reports*, *8*(1). https://doi.org/10.1038/s41598-018-20979-w

Jolivet, L. (2003). Subduction tectonics and exhumation of high-pressure metamorphic rocks in the Mediterranean orogens. *American Journal Of Science*, 303(5), 353-409. https://doi.org/10.2475/ajs.303.5.353

Jolivet, L., Daniel, J., Truffert, C., & Goffé, B. (1994). Exhumation of deep crustal metamorphic rocks and crustal extension in arc and back-arc regions. *Lithos,* 33(1-3), 3-30. https://doi.org/10.1016/0024-4937(94)90051-5

Jolivet, L., Faccenna, C., Goffé, B., Mattei, M., Rossetti, F., & Brunet, C. et al. (1998). Midcrustal shear zones in postorogenic extension: Example from the northern Tyrrhenian Sea. *Journal Of Geophysical Research: Solid Earth*, *103*(B6), 123-160. https://doi.org/10.1029/97jb03616

Jolivet, L., Goffé, B., Monié, P., Truffert-Luxey, C., Patriat, M., & Bonneau, M. (1996). Miocene detachment in Crete and exhumation P-T-t paths of high-pressure metamorphic rocks. *Tectonics*, 15(6), 1129-1153. https://doi.org/10.1029/96tc01417

Keller, J., & Coward, M. (1996). The structure and evolution of the Northern Tyrrhenian Sea. *Geological Magazine*, *133*(1), 1-16. https://doi.org/10.1017/s0016756800007214

Keller, J. And Pialli, G. (1990) Tectonics of the Island of Elba; a reappraisal, *Bollettino della Societá Geologica Italiana*, 109(2), 413-425.

Ketcham, R., Gautheron, C., & Tassan-Got, L. (2011). Accounting for long alpha-particle stopping distances in (U–Th–Sm)/He geochronology: Refinement of the baseline case. *Geochimica Et Cosmochimica Acta*, *75*(24), 7779-7791. https://doi.org/10.1016/j.gca.2011.10.011

Kligfield, R., Hunziker, J., Dallmeyer, R., & Schamel, S. (1986). Dating of deformation phases using K-Ar and 40Ar/39Ar techniques: results from the northern apennines. *Journal Of Structural Geology*, *8*(7), 781-798. https://doi.org/10.1016/0191-8141(86)90025-8

Lallemand, S., Heuret, A., & Boutelier, D. (2005). On the relationships between slab dip, back-arc stress, upper plate absolute motion, and crustal nature in subduction zones. *Geochemistry, Geophysics, Geosystems*, *6*(9), n/a-n/a. https://doi.org/10.1029/2005gc000917

Lonergan, L., & White, N. (1997). Origin of the Betic-Rif mountain belt. *Tectonics*, *16*(3), 504-522. https://doi.org/10.1029/96tc03937

Lustrino, M., Morra, V., Fedele, L. & Franciosi, L. (2009). Beginning of the Apennine subduction system in central western Mediterranean: Constraints from Cenozoic "orogenic" magmatic activity of Sardinia, Italy. *Tectonics 28*, https://doi.org/10.1029/2008tc002419

Maineri, C., Benvenuti, M., Costagliola, P., Dini, A., Lattanzi, P., Ruggieri, G., & Villa, I. (2002). Sericitic alteration at the La Crocetta deposit (Elba Island, Italy): interplay between magmatism, tectonics and hydrothermal activity. *Mineralium Deposita*, *38*(1), 67-86. https://doi.org/10.1007/s00126-002-0279-2

Malavieille, J. (2010). Impact of erosion, sedimentation, and structural heritage on the structure and kinematics of orogenic wedges: Analog models and case studies. *GSA Today*, 4-10. https://doi.org/10.1130/gsatg48a.1

Malinverno, A., & Ryan, W. (1986). Extension in the Tyrrhenian Sea and shortening in the Apennines as result of arc migration driven by sinking of the lithosphere. *Tectonics*, *5*(2), 227-245. https://doi.org/10.1029/tc005i002p00227

Maluski, H. (1977). Application de la methode 40Ar-39Ar aux mineraux des roches cristallines perturbees par des evenements thermiques et tectoniques en Corse. *Bulletin De La Société Géologique De France*, S7-XIX(4), 849-855. https://doi.org/10.2113/gssgfbull.s7-xix.4.849

Marroni, M., Meneghini, F., & Pandolfi, L. (2004). From accretion to exhumation in a fossil accretionary wedge: a case history from Gottero unit (Northern Apennines, Italy). *Geodinamica Acta*, *17*(1), 41-53. https://doi.org/10.3166/ga.17.41-53

Marroni, M., & Treves, B. (1998). Hidden Terranes in the Northern Apennines, Italy: A Record of Late Cretaceous-Oligocene Transpressional Tectonics. *The Journal Of Geology*, *106*(2), 149-162. https://doi.org/10.1086/516013

Massa, G., Musumeci, G., Mazzarini, F., & Pieruccioni, D. (2016). Coexistence of contractional and extensional tectonics during the northern Apennines orogeny: the late Miocene out-of-sequence thrust in the Elba Island nappe stack. *Geological Journal*, *52*(3), 353-368. https://doi.org/10.1002/gj.2761

Mazzarini, F., Musumeci, G., & Cruden, A. (2011). Vein development during folding in the upper brittle crust: The case of tourmaline-rich veins of eastern Elba Island, northern Tyrrhenian Sea, Italy. Journal Of Structural Geology, 33(10), 1509-1522. https://doi.org/10.1016/j.jsg.2011.07.001

Molli, G., & Malavieille, J. (2011). Orogenic processes and the Corsica/Apennines geodynamic evolution: insights from Taiwan. *International Journal Of Earth Sciences*, 100(5), 1207-1224. https://doi.org/10.1007/s00531-010-0598-y

Molli, G., & Meccheri, M. (2012). Structural inheritance and style of reactivation at mid-crustal levels: A case study from the Alpi Apuane (Tuscany, Italy). *Tectonophysics*, 579, 74-87. https://doi.org/10.1016/j.tecto.2012.06.044

Moorbath, S. (2005). Dating earliest life. *Nature*, 434(7030), 155-155. https://doi.org/10.1038/434155a

Musumeci, G., Mazzarini, F., Tiepolo, M., & Di Vincenzo, G. (2010). U-Pb and 40Ar/39Ar geochronology of Palaeozoic units in the northern Apennines: determining protolith age and alpine evolution using the Calamita Schist and Ortano Porphyroid. *Geological Journal*, *46*(4), 288-310. https://doi.org/10.1002/gj.1266

Musumeci, G., Mazzarini, F. and Cruden, A. (2015). The Zuccale Fault, Elba Island, Italy: A new perspective from fault architecture. *Tectonics*, 34(6), 1195-1218. https://doi.org/10.1002/2014tc003809

Musumeci, G., & Vaselli, L. (2012). Neogene deformation and granite emplacement in the metamorphic units of northern Apennines (Italy): Insights from mylonitic marbles in the Porto Azzurro pluton contact aureole (Elba Island). *Geosphere*, *8*(2), 470-490. https://doi.org/10.1130/ges00665.1

Pandeli, E., Principi, G., Bortolotti, V., Benvenuti, M., Fazzuoli, M., Dini, A., Fanucci, F., Menna, F. and Nirta, G. (2013). The Elba Island: an intriguing geological puzzle in the Northern Tyrrhenian Sea. *Geological Field Trips*, 5(2.1), 1-114.

Pandeli, E., Puxeddu, M., Ruggieri, G. (2001)The metasiliciclastic-carbonate sequence of the Acquadolce Unit (Eastern Elba Island): new petrographic data and paleogeographic interpretation, *Ofioliti*, 2001, 26 (2a), 207-218.

Papeschi, S., Musumeci, G., Massonne, H., Mazzarini, F., Ryan, E., & Viola, G. (2020). High-P (P = 1.5–1.8 GPa) blueschist from Elba: Implications for underthrusting and exhumation of continental units in the Northern Apennines. *Journal Of Metamorphic Geology*, *38*(5), 495-525. https://doi.org/10.1111/jmg.12530

Peccerillo, A., and Donati, C (2003) Chapter 1 – The Tuscan Magmatic Province. *Periodico di Mineralogia,* 72, 27

Peyton, S. L. and Carrapa, B. (2013), An introduction to low-temperature thermochronologic techniques, methodology, and applications, In: *C Knight. and J. Cuzella, eds., Application of structural methods to Rocky Mountain hydrocarbon exploration and development: AAPG Studies in Geology,* 65, p. 15–36.

Reiners, P. (2005). Zircon (U-Th)/He Thermochronometry. *Reviews In Mineralogy And Geochemistry*, *58*(1), 151-179. https://doi.org/10.2138/rmg.2005.58.6

Reiners, P., Farley, K., & Hickes, H. (2002). He diffusion and (U–Th)/He thermochronometry of zircon: initial results from Fish Canyon Tuff and Gold Butte. *Tectonophysics*, *349*(1-4), 297-308. https://doi.org/10.1016/s0040-1951(02)00058-6

Reiners, P., Spell, T., Nicolescu, S., & Zanetti, K. (2004). Zircon (U-Th)/He thermochronology: He diffusion and comparisons with 40Ar/39Ar dating. *Geochimica Et Cosmochimica Acta*, *68*(8), 1857-1887. https://doi.org/10.1016/j.gca.2003.10.021

Ring, U., & Glodny, J. (2010). No need for lithospheric extension for exhuming (U)HP rocks by normal faulting. Journal Of The Geological Society, 167(2), 225-228. https://doi.org/10.1144/0016-76492009-134

Robertson, A., & Grasso, M. (1995). Overview of the Late Tertiary?Recent tectonic and palaeo-environmental development of the Mediterranean region. *Terra Nova*, *7*(2), 114-127. https://doi.org/10.1111/j.1365-3121.1995.tb00680.x

Rosenbaum, G., & Lister, G. (2004). Neogene and Quaternary rollback evolution of the Tyrrhenian Sea, the Apennines, and the Sicilian Maghrebides. *Tectonics*, *23*(1), n/a-n/a. https://doi.org/10.1029/2003tc001518

Rossetti, F., Faccenna, C., Jolivet, L., Funiciello, R., Tecce, F., & Brunet, C. (1999). Syn-versus post-orogenic extension: the case study of Giglio Island (Northern Tyrrhenian Sea, Italy). *Tectonophysics*, 304(1-2), 71-93. https://doi.org/10.1016/s0040-1951(98)00304-7

Rossetti, F., Faccenna, C., Jolivet, L., Goffe´ , B. & Funiciello, R. (2002). Structural signature and exhumation P –T –t paths of the blueschist units exposed in the interior of the Northern Apennine chain, tectonic implication. *Bollettino della Societa` Geologica Italiana, volume speciale*, 1, 829– 842.

Royden, L., & Burchfiel, B. (1989). Are systematic variations in thrust belt style related to plate boundary processes? (The western Alps versus the Carpathians). *Tectonics*, *8*(1), 51-61. https://doi.org/10.1029/tc008i001p00051

Ryan, E. J. (2017) The Structural and Metamorphic Evolution of the Eastern Elba Nappe Stack, innermost Northern Apennines, Central Italy (Master thesis, Norwegian University of Science and Technology, Trondheim, Norway). Retrieved from https://ntnuopen.ntnu.no/ntnu-xmlui/handle/11250/2446953

Şengör, A., Yılmaz, Y., & Sungurlu, O. (1984). Tectonics of the Mediterranean Cimmerides: nature and evolution of the western termination of Palaeo-Tethys. *Geological Society, London, Special Publications*, *17*(1), 77-112. https://doi.org/10.1144/gsl.sp.1984.017.01.04

Séranne, M. (1999). The Gulf of Lion continental margin (NW Mediterranean) revisited by IBS: an overview. *Geological Society, London, Special Publications*, *156*(1), 15-36. https://doi.org/10.1144/gsl.sp.1999.156.01.03

Shreve, R., & Cloos, M. (1986). Dynamics of sediment subduction, melange formation, and prism accretion. *Journal Of Geophysical Research*, 91(B10), 10229. https://doi.org/10.1029/jb091ib10p10229

Shuster, D., Flowers, R., & Farley, K. (2009). The influence of artificial radiation damage and thermal annealing on helium diffusion kinetics in apatite. *Geochimica Et Cosmochimica Acta*, *73*(1), 183-196. https://doi.org/10.1016/j.gca.2008.10.013

Sirevaag, H. (2013). Nature and Origin of the Cover Sequence of the Tuscan Basement on Elba Island: Evidence from Detrital Zircon Dating (Master thesis, University of Bergen, Bergen, Norway). Retrieved from http://bora.uib.no/handle/1956/7008

Stampfli, G. (2000). Tethyan oceans. *Geological Society, London, Special Publications, 173(1)* , 1-23. https://doi.org/10.1144/gsl.sp.2000.173.01.01

Stampfli, G., Borel, G., Cavazza, W., Mosar, J., & Ziegler, P. (2001). Palaeotectonic and palaeogeographic evolution of the western Tethys and PeriTethyan domain (IGCP Project 369). *Episodes*, 24(4), 222-228. https://doi.org/10.18814/epiiugs/2001/v24i4/001

Stampfli G.M., Borel G.D. (2004) The TRANSMED Transects in Space and Time: Constraints on the Paleotectonic Evolution of the Mediterranean Domain. *In: Cavazza W., Roure F., Spakman W., Stampfli G.M., Ziegler P.A. (eds) The TRANSMED Atlas. The Mediterranean Region from Crust to Mantle. Springer, Berlin, Heidelberg.* https://doi.org/10.1007/978-3-642-18919-7_3

Storti, F., & McClay, K. (1995). Influence of syntectonic sedimentation on thrust wedges in analogue models. *Geology*, *23*(11), 999. https://doi.org/10.1130/0091-7613(1995)023<0999:iossot>2.3.co;2

Tagami, T., Farley, K., & Stockli, D. (2003). (U–Th)/He geochronology of single zircon grains of known Tertiary eruption age. *Earth And Planetary Science Letters*, *207*(1-4), 57-67. https://doi.org/10.1016/s0012-821x(02)01144-5

Trevisan, L. 1950. L'Elba orientale e la sua tettonica di scivolamento per gravita`. *Memorie dell'Istituto Geologico dell'Universita` di Padova*, 16, 1–30.

Trincardi, F., & Zitellini, N. (1987). The rifting of the Tyrrhenian Basin. *Geo-Marine Letters*, 7(1), 1-6. https://doi.org/10.1007/bf02310459

Tvedt, A. B. M. (2011) Strain Analyses and thermochronology in the Eastern Elba fold and thrust belt (Master thesis, University of Bergen, Norway).

Uyeda, S., & Kanamori, H. (1979). Back-arc opening and the mode of subduction. *Journal Of Geophysical Research*, *84*(B3), 1049. https://doi.org/10.1029/jb084ib03p01049

Vanneschi, C., Salvini, R., Massa, G., Riccucci, S., & Borsani, A. (2014). Geological 3D modeling for excavation activity in an underground marble quarry in the Apuan Alps (Italy). *Computers & Geosciences*, 69, 41-54. https://doi.org/10.1016/j.cageo.2014.04.009

Viola, G., Torgersen, E., Mazzarini, F., Musumeci, G., Lelij, R., Schönenberger, J., & Garofalo, P. (2018). New Constraints on the Evolution of the Inner Northern Apennines by K-Ar Dating of Late Miocene-Early Pliocene Compression on the Island of Elba, Italy. *Tectonics*, *37*(9), 3229-3243. https://doi.org/10.1029/2018tc005182

Viti, M., Mantovani, E., Babbucci, D., Tamburelli, C., & Cenni, N. (2016). Seismotectonics of the Padanian Region and Surrounding Belts: Which Driving Mechanism?. *International Journal Of Geosciences*, *07*(12), 1412-1451. https://doi.org/10.4236/ijg.2016.712100

von Raumer, J., Stampfli, G., & Bussy, F. (2003). Gondwana-derived microcontinents — the constituents of the Variscan and Alpine collisional orogens. *Tectonophysics*, *365*(1-4), 7-22. https://doi.org/10.1016/s0040-1951(03)00015-5

Watson, E. (1979). Zircon saturation in felsic liquids: Experimental results and applications to trace element geochemistry. *Contributions To Mineralogy And Petrology*, *70*(4), 407-419. https://doi.org/10.1007/bf00371047

Westerman, D., Dini, A., Innocenti, F., & Rocchi, S. (2004). Rise and fall of a nested Christmas-tree laccolith complex, Elba Island, Italy. *Geological Society, London, Special Publications*, 234(1), 195-213. https://doi.org/10.1144/gsl.sp.2004.234.01.12

Whitney, D., & Evans, B. (2009). Abbreviations for names of rock-forming minerals. *American Mineralogist*, *95*(1), 185-187. https://doi.org/10.2138/am.2010.3371

Wolf, R., Farley, K., & Silver, L. (1996). Helium diffusion and low-temperature thermochronometry of apatite. *Geochimica Et Cosmochimica Acta*, *60*(21), 4231-4240. https://doi.org/10.1016/s0016-7037(96)00192-5

Wolfe, M., & Stockli, D. (2010). Zircon (U–Th)/He thermochronometry in the KTB drill hole, Germany, and its implications for bulk He diffusion kinetics in zircon. *Earth And Planetary Science Letters*, *295*(1-2), 69-82. https://doi.org/10.1016/j.epsl.2010.03.025

Wortel, M., & Spakman, W. (2000). Subduction and Slab Detachment in the Mediterranean-Carpathian Region. *Science*, *290*(5498), 1910-1917. https://doi.org/10.1126/science.290.5498.1910

Wölfler, A., Kurz, W., Danišík, M., & Rabitsch, R. (2010). Dating of fault zone activity by apatite fission track and apatite (U-Th)/He thermochronometry: a case study from the Lavanttal fault system (Eastern Alps). *Terra Nova*, 22, 274–282. https://doi.org/10.1111/j.1365-3121.2010.00943.x

Zhang, L., & Wang, Y. (2020). The exhumation of high- and ultrahigh-pressure metamorphic terranes in subduction zone: Questions and discussions. *Science China Earth Sciences*. https://doi.org/10.1007/s11430-020-9579-3

Zeitler P.K. (2014) U-Th/He Dating. In: *Rink W., Thompson J. (eds) Encyclopedia of Scientific Dating Methods. Springer, Dordrecht.* https://doi.org/10.1007/978-94-007-6326-5_131-1

Zeitler, P., Herczeg, A., McDougall, I., & Honda, M. (1987). U-Th-He dating of apatite: A potential thermochronometer. *Geochimica Et Cosmochimica Acta*, *51*(10), 2865-2868. https://doi.org/10.1016/0016-7037(87)90164-5

10 Appendix

Appendix I - Outcrop descriptions
Appendix II – Maps and cross-section

Outcrop	Locality	Description	Foliation	Linetaion	Fold axis	Fault
1	Capo d'Arco Road	Phyllites have white, elongated streaks and isoclinal folds. Sheared clasts indicating top-to-the-east movement. Faint lineations. Quartz vein boudinage. All structures cm scaled.	005/31° 213/43°	39°/225 40°/124 40°/240	14°/131	092/54°
2	Capo d'Arco Road	More massive layers, probably metasiltstone. Contains calc-schist lenses.	040/29°			
3	Capo d'arco Road	Collected sample for thin section labelled TOL-E	048/52° 066/48°		38°/058	
4	Capo d'Arco Road	Dark, very fine-grained quartz, sometimes with white thin quartz folds and streaks. Collected sample for thin section labelled TOL-F	030/22° 019/36° 023/35° 040/30° 026/18° 065/26°			
5	Ortano Road	Phyllites, but with minimal white streaks	235/35°	32°/210 31°/248		
6	Felciaio Beach	Lineations in the form of rods are sub-horizontal, not down-dip as expected. Less phyllitic, more obvious layers that are folded differently than in Eastern Elba	165/57°	18°/212		
7	Felciaio Beach	Orange contact metamorphic minerals - cordierite. Some sections have abundant isoclinal quartz folds.				
8	Felciaio Beach	Layers appear to be refolded. Collected sample for thin section labelled TOL-A/B/C				
9	Rio Marina Coastline	Large cliffside with graphitic phyllites containing m-scaled calc-schist lenses. Sample 3 collected for thermochronology	288/59°	10°/251	05°/171	315/55°
10	Capo d'Arco	Undulating foliaiton forming open folds. This and nearby outcrops have many thicker (1-2 cm) quartz streaks, sometimes as isoclinal folds, sometimes as streaks.	033/15° 059/35° 088/59° 069/50°			
11	Capo d'Arco	Rodding lineations		05°/330		
12	Capo d'Arco	Undulating foliation not so distinct further south of this point.	199/20° 268/16° 109/25° 119/31°	30°/153	05°/111 37°/136	
13	Capo d'Arco	Flaky phyllites with occasional rootless quartz fold hinges parallel to foliation.	279/26° 266/18° 289/35° 096/15° 089/19° 331/15° 292/21° 285/41° 299/38°		06°/092?	
14	Rio Marina Harbor	Calc-schist lense by Rio Marina lighthouse. Colorful layers with several folds, both similar and sheath folds.	328/25° 291/30° 331/20°	05°/255	20°/274 02°/201 20°/295 10°/269 25°/270 40°/293	